

https://dspace.org/

The synthesis and characterization of activated carbon from sewage sludge as low cost bio-adsorbent for nitrate and cationic dye pollution remediation

Masengo, John Longo

2021
https://hdl.handle.net/10539/32952

Downloaded from a DSpace repository. https://dspace.org/



UNIVERSITY OF THE
WITWATERSRAND,
JOHANNESBURG

THE SYNTHESIS AND CHARACTERIZATION OF ACTIVATED CARBON FROM SEWAGE SLUDGE AS LOW COST BIO-ADSORBENT FOR NITRATE AND CATIONIC DYE POLLUTION REMEDIATION

John Longo Masengo

Student Number: 2244474

A dissertation submitted to the Faculty of Engineering and the Built Environment, University of the Witwatersrand, Johannesburg, in fulfilment of the requirements for the degree of MSc in Engineering.

Supervisor: Prof Jean Mulopo

September, 2021

KEYWORDS

Activated carbon, Sewage sludge, Bio-adsorbent, Nitrate, Cationic dye pollution, Remediation, Synthesis and Characterization

ABSTRACT

Sewage sludge is an inevitable waste from wastewater treatment plant. in South Africa, landfilling of sewage sludge remains the principal route of management. This study aims to synthetise bio-adsorbent from sewage sludge and discard coal.

This study plan to synthetise bio-adsorbent from sewage sludge and discard coal as precursor. To achieve this purpose: two types of municipal wastewater sewage sludge were collected from the ERWAT wastewater treatment plant in the Mid-Vaal district (South Africa). The secondary sludge, which was a dissolved air flotation stage outlet, was labeled as (D), while the digested and dewatered (with filter belt) sludge (primary and secondary) ready for disposal was labelled as (D) (S). The activating reagent concentration (Potassium Hydroxide: KOH), temperature, and mixture with discard coal were chosen as variables to consider in the sewage preparation based on literature. Precursors sludge TGA curves with temperatures varying from 30 °C to 900 °C in nitrogen (N_2) atmosphere were used to determine the minimum pyrolyzed temperature (minimal weight variance located about 600 °C). Two numerical variables (pyrolysis temperature and KOH concentration) and two categorical variables (types of sewage sludge samples blended with/without discard coal) were used to synthesize activated carbon from sludge. The effect of the synthesis variables on the low cost activated carbon derived properties in comparison to commercial activated carbon was investigated using response surface methodology (RSM) with eight responses. R1 (Specific surface area: m^2/g), R2 (micropore surface area/total surface area*100: %), R3 (Cations Exchange Capacity (CEC): meq/100g), R4 (pH_{pzc}), R5 (Acidity: mmol/g), R6 (Basicity: mmol/g), R7 (N/C ratio), R8 (H/C ratio) were the eight responses considered.

In contrast to the precursors, FT-IR (Fourier Transform Infrared Spectroscopy), SEM/EDS (Scanning Electron Microscopy-Energy Dispersive Spectroscopy), BET (Brunauer–Emmett–Teller), and XRD (X-Ray Diffraction) study reveal evidence of surface functionalities, morphology, texture, and crystalline structures transformation after activation. Furthermore, the Toxicity Characteristic Leaching Procedure (TCLP) test revealed that after activation, the concentrations of Cu, Zn, Pb, Ni, Co, Cr, Fe, and Mn decreased significantly, indicating that the metals had stabilized. The effect of

sludge type was also examined, and two types of bio-adsorbents with the best surface areas were chosen for oxidation ammonium persulfate: SC-3-600 (281,72 m^2/g) and SC-5-900 (422,09 m^2/g) from S sludge, and DC-5-750 (312,72 m^2/g) and DC-7-900 (247,57 m^2/g) from D sludge. After activating precursors synthesized with sewage and waste coal, the bio-absorbent was obtained. FT-IR analysis revealed the introduction of an acidic surface functional group after oxidation with ammonium persulfate in all cases, although Raman spectroscopy revealed a minor graphitization advancement over disordered carbon structure. However, after oxidation with a 2M ammonium persulfate dissolved in 1M H_2SO_4 solution, the texture of SC-3-600 and SC-5-900 was seriously affected, dropping from 281,72 m^2/g and 422,09 m^2/g, respectively, to 46,57 m^2/g and 313,05 m^2/g after oxidation. The differences were less significant in the case of DC-5-750 and DC-7-900, which started with a surface area of 312,72 m^2/g and 247,57 m^2/g, respectively, and ended up with 282,22 m^2/g and 295,31 m^2/g after oxidation. The highest nitrate adsorption capacity was found in an acidic solution (pH 2), while the highest methyl red adsorption capacity was found in a mild acidity solution (pH4).

For both nitrate and methyl red, the adsorption process using synthesized adsorptions was primarily represented by the pseudo kinetic model rather than the pseudo first-order kinetic model, and the intraparticle model diffusion was not found to be the sole controlling mechanism in both cases. For nitrate, the Langmuir isotherm model suits the adsorption process better in the following order: For methyl red, DC-5-750 (26,735 mg/g) > Com-AC (20,618 mg/g) > DC-7-750 M1 (17,064 mg/g) DC-5-750M2 (175, 438 mg/g) > DC-7-750 (147,058 mg/g) > Com-AC (196,07 mg/g). The adsorption was favorable in all cases because R_L (Langmuir constant) was between 0 and 1. Thermodynamic data analysis revealed that nitrate uptake was exothermic, spontaneous at lower temperatures, and had an S value of < 0, while adsorptive methyl red (MR) removal was endothermic, feasible, and spontaneous with an S value of >0.

TABLE OF CONTENTS

Keywords i
Abstract ii
Table of Contents iv
List of Figures vi
List of Tables ix
List of Abbreviations xi
Declaration xii
Acknowledgements xiii
Chapter 1: Introduction 1
1.1 Research problem 1
1.2 Importance of research 3
1.3 Scope of research and hypothesis 3
1.4 Objectives of the study 4
1.5 Research methodology 4
Chapter 2: Literature Review 7
2.1 general Background 7
2.2 Origin and utilization of Activated Carbon 9
2.3 Preparation of activated carbon 10
2.4 Properties 12
2.5 Surface modifications 20
2.6 Adsorption on carbon based adsorbent 25
2.7 Synthesis of adsorbent from sewage sludge by chemical activation 34
Chapter 3: Materials and Methodologies 41
3.1 Samples and chemicals 41
3.2 Raw materials processing 43
3.3 synthesis and characterization of Sludge based activated carbon 44
3.4 Use of the experimental design for adsorbent synthesis 46
3.5 modifications with Ammonium Persulfate 50
3.6 adsorption test 51
Chapter 4: Synthesis and characterization of SBAC 53
4.1 precursors pre-treatment and preliminary characterizations 53
4.2 precursors and sludge based adsorbent analysis 55
4.3 design Responses 67
4.4 toxicity characteristic leaching procedure 107

Chapter 5: Wet oxidation and adsorption test 109
5.1 Modification 109
5.2 Adsorption Tests Application 113
Chapter 6: Conclusions 135
Bibliography 137
Appendices 155

LIST OF FIGURES

Figure 2.1 Illustration of 2-D plane layer of (a) graphitizable carbon and (b) non-graphitizable carbon (Marsh & Reinoso, 2006) 9

Figure 2.2 illustration of carbonized products with a likewise graphitic structure (Gong, 2013) 10

Figure 2.3 Types of porosity in activated carbon (Bandosz, 2006) 13

Figure 2.4 types of isotherm shape with Nitrogen adsorption/desorption (Marsh & Reinoso, 2006) 15

Figure 2.5 structure and classification of oxygen functionalities of carbon surface (Shafeeyan et al., 2010) 17

Figure 2.6 Nitrogen containing functional groups in activated carbon. N-6: pyridinic N, N-5:pyrrolic/pyridine, N-Q: quaternary and N-X: N-oxides (Tascón, 2012) 18

Figure 2.7 Behaviour of functional groups related to point of zero charge and the pH of the medium (Bandosz, 2006) 20

Figure 3.1 (a) Dissolved Air Flotation and (b) Final Sludge. 41

Figure 3.2 Resume of principal practical research activities 42

Figure 3.3 Photography of the sewage air-dried, D in the plastic cylinder and S laid on the bash 43

Figure 4.1 Thermogravimetric curves of Sludge precursor 55

Figure 4.2 microscopic observation of sewage sludge precursor D: (a) and (b), S: (c) and (d). 56

Figure 4.3 Elemental analysis of D precursors particles by EDS 57

Figure 4.4 Elemental EDS analysis of S sample 58

Figure 4.5 SEM microscopic analysis of SBAC, (a) multiple particle (b) focus on particle without cavity after activation and (c) qualitative analysis of the targeted particle 59

Figure 4.6 FT-IR spectra for precursors 60

Figure 4.7 FT-IR spectra of SBAC with sludge D as precursor 61

Figure 4.8 FT-IR spectra of SBAC with sludge S as precursor 62

Figure 4.9 FT-IR spectra of D-5-600 and D C-5-600 63

Figure 4.10 FT-IR spectra of S-3-600 and SC-3-600 64

Figure 4.11 FT-IR spectra of SC-3-600 and SC-3-900 65

Figure 4.12 FT-IR spectra of D-3-600 and S-3-600 65

Figure 4.13 XRD graph of feedstock (a), SBAC and Com-AC (b) 67

Figure 4.14 graphic of SBAC surface area from Sludge D without discard coal 70

Figure 4.15 graphic of surface area from Sludge D mixed with discard coal 70

Figure 4.16 graphic of SBAC surface area from Sludge S without discard coal 71
Figure 4.17 graphic of SBAC surface area from Sludge S with discard coal 72
Figure 4.18 Graphic of SBAC microporosity from sludge D without Discard coal 74
Figure 4.19 Graphic of SBAC microporosity from sludge D with Discard coal 75
Figure 4.20 Graphic of SBAC microporosity from S-sludge without discard coal 75
Figure 4.21 Graphic of SBAC microporosity from Sludge S with discard coal 76
Figure 4.22 pore size distribution of adsorbents 78
Figure 4.23 N2 adsorption-desorption isotherm (a) DC-5-750 , (b) DC-7-900, (c) SC-3-600 and (d) SC-5-900 79
Figure 4.24 graphic of SBAC CEC from sludge D without discard coal 86
Figure 4.25 graphic of SBAC CEC from sludge D with discard coal 87
Figure 4.26 graphic of SBAC CEC from sludge S without discard coal 88
Figure 4.27 graphic of SBAC CEC from sludge S with discard coal 88
Figure 4.28 Graphic of pHpzc response for SBAC from sludge D without discard coal 91
Figure 4.29 Graphic of pHpzc response for SBAC from sludge D with discard coal 91
Figure 4.30 Graphic of pHpzc response for SBAC from sludge S without discard coal 92
Figure 4.31 Graphic of pHpzc response for SBAC from sludge S with discard coal 92
Figure 4.32 graphic of SBAC acidity from sludge D without discard coal 96
Figure 4.33 graphic of SBAC acidity from sludge D with discard coal 96
Figure 4.34 graphic of SBAC acidity from sludge S without discard coal 97
Figure 4.35 graphic of SBAC acidity from sludge S with discard coal 97
Figure 4.36 graphic of SBAC N/C ratio from Sludge D without discard coal 100
Figure 4.37 graphic of SBAC N/C ratio from Sludge D with discard coal 101
Figure 4.38 graphic of SBAC N/C ratio from sludge S without discard coal 101
Figure 4.39 graphic of SBAC N/C ratio from sludge S with discard coal 102
Figure 4.40 graphic of SBAC H/C ratio from sludge D without discard coal 105
Figure 4.41 graphic of SBAC H/C ratio from sludge D with discard coal 105
Figure 4.42 graphic of SBAC H/C ratio from sludge S with discard coal 106
Figure 5.1 FT-IR spectra of Com-AC, DC-5-750 and its 2 modified sorbents 109
Figure 5.2 morphology of (a) DC-5-750, (b) DC-5-750 M1 and (c) Com-AC 110
Figure 5.3 XRD pattern of Com-AC, unmodified (DC-5-750) and its modified sorbent 111

Figure 5.4 preliminary adsorption capacity evaluation of nitrate adsorption 114
Figure 5.5 effect of time on nitrate adsorption capacity 115
Figure 5.6 nitrate PSO kinetic model plot 115
Figure 5.7 nitrate PSO kinetic plots 116
Figure 5.8 intraparticle model diffusion of nitrate adsorption 116
Figure 5.9 Effect of pH solution on nitrate adsorption 118
Figure 5.10 effect of initial nitrate concentration on adsorbent adsorption capacity 119
Figure 5.11 effect of nitrate adsorption initial concentration on percentage adsorbent uptake 119
Figure 5.12 Langmuir isotherm plot of nitrate adsorption 120
Figure 5.13 Freundlich isotherm plot of nitrate adsorption 120
Figure 5.14 plot of nitrate ln(qe/ce) vs 1/T 122
Figure 5.15 preliminary adsorption capacity results of MR adsorption 124
Figure 5.16 effect of contact time on adsorption capacity of MR 125
Figure 5.17 methyl red PFO kinetic model 125
Figure 5.18 methyl red PSO kinetic model 126
Figure 5.19 methyl red intraparticle diffusion model 126
Figure 5.20 effect of solution pH on MR adsorption capacity of adsorbent 128
Figure 5.21 adsorption capacity of sorbent in fonction of MR initial concentration 128
Figure 5.22 MR percentage removed in function of initial concentration 129
Figure 5.23 Langmuir isotherm plot of MR adsorption 129
Figure 5.24 Freundlich Isotherm plot of MR adsorption 130
Figure 5.25 effect of ionic strength 132
Figure 5.26 plot of ln(qe/ce) vs 1/T of MR adsorption 133

LIST OF TABLES

Table 2.1 benefit and drawback of dye uptake methods (Afroze & Sen, 2018; Yagub et al., 2014) 7
Table 2.2 Advantages and disadvantage of activation routes (Hadi et al., 2015) 12
Table 2.3 Publications on adsorption with modified activated carbon 23
Table 2.4 Equilibrium adsorption Isotherms (Singh et al., 2018) 32
Table 2.5 SBAC synthesis conditions and adsorption capacity 37
Table 2.6 Aqueous phase modified SBAC and adsorption capacity 39
Table 3.1 previous research of SBAC preparation using RSM 46
Table 3.2 Experiments generated by Design Expect 12.0 49
Table 3.3 Rearranged experiment 50
Table 3.4 wet oxidation conditions 51
Table 3.5 Adsorption test conditions 52
Table 4.1 Moisture content of non-dried and sun dried sample 53
Table 4.2 Precursors properties 54
Table 4.3 Analysis of variance (ANOVA) of surface area response 68
Table 4.4 Actual equation of microporosity percentage response 68
Table 4.5 Analysis of variance (ANOVA) of Microporosity percentage response 73
Table 4.6 Actual equation of microporosity percentage response 73
Table 4.7 Comparison of structural properties of chemically activated SBAC from literature 76
Table 4.8 Summary of experimental design responses 80
Table.4.9 ANOVA of CEC response 83
Table 4.10 Actual equation of CEC response 84
Table 4.11 brief comparison of CEC 85
Table 4.12 ANOVA of pHpzc Response 89
Table 4.13 Actual equation for pHPZC 90
Table 4.14 Acidity and basicity of SBAC 93
Table 4.15 ANOVA of acidity response 94
Table 4.16 Actual equation of Acidity response 94
Table 4.17 ANOVA of basicity response 98
Table 4.18 ANOVA of N/C ratio response 99
Table 4.19 Actual equation for N/C response 99

Table 4.20 ANOVA of H/C response 102
Table 4.21 Actual equation of H/C response 103
Table 4.22 Heavy metal concentration leached with TCLP procedure from precursors and sorbents 108
Table 5.1 Physical structure and ultimate analysis results of SBAC after and before modifications 112
Table 5.2 Parameters of PFO, PSO kinetics and intraparticle diffusion nitrate model 117
Table 5.3 Value of isotherms parameters of nitrate removal 121
Table 5.4 Comparison of Langmuir maximum capacity with literature 121
Table 5.5 Value of nitrate adsorption thermodynamic parameters 123
Table 5.6 Parameters value of methyl red PFO and PSO kinetic and intraparticle model 127
Table 5.7 Parameters value of Langmuir and Freundlich isotherm 131
Table 5.8 Comparison of adsorption capacity with literature values 131
Table 5.9 Value of thermodynamic parameter of MR adsorption 134

LIST OF ABBREVIATIONS

AC	Activated carbon
ANOVA	Analysis of variance
APS	Ammonium persulfate
BET	Brauner-Emmett-Teller
CEC	Cations Exchange Capacity
MR	Methyl Red
PFO	Pseudo first order
PSD	Pore size distribution
PSO	Pseudo second order
PZC	Point of zero charge
RSM	Response surface methodology
SBAC	Sludge based activated carbon
TCLP	Toxicity Characteristic Leaching Procedure
TGA	Thermogravimetric Analysis
TPD	Temperature programme desorption

DECLARATION

I, John Longo Masengo, declare that this dissertation is my own work. It is currently submitted for the degree of Masters of Science in engineering to the University of the Witwatersrand. It has not been submitted elsewhere for examination

Signature: _John Longo Masengo 

02 day of ____September_____ 2021

ACKNOWLEDGEMENTS

Isaiah 41:10

The current dissertation is the culmination of a tremendous amount of work from those who have assisted this project a reality, and it is difficult to find the right words to convey our gratitude.

We would like to express our gratitude to Prof Jean Mulopo for his unconditional support who during the completion of this study despite his various commitments. His advices, comments, and motivation, combined with his help, were invaluable in completing the study, not to mention his encouragement to keep going.

We cannot afford to ignore contribution of Staff of the School of Chemical and Metallurgical Engineering personal who provided their time for analyses namely Motlatsi Phali, Letta Ntuli, Petra and Sonia.

To my father Jean Ilunga Masengo and my mother Edwin Kumwimba Banza I thank them for their incredible will to support our formation and encouragements.

To my siblings for the cheer moment, we shared since childhood: Thethe Kyungu, Papa Levi Shimbi, Joe Masengo, Jeanine Kabongo, Jean-Paul Ilunga, William Kabulo and Mary Kumwimba.

Thank you to our brother-in-law Mujinga Kipanzula, my friends Simeon Monga Lubinda and Abigael Umba and uncle Shimbi Kabulo.

To our fellow postgraduate colleagues and Gentil Kahilu for friendly and cooperative atmosphere that reigns in the office.

We also thank all those who contributed to the completion of this project

CHAPTER 1: INTRODUCTION

1.1 Research problem

South African population has experienced a rapid growth in the last 2-3 decades i.e. 48.8 million in 2005, 51.58 million in 2010 to 57.7 million 2018 (Stats SA, 2018) of which more than half currently lives and works in densely populated urban areas (DWA, 2013b). This rapid population growth coupled with rapid urbanisation have put an extra pressure on existing Wastewater Treatment Plants (WWTP) facilities which has resulted in the short to medium term in an increased generation of sewage sludge at these facilities (Libhaber & Orozco-Jaramillo, 2012).

Several lines of evidence have suggested that the disposal of sewage sludge in landfills is not a sustainable option for sewage sludges management (Almahbashi et al., 2020; Devi & Saroha, 2016; Kacprzak et al., 2017; Tesfamariam, 2010; G. Xu et al., 2015), even though approximately 80% of wastewater treatment facilities still dispose their sewage sludge on dedicated sites (Herselman et al., 2006) despite the potential dangers of contamination of the soil, subsoil (Kacprzak et al., 2017). The South African department of Water Affairs and Forestry has identified 4 areas of utilization of sewage sludges namely i) agriculture use (fertilizer), ii) beneficiation (rehabilitation site, adsorbent, nursery growth medium), iii) thermal management practices and iv) commercial products (manufacturing of pellet, bricks, paving and artificial rock)(Herselman & Moodley, 2009). However; the utilization of fertilizers produced from sewage sludge is still relatively limited due to both quality limitations (Faecal coliform maximum < 10000 CFU/g dry, Helminth Ova < 1 viable ova/g dry, pollution: As < 40 ppm, Cd< 40 ppm, Cr <1200 ppm, Cu < 1500 ppm, Pb < 300 ppm, Hg < 15 ppm, Ni < 420 ppm, Zinc < 2500 ppm) and quantity limitation (less than 10t/ha used per year) (Snyman & Herselman, 2006).

On the other hand; despite the fact that the South African mining industry contributes by a significant portion to the Gross Domestic Product (approximately:9 %) (Stats SA, 2019), it remains a well-known source of pollution and one of the largest water consumers after the agriculture sector (DWA, 2013a). In South Africa the coal and gold mining spanned from the end of the ninetieth century. In the Witwatersrand gold reef, more than 6 billion metric tons of gold ore has been extracted, milled, and

treated over the last century, after-effect, a proportion of world's deepest gold mines (3,777 m) the with significant draining, pumping and exhausting process, the daily flow of mine water up to 130 Ml. Initial evaluation of the decant volume per day ranged between 7 Ml and 12.5 Ml (Hobbs & Cobbing, 2007; Rösner & Van Schalkwyk, 2000). In 2005, the rate of decant was assessed between 18 and 36 Ml/d, after a new decant had been announced earlier in the same year, located on surface at an abandoned shaft to the east on the slope above the black reef incline (Hobbs & Cobbing, 2007; Rösner & Van Schalkwyk, 2000). The discontinuation of gold mines on the Witwatersrand has been correlated to environmental risk because of Acid Mine of Drainage (AMD) seepage from flooded underground mine workings, especially the prospective repercussions on the ground water and its environment. seepage of polluted leachate from tailings piles or dams can be a potential source of surface and ground water pollution in many mining areas (Mulopo, 2017). The impacts of AMD on catchments are unwholesome, for instance, despite of its contribution of 4,6% of total water usage, 78.4% of the total sulphate load is ascribed to mine water in the Olifants river catchment. Arguably water high quality for safe environmental discharge or reuse is the main asset that can be recovered from AMD remediation (Mulopo, 2017). Recently, physical treatment technologies such as membrane based processes have been investigated and even implemented as a supplementary operation in AMD remediation to provide treated water of very high quality (Masindi et al., 2018; Mulopo, 2017; Simate & Ndlovu, 2014). However; the recent culmination of various factors including the relative decrease in costs associated with membrane applications, the improved understanding of the environmental impacts of AMD pollution, and the more enacted stringent legislation on discharge water quality, have put in the spotlight the apparent advantages of physical technology and/or their complementarity with existing treatment technologies mainly chemical and biological based (Mulopo, 2017). In particular, the uptake of organic as well as inorganic pollutants from acid mine drainage, is a very important application of activated carbons (Mulopo, 2017). It has been reported that around 80% (300,000 tons/year) of the world of activated carbon manufactured around the world is used in liquid phase applications (Bansal & Goyal, 2005).

1.2 Importance of research

Activated carbon is a carbonaceous solid material resistant to high temperatures with a high adsorption capacity defined by the pores volume and the various surface functional groups (Marsh & Reinoso, 2006).

Globally increasing demand for adsorbent materials for environmental processes such as wastewater treatment has motivated additional study in the synthesis of activated carbons. Activated carbon precursors can be derived from a variety of carbon-rich materials, including non-traditional sources such as sewage sludge.

The past two decades has seen an increase in studies pertaining to the synthesis of activated carbon from sewage sludge (Aliakbari et al., 2018; Almahbashi et al., 2020; Devi & Saroha, 2016; dos Reis, Adebayo, et al., 2016; Hadi et al., 2015; Liadi et al., 2020; Xu et al., 2017).

1.3 Scope of research and hypothesis

However, an in-depth examination of the current body of works reveals knowledge gaps i.e. very few studies take into account the specific chemical composition of the source materials used. The synthesis of the activated carbon from sewage sludge has been generally geared towards specific applications and therefore focused on results than on the understanding of the intrinsic mechanism within the materials.

To our knowledge, there are no reports on the oxidation of activated carbon from sewage sludge using ammonium peroxydisulfate.

Therefore, the following assumptions are considered in this project:

- waste coal will impact positively the AC surface area due to its higher carbon content than sludge.
- Pyrolysis will result in formation of porosity, stable metals oxide and elimination volatile compound
- pH point of zero charge will affect protonation or deprotonation of activated carbon surface

1.4 Objectives of the study

The main objective of this project is to synthesize and characterize activated carbon derived from sewage sludge collected from ERWAT facilities in Midrand (South Africa) as a low-cost bio-adsorbent for coal acid mine drainage remediation.

The specific objectives are:

a) to study the effect of different synthesis variables on the structural properties of the activated carbon prepared and attempt to establish how one can get a predefined activated carbon from sewage sludge by changing the parameters used for its synthesis.

b) to characterize activated carbons produced (surface area, porosity, pores (mesoporous volume) versus commercially available activated carbon via SEM, EDS, XRD FT-IR and BET analyses.

c) to study the oxidation of activated carbon.

d) to determine the effectiveness of synthesized activated carbon in nitrate and methyl red remediation via adsorption.

1.5 Research methodology

The chemical structure of the activated carbon surface is transformed during the chemical activation process in order to obtain the optimum porous surface. The surface of the activated carbons is generally filled with oxygenated sites and possibly amine sites if the source material has been chemically treated. Further oxygen complexes are formed when the activated carbon is treated with oxidising agents in the gas phase or in solution. These treatments create 3 types of oxides on the surface namely acidic, basic and neutral. Acidic sites make activated carbon more hydrophilic, lower the pH in aqueous suspension and increase the negative charge density at the surface whereas basic sites are essentially of the Lewis type associated with π-rich regions located at the basal planes. The oxidation process increases the oxygen content by decreasing the electronic density of the basal planes and, consequently, decreases the basicity at the surface (Tascón, 2012). Therefore, the knowledge of the chemical nature of the activated carbon surface is essential to understand the adsorption of certain inorganic compounds in aqueous solution by activated carbon as in the case of metals removals from AMD.

the oxidation of activated carbon is carried out after the activation process. This project will particularly assess the activated carbon oxidation using ammonium peroxydisulfate [$(NH_4)_2S_2O_8$]. In general, the oxidation process is meant to lead to the formation of carboxylic sites, or the transformation of oxygen sites into carboxylic sites. In this project, we chose ammonium peroxydisulfate because its ability to oxidises the surface without modifying drastically the porous structure (Ang et al., 2020; Moreno-Castilla et al., 1995) and enhancing surface acidity by increasing carboxylic group presence (Dai et al., 2017; Moreno-Castilla et al., 2000).

CHAPTER 2: LITERATURE REVIEW

2.1 general Background

Sewage sludge is a solid reject from a wastewater treatment plant that can be classified as primary or secondary sewage sludge based on its origin. The first category is the underflow from settling vessels after inlet physical treatment (sedimentation, flocculation, filtration, etc.) and is primarily inorganic; the secondary, also known as biological sludge, is issued from biological process (activated sludge) (Devi & Saroha, 2016; Smith et al., 2009). On the other hand, due to their recalcitrant and non-biodegradable nature, the presence of dyes in wastewater from coloration processes in diverse industries such as tanning leather, paper, and paints constitutes a concern for the environment. Dye inhalation can cause digestive tract and eye/skin irritation (Khan et al., 2018; Yagub et al., 2014). Table 2.1 summarizes the benefits and drawbacks of dye removal methods.

Table 2.1 benefit and drawback of dye uptake methods (Afroze & Sen, 2018; Yagub et al., 2014)

Methods	Benefit	Drawback
Chemical treatment		
Oxidation	Simple to implement	Higher energy consumption and by product generation
Ozonation	Applied in gaseous phases doesn't expand volume of wastewater or sludge	little half-life (20 min)
Photochemical	No sludge generation and diminution of odors	by product generation
Electrochemical destruction	No chemical utilization and sludge accumulation	High energy consumption, the higher flowrate diminish dye uptake
Biological treatment		
Anaerobic textile–dye bioremediation systems	Azo as well as water-soluble dyes can degraded	Anaerobic decline output methane and hydrogen sulphide

Adsorption by living/dead microbial biomass	Some type of dye have propensity to be linked with microbial organism	Not efficient for all dye
Physical treatment		
Ion exchange	Regeneration: absorbent recovery	Not potent for all dyes
Membrane filtration	Not suitable for all types of dyes	Enriched sludge generation
Activated carbon adsorption	reduction of the volume of biological and/or chemical sludge to be disposed, high efficacy in up-taking diluted impurities,	Cost of activated carbon

Nitrate removal from polluted underground and surface water caused by human activities (agriculture and modernisation) has piqued the interest of researchers in recent decades (Nassar et al., 2020). Due to its higher solubility in water, nitrate can be found in a variety of water bodies, which can negatively impact the flora through eutrophication or, in the case of ingurgitation in the human body, lead to the formation of cancerous compounds (nitrosamine) (Long et al., 2019).

Recently, biological treatment, chemical, and physical removal approaches have been promoted to combat nitrate pollution. Among these technologies, adsorption has been regarded as an eco-friendly process with significant removal efficacy and in particular, carbon-based adsorbent (carbon graphene, activated carbon, carbon nanotube, and biochar) research has surpassed other adsorbent types of research (Long et al., 2019).

Among the various adsorbents used in wastewater treatment, such as zeolite, activated alumina, silica gel, activated carbon (AC) is by far the most commonly used due to its flexibility in removing both inorganic and organic contaminants and its consistency in acidic or basic solutions (Gupta & Garg, 2015; Taenzana, 2011).

However, the major drawback of engineered activated carbon, also known as industrial activated carbon, remains its high cost. In this regard, many studies have been undertaken aiming to promote the synthesis of low cost activated carbon from diverse carbonaceous feedstock such as coconut (Song et al., 2010), waste tea (Gokce

& Aktas, 2014), cow bone (Cechinel & de Souza, 2014), palm kernel shell (Pam et al., 2018), and sewage sludge (Almahbashi et al., 2020; Gupta & Garg, 2015; Li et al., 2019; Liadi et al., 2020).

2.2 Origin and utilization of Activated Carbon

Activated carbon can be made from a variety of carbonaceous solid precursors such as wood, lignocellulosic biomass, peat, lignite, and coals (Bandosz, 2006; Marsh & Reinoso, 2006). However, there are some limitations to the types of carbonaceous solid precursors that can be used to make activated carbon A stabilized solid char made from a thermosetting material, on the other hand, satisfies the requirements for a suitable raw material (Bandosz, 2006). Generally, an activated carbon is carbonaceous material with a non-graphitic structure and its porosity is generated by the presence of a non-parallel units in the lattice (Figure 2.1).

As a versatile compound activated carbon utilization is not restrained to adsorption of pollutants in the gas or liquid phase (Bansal & Goyal, 2005).

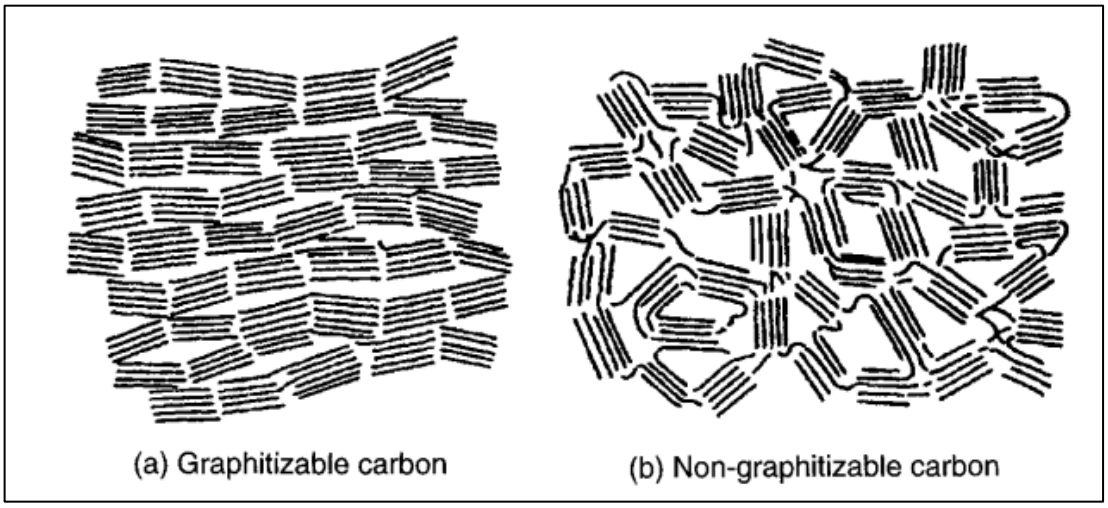


Figure 2.1 Illustration of 2-D plane layer of (a) graphitizable carbon and (b) non-graphitizable carbon (Marsh & Reinoso, 2006)

Wood, coconut shells, fruit stones, coals, lignite, petroleum coke, etc. are all low-priced materials with a high carbon and a low inorganic content, as results, they are suitable candidates to utilize as an activated carbon precursor (Bansal & Goyal, 2005; Marsh & Reinoso, 2006).

The following criteria are used to choose the necessary raw material for the synthesis of activated carbon (Bansal & Goyal, 2005; Marsh & Reinoso, 2006):

a. a high capacity performance, as well as high density and hardness.

b. the least amount of inorganic matter Due to their lack of porosity, their presence decreases adsorption potential, which is related to mass absorbed per unit of adsorbent.

c. Cost and availability: The price of the finished product is affected by the cost of the raw materials; however, the greater the mass loss occurs during the process, the higher the price of the product.

2.3 Preparation of activated carbon

Activated carbon is currently produced either thermally or chemically. (Bandosz, 2006; Bansal & Goyal, 2005; Marsh & Reinoso, 2006)

2.3.1 **Physical**

Physical or thermal activation is a two-step process, starting with carbonization then activation, The first step is carried out under an inert atmosphere at the temperature comprises between 500 ° C and 800° C (Bansal & Goyal, 2005). Carbonization results in the elimination of most of the non-carbon elements such as oxygen, hydrogen, nitrogen sulphur, and generation of a compound constitute of fixed carbon (char) with aromatic sheets structure. The free interstices between sheets (Figure 2.2) may be filled or blocked with the internal carbon mass (or tar) from the decomposition, which confers less porous structure to the carbonized products (Gong, 2013).

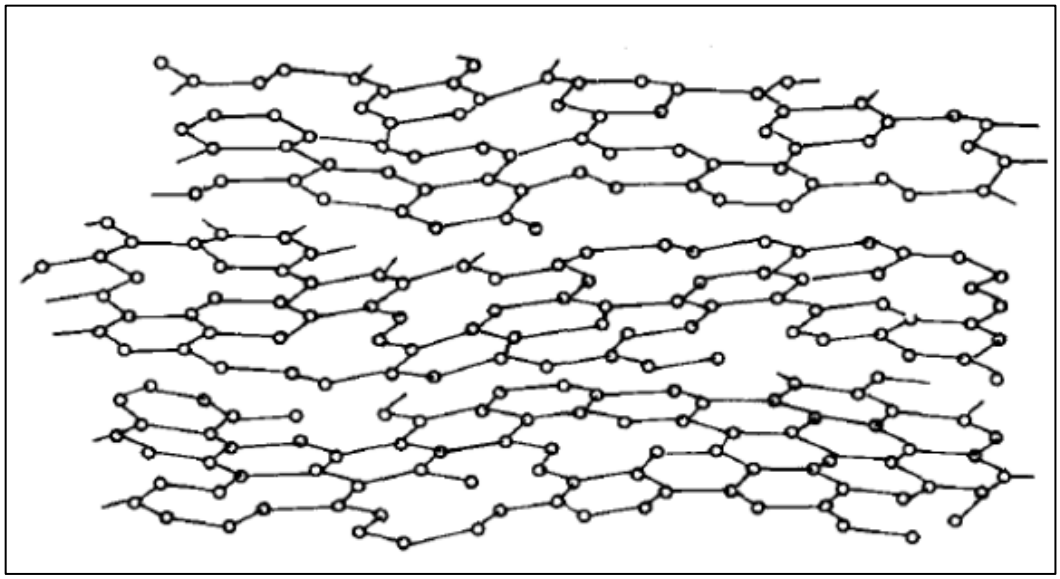


Figure 2.2 illustration of carbonized products with a likewise graphitic structure (Gong, 2013)

The second stage (activation) aims to improve the porosity of carbonized materials for their intended uses by forming new cavities and expanding existing voids, implying surface modification. Carbon atoms can be removed from within porous carbons by gasification using carbon dioxide (equation 2.1) or water vapour (equation 2.2), at temperatures between 800 and 1100 °C (Marsh & Reinoso, 2006).

$$C + CO_2 = 2\,CO \quad (2.1)$$

$$C + H_2O = CO + H_2 \quad (2.2)$$

2.3.2 **Chemical**

Chemical activation is a one-step process in which pyrolysis and activation occur simultaneously, and the carbonaceous precursor is physically mixed (dried) or impregnated with a dehydrating activating agent, such as potassium hydroxide, phosphoric acid or zinc chloride, and then heated under an inert atmosphere at a temperature comprises between at 400 ° C and 800 ° C (Hadi et al., 2015).

2.3.3 **Advantages and disadvantages of chemical or physical activations**

The choice of a given activation technique is influenced by its disadvantages and advantages, which are summarized in Table 2.2 below.

Table 2.2 Advantages and disadvantage of activation routes (Hadi et al., 2015)

Activation Procedure	Advantages	Disadvantages
Chemical	High surface area Lower temperature activation Shorter period time	Post-treatment required: acid washing, Corrosiveness of the process Introduction of inorganic compound from the activating agent
Physical	Non-Corrosive No washed or post-treatment required	High temperature (800 ° C 1100 ° C) Low surface area Longer period of activation: 2 steps

A part from the drawbacks of the physical activation method mentioned in table 2.2, one of them is the equipment limitations caused by CO_2 injection (Gong, 2013).

2.4 Properties

2.4.1 **Pore Surface structure**

Pore size distribution

Pore size distribution (PSD) is a key feature of adsorbents that specifies the amount of total pore volume accessible to various types of compounds (molecules, atoms, etc.) based on their size and shape. Micropores (less than 2 nm), mesopores (2–50 nm), and macropores (greater than 50 nm) are the 3 types of pores classified by the International Union of Physical and Applied Chemistry (IUPAC) Pores can be either regular or irregular in shape (see Figure 2.3).

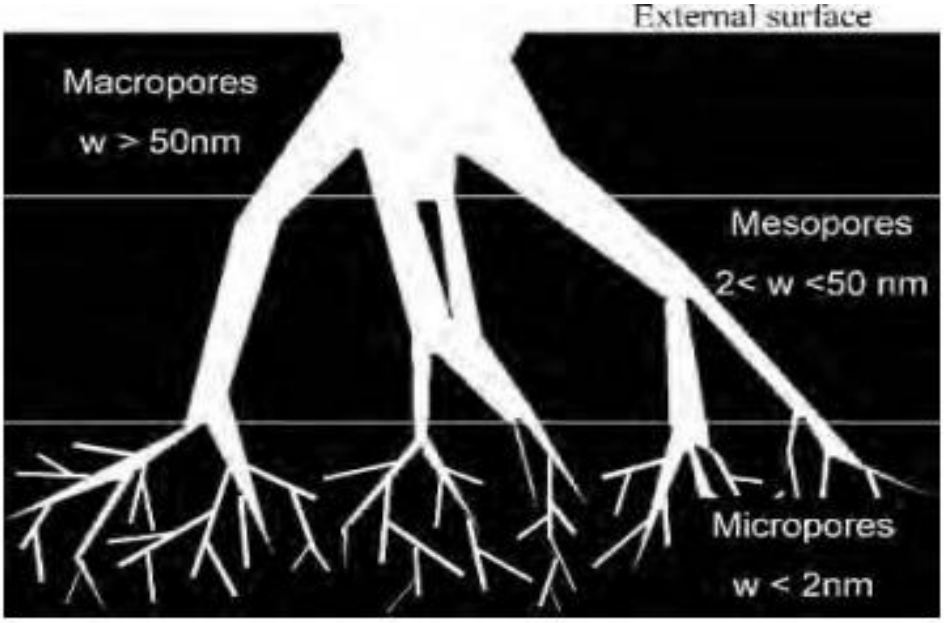


Figure 2.3 Types of porosity in activated carbon (Bandosz, 2006)

Since organic molecules vary in size, attention should be paid to porous structure, especially the presence of mesopores in the case of non-polar compound adsorption, since large molecules may have limited access to micropore volume (Bansal & Goyal, 2005).

Surface area

Surface area is a convenient mean to gauge adsorption capacity on the atomic scale and in this regard, the Brauner-Emmett-Teller (BET) method is the most conventional method to evaluate surface area (Tascón, 2012). In this technique, the surface area is determined by the amount of N_2 adsorbed and desorbed at 77 K under a range of relative pressure (p/p_0), the isotherm generated data on the types of size (micro, meso and macropore) based on adsorption model and the total area will be filled with nitrogen (Marsh & Reinoso, 2006).

$$\boldsymbol{S}_{\mathrm{BET}} = \frac{V_m N_a \sigma_x}{V} \quad (2.3)$$

where V_m is the volume of gas for an adsorbed monolayer, V is the molar volume of the

adsorbed gas, N_a is the Avogadro number and σ_x is the area covered by one nitrogen molecules

The BET theory is based on the followed assumptions: i) The adsorbent's surface is identical, resulting in no difference in the heat of the first adsorption monolayer. (ii) There are no interactions between adsorbed particles because the iterative process produces a new adsorption surface for the next compound (iii) the heat of adsorption of all monolayers except the first equal to the heat of condensation (Taenzana, 2011; Tascón, 2012). Equations (2.3 and 2.4) are based on the above-mentioned assumptions:

$$\frac{p/p_0}{n_a\left[1-\left(p/p_0\right)\right]} = \frac{1}{n_m C} + \frac{C-1}{n_m C} \cdot \frac{p}{p_0} \quad (2.4).$$

where n_a is the adsorbed amount and C is an empirical constant that gives an indication of the attractive adsorbent-adsorbate interactions. Emmett and Teller originally found that various adsorbents gave linear BET plots over the relative pressure range P/P_0= 0.05–0.3. Adsorbents can be classifieds according to their isotherm shape (Figure 2.4). The type I isotherm is a characteristic of exclusive microporous adsorbent whose curve attain maximum adsorption without inflection. Type II showed an inflection in the area $p/p_0 > 0{,}01$ and $p/p_0 > 0{,}9$ implying that the adsorbent is microporous with an open surface. The type IV isotherm curve parallels that of type III, with the exception that adsorption occurs in mesopores rather than open surfaces; the presence of hysteresis is due to the disparity between capillary condensation filling and evacuating in mesopores; in this case, the adsorbent is known as mesopore; and finally, type VI is for surfaces with an excessive homogeneous structure with ultramicroscopic adsorption. (Marsh & Reinoso, 2006).

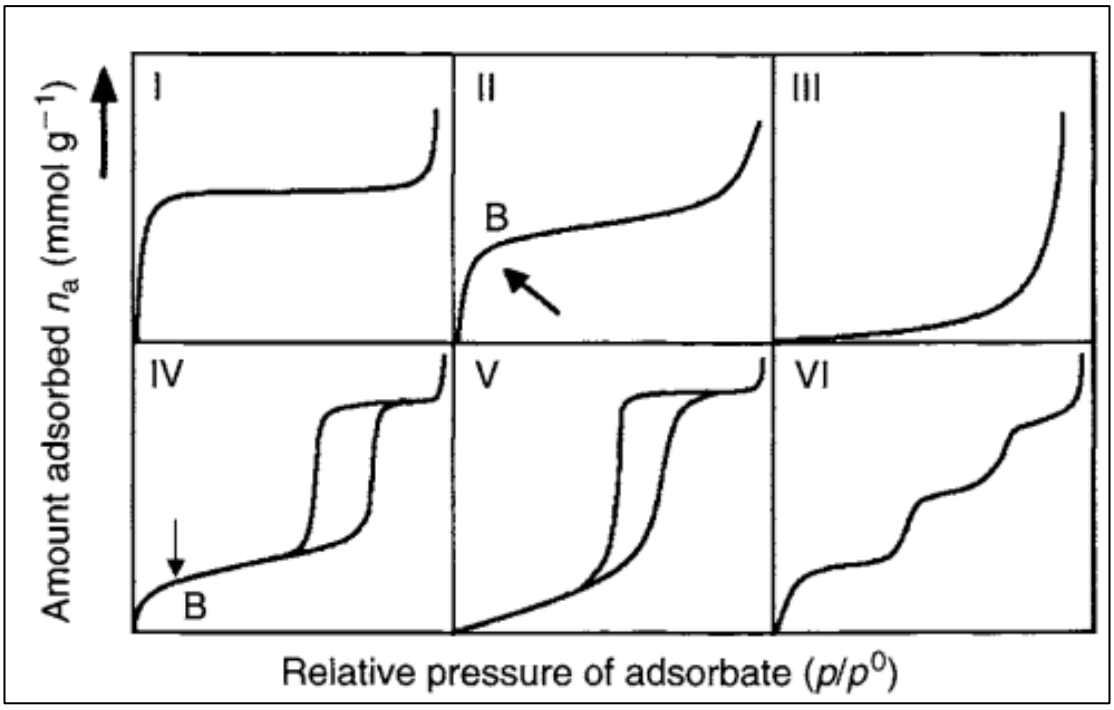


Figure 2.4 types of isotherm shape with Nitrogen adsorption/desorption (Marsh & Reinoso, 2006)

Pore volume

The micropore volume of activated carbon ranges from 0.15 to 0.50 cm^3/g, and is responsible for at least 95 percent of sorption ability; mesopore volume is less than 0.10 cm^3/g, and their contribution to adsorption capacity is less than 5%; macropore volume ranges from 0.2 to 0.5 cm^3/g, and their surface area is marginal (less than 2 m^2/g); therefore, the widest pores constitute a transit wand (Tascón, 2012). While their high surface (> 1000 m^2/g) allows for rapid adsorption, the mere pore volume (0.6 m^3/g) limits the retention of the adsorbed compound in activated carbon for gas-adsorbing applications (Perrich, 2018).

Iodine number

Iodine number expresses the capacity of 1 g activated carbon to absorb milligrams of iodine with an iodine concentration of 0.02N in the residual filtrate. Since iodine, it is adsorbed in the pores, therefore, it is also a quantification of pore volume (Perrich, 2018).

2.4.2 **Surface properties**

The chemical composition of the functional groups is closely related to the physicochemical properties of carbon materials, and this knowledge becomes crucial in providing a more precise and coherent image of the surface and predicting the

applications of carbon materials (Bandosz, 2006). The sorbates (molecules or atoms) are stuck on the carbon (sorbent) surface by physical interactions (electrostatic and dispersive forces) and/or chemical bonds (Bandosz, 2006); except for adsorption of gases and vapours, which is exclusively physical and does not include participation or creation of chemical bonds (Marsh & Reinoso, 2006), a relatively large specific surfactant is needed for adsorption of gases and vapours (Bandosz, 2006). The wettability, polarity, and acidity/basicity properties of activated carbon are conferred by the chemical structure of the compound present at the surface (Bansal & Goyal, 2005; Marsh & Reinoso, 2006; Tascón, 2012). While genuine carbon is hydrophobic and non-polar, these properties are regarded as a benefit to avoid water adsorption, which reduces the pore volume designed to host adsorbed impurities, the presence of surface groups drives activated carbon hydrophilic and polar, increasing the ion exchange capacity and making the adsorbent more efficient for metal uptake in industrial and domestic wastewaters (Bansal & Goyal, 2005; Tascón, 2012). The presence of acid, base, and neutral functional groups on the surface of activated carbon makes it amphoteric; acidic surface groups are produced when carbon is treated with oxygen at temperatures below 400°C or in liquid phase with an oxidant at ambient temperature. When the temperature is between 350 and 750°C, these surface groups are thermally less stable and dissociate to produce CO_2 during heat treatment in a vacuum or an inert atmosphere. Carboxylic, lactone, and phenolic groups are thought to be present on the carbon surface, making it hydrophilic and polar (Bansal & Goyal, 2005).

Surfaces functionalities

The surface of activated carbons consists of hydrophobic graphene layers and hydrophilic functional groups. Organic compounds adsorb on hydrophobic surfaces, while polar species adsorb on hydrophilic surfaces. (Song et al., 2010).

Oxygen functional groups are the most important among other groups: sulphur, phosphorous, halogens and nitrogen-containing functional groups, the latter one is the second in terms of research after the major groups (Tascón, 2012).

a. *Oxygen functionalities*

Oxygen is the most abundant element of heteroatoms, and it is the second most abundant on the surface after carbon(Tascón, 2012).Heteroatoms such as carboxyl, lactones, phenol, and lactol are assumed to be responsible for acidity and Chromene, Ketones, and pyrones of basicity as shown in Figure 2.5 (Shafeeyan et al., 2010).

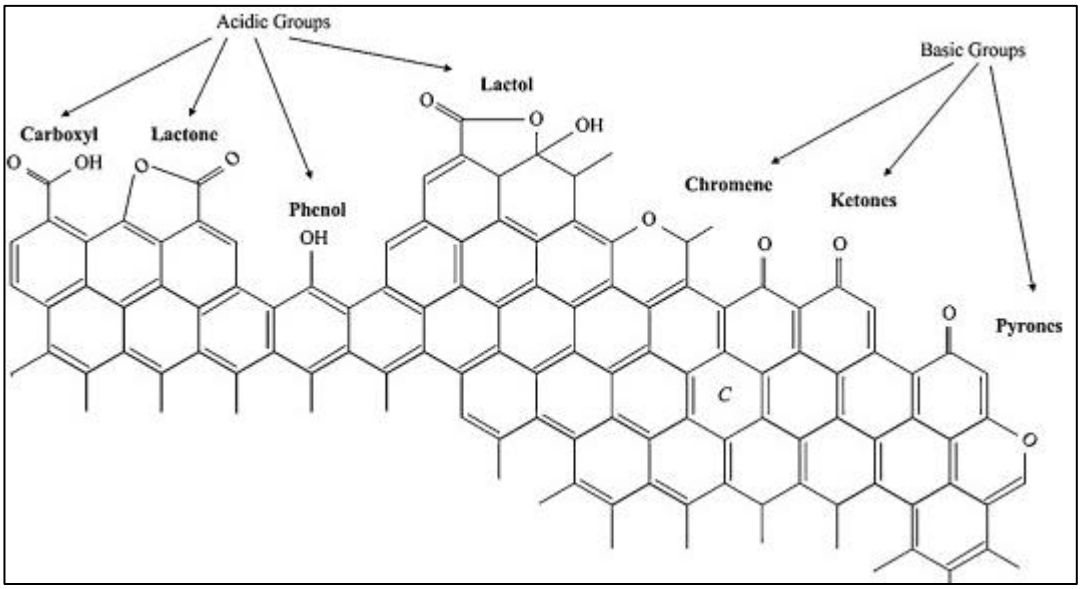


Figure 2.5 structure and classification of oxygen functionalities of carbon surface (Shafeeyan et al., 2010)

b. *Nitrogen containing functional groups*

The presence of nitrogen heteroatoms is negligible in nature; however, they can be introduced by reactions with nitrogen compounds (ammonia, urea, melamine, HCN) or from nitrogen raw materials (carbazole, nitrogen-enriched polymer, acridine). Nitrogen atoms in the carbon structure increase surface polarity, whether negatively (pyridinic group) or positively (replacement C atoms by N in the graphitic layer) (Tascón, 2012). At low temperatures, the adsorbent is merely acidic and likely basic; at higher temperatures, replacement of carbon atoms by nitrogen atoms occurs, and pyrrolic and pyridine compounds induce basicity, the degree of basicity or basicity depends on the variety of heteroatoms (Figure 2.6). (Bandosz, 2006; Tascón, 2012).

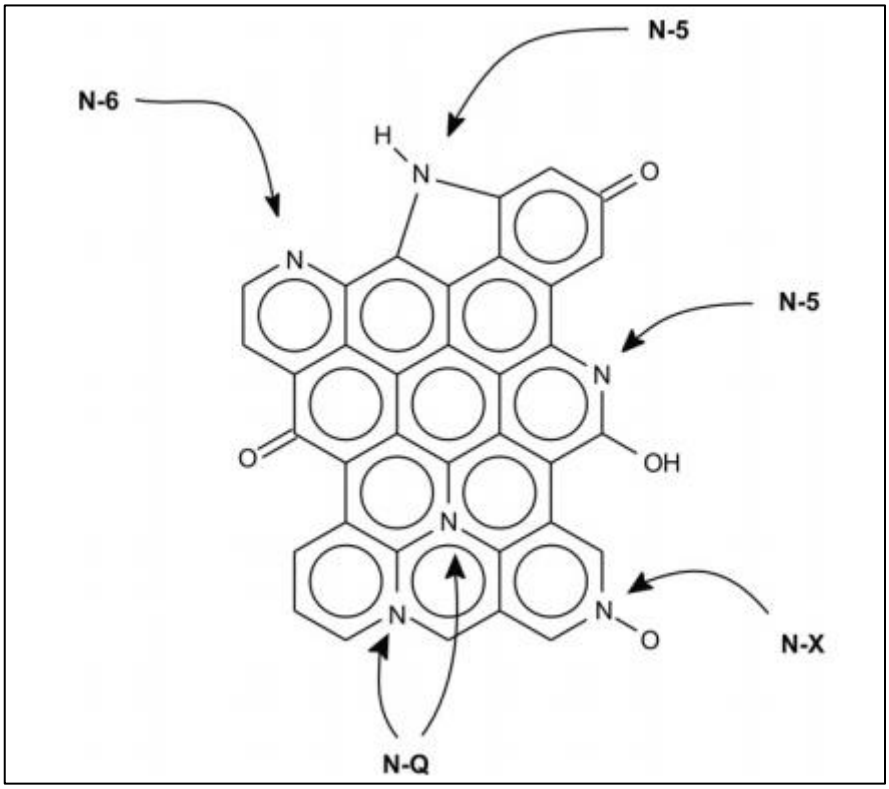


Figure 2.6 Nitrogen containing functional groups in activated carbon. N-6: pyridinic N, N-5:pyrrolic/pyridine, N-Q: quaternary and N-X: N-oxides (Tascón, 2012)

Characterization of surface chemistry

The following techniques can be used to determine the surface composition and concentration: temperature-programmed desorption (TPD), acid/base titration, potentiometric, and FT-IR (Tascón, 2012) , and X-ray spectroscopy can be used to determine the crystallographic structure (Bansal & Goyal, 2005). When it comes to knowledge about quantity and consistency, certain methods are thought to be complementary. Temperature Programmed Desorption (TPD), for example, reliably reveals more oxygen-containing groups than Boehm titration, but quantitative data is less reliable (Bandosz, 2006). Since infrared radiation interacts differently with bonds of different compounds (Marsh & Reinoso, 2006; Smith, 1998), FT-IR peak wavenumbers (cm^{-1}) are related to compound functional groups studied. FT-IR technique allows the determination of surface functional groups at lower concentrations(Bansal & Goyal, 2005).

Since bending vibrations occur in the molecules and the fingerprint region is special for each compound, it is not possible to relate wavenumber to a specific compound in the 1500 cm^{-1} to 500 cm^{-1} range, also known as the fingerprint region (Smith, 1998) .

The less the functional group is present for a given wavelength peak, the closer the transmittance is to 100% (Mmonatau, 2018). Acid/base titration can be used to assess surface acidity (Boehm, 2002), and despite its inability to differentiate other surface functional groups (sulphur, nitrogen, phosphorus) from oxygen functional groups (carboxylic acids, lactones, or phenol) (Tsechansky & Graber, 2014), the Boehm method remains the most commonly used titration technique due to its reliability, simplicity, speed, and reproducibility . The basic assumption of the Boehm method is that the surface functionalities are neutralized according to their acid intensity, with a base with a defined pKa neutralizing the targeted functional group with a lower pKa (Boehm, 2002; Tsechansky & Graber, 2014). In Boehm techniques, 3 bases are used for titration. First, $NaHCO_3$ (pKa 6.37) neutralizes strongly acidic groups (carboxylic); second, the supplement group neutralized by Na_2CO_3 (pKa 10.25) is assumed to be lactones; and finally, the feeble group neutralized by NaOH (pKa 15.74) but not by $NaHCO_3$ or Na_2CO_3 is assumed to be phenols (Bhadra et al., 2016; Dai et al., 2017).

Point of zero charge

The point of zero charge (PZC), which is defined as the pH where adsorption does not occur due to the neutrality of the adsorbent surface, is one of the most important properties of activated carbons. As shown in Figure 2.7, the charge of positive surface sites is equal to that of negative ones at the PZC point. When the pH of the solution is higher than the pH of the PZC point, acidic functionalities split and free protons into the medium, causing the carbon surface to become negatively charged, which favours cation sorption. When the pH is lower than the pH of the PZC point, anions are adsorbed more favourably because basic sites combine with protons from the medium, causing the surface to become positively charged, which favours anions sorption (Bandosz, 2006). Activated carbons are typically divided into 2 categories depending on the basicity or acidity of the pHpzc: basic (H) and acidic (L) (acidic), The first group has a low density of oxygen-containing functional groups with simple pHpzc values; they are hydrophobic and adsorb heavy acids, while the second group has a

higher density of oxygen-containing functional groups with acidic pHpzc values; they are hydrophilic and adsorb bases (Bandosz, 2006).

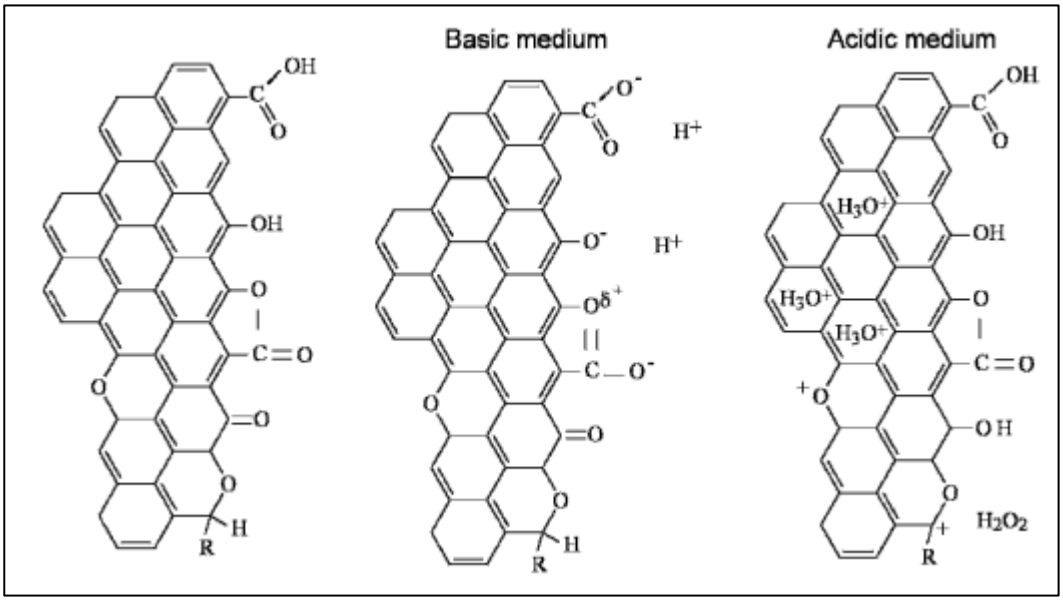


Figure 2.7 Behaviour of functional groups related to point of zero charge and the pH of the medium (Bandosz, 2006)

Besides the properties related to adsorption of anions or cations, the point of zero charge can be regarded as a mean to gauge oxidation of the surface of carbons, since it shows variation in surface acidity /basicity before and after modification process (Bandosz, 2006), for instance, $ZnCl_2$ activation and HCl washing are known to produce acidic Activated carbon and HNO_3 modification renders the surface even more acidic by introducing oxygen-containing functional groups (Smith et al., 2009).

2.5 Surface modifications

The introduction of heteroatoms into the carbon skeleton renders the carbon surface more attractive to polar molecules, although heat treatment in presence of oxidant gas/vapour (dry oxidation) increases oxygen surface groups, heat treatment at an elevated temperature and under inert atmosphere leads to opposite expectations (Daud & Houshamnd, 2010). Rivera-Utrilla, et al., (2011) classified the modifications technique into 4 categories namely oxidation, sulfuration, ammonification, and coordinated ligand anchorage. Despite its main shortcoming is the surface area reduction during the process, oxidation remains the most popular due to its simplicity

especially wet oxidation (Bhatnagar et al., 2013; Daud & Houshamnd, 2010; Tascón, 2012).

Oxidation is mainly used to introduce oxygen-containing functional groups on the surface of AC (Daud & Houshamnd, 2010), Generally, it is achieved in gas phase (air, oxygen, ozone) or aqueous phase (H_2O_2, HNO_3, H_2SO_4, $(NH_4)_2S_2O_8$, etc.) (Rivera-Utrilla et al., 2011; Shafeeyan et al., 2010; Tascón, 2012). Because of the enhancement of oxygen functionalities, oxidation with HNO_3 is more efficient when temperatures are close to 100 °C, which is a disadvantage when compared to oxidant reagents used at close or room temperature, such as H_2O_2 (Rivera-Utrilla et al., 2011) or $(NH_4)_2S_2O_8$ (Han et al., 2015). The effect of oxidation on the structure of activated carbon has been a topic of debate among researchers. On the one hand, as noted, wet oxidation is thought to change the textural structure of activated carbon, especially its surface area: Moreno-Castilla et al.(2000) found that oxidation for 48 hours with $(NH_4)_2S_2O_8$ (saturated solution in 1M H_2SO_4) and H_2O_2 (9.8 M) impedes the structure of the unmodified material lightly compared to HNO_3 (13.9 M). The S_{BET} varied from 1290 m^2/g for the unmodified material to 1200 m^2/g when treated with H_2O_2, 1090 m^2/g with $(NH_4)_2S_2O_3$ and 789 m^2/g for HNO_3. Alvarez-Merino et al. (2005) used the same technique as (Moreno-Castilla et al., 1997) to adjust granular activated carbon and found that the S_{BET} decreased significantly from 1150 $m^2.g^{-1}$ before modification to 1050 $m^2.g^{-1}$ after modification. Han et al. (2015) investigated the effect of oxidation time and Ammonium persulfate (APS) concentration in mild conditions on the structure of activated carbon with an S_{BET} of 2323 m^2/g. The S_{BET} reduction was 31 percent and 39 percent for 0.75 h and 1.5 h, respectively, and reached 61 percent for 6 h. Li et al. (2011) investigated the effect of temperature, APS concentration, and impregnation time on the structure of an activated carbon with an SBET of 2311 m^2/g, modified with 2.0 mol/L APS in 1M H_2SO_4, treated at 60 °C for 24 hours, the SBET sharply decreased to 469 m^2/g, whereas for a shorter period of time (3 hours), it was 1438 m^2/g. The effect of oxidant concentration on the surface area was demonstrated by Tamai et al. (2006). High oxidative conditions led to a sharp decrease in surface area from 2190 m^2/g with a ratio of 1 to 1370 m^2/g with a ratio of 3, in the first method, from an S_{BET} of 2600 m^2/g after adjustment for 0.5h at room temperature with (HNO_3/ H_2SO_4) or (cetylamine/ethanol) solutions, in the second method, the surface area decrease was associated to the cetylamine solution concentration augmentation. Daud

& Houshamnd (2010) on the other hand, have mentioned antipode results predicted from wet oxidation, such as the augmentation of the surface area of modified products. Domingo-Garcia et al. (2000) used APS and HNO_3 to modify an activated carbon with an initial S_{BET} of 1026 m^2/g; the S_{BET} of the product was 1129 m^2/g and 1196 m^2/g, respectively. Aburub & Wurster (2006) registered a light growth of S_{BET} from 1311 m^2/g to1372 m^2/g after 2 hours of treatment with an equimolar solution (H_2SO_4 / HNO_3) Changes in the surface area have been due to the transformation of micropore to mesopore or surface etching in the case of increased surface area, or the collapsing of micropore walls to become thinner or the dismantlement of porosity in the case of reduced surface area (Daud & Houshamnd, 2010; Moreno-Castilla et al., 2000; Tamai et al., 2006). The value of mastering the extremes of wet oxidation by controlling and overseeing oxidant concentration, oxidation time, and oxidation temperature was demonstrated by the increase or decrease in surface area. It is recommended to consider all parameters, for example, oxidation carried out with a lower concentrated oxidant for a long period of time may result in severe oxidation. This means that gravity is calculated by more than just focus. Surface functionalities and textural properties differed depending on oxidation conditions; however, extreme oxidation does not result in complete functionalization of the activated carbon surface (Daud & Houshamnd, 2010) . When exposed to extreme oxidation conditions, the surface area decreases significantly, from 1380 m^2/g to 6.5 m^2/g after 10 days at 20 °C and 5.5 m^2/g after 4 days at 30 °C (Machida et al., 2015). Wet oxidation is more likely to provide more functional groups on activated carbon with more advanced textures (meso and macroporosity, and increased microvolumes) and larger surface area (Daud & Houshamnd, 2010). In terms of functional groups produced by wet oxidation, carboxylic, phenolics, lactones, and carbonyl groups are generally more important after oxidation than before, depending on the types of oxidant used, carboxylic: $(NH_4)_2S_2O_3 > HNO_3 > H_2O_2$, phenol: $H_2O_2 > HNO_3 > (NH_4)_2S_2O_3$, lactones: $HNO_3 > H_2O_2 > (NH_4)_2S_2O_3$, overall acidity: $HNO_3 > (NH_4)_2S_2O_3 > H_2O_2$.(Daud & Houshamnd, 2010) . As outlined in Table 2.3, numerous peer-reviewed journal articles have highlighted the benefits of the modification, which increases impurities absorption of oxidised activated carbon in liquid phases adsorption for both inorganic (Dai et al., 2017; Machida et al., 2015; Pam et al., 2018; Song et al., 2010; Yao et al., 2016) and organic compounds (Bhadra et al., 2016; Gokce & Aktas, 2014; Han et al., 2015; Shaarani & Hameed, 2011). Song, et al. (2010) found that the activated carbon

from coconut had a 2.5-fold lower Pb^{2+} adsorption capacity than the modified. Similarly, Yao, et al. (2016) found that the surface dwindled after modification (375,96 m^2/g) compared to 1719,32 m^2/g for the unmodified, with a Pb^{2+} adsorption capacity of 60,5 mg/g, less than one-half of the modified (93.5 mg/g).Despite the increase in the functional group, the decrease in surface area and pores collapsing hinder adsorption capability, so surface modification is not always beneficial when carried out in severe conditions. Modified and unmodified activated carbon had comparable adsorption capacities, according to Machida et al. (2015).

Table 2.3 Publications on adsorption with modified activated carbon

References	Activated Carbon State	Modification Conditions			S_{BET} (m^2/g)	pH_{PZC}	Adsorption
		Oxidant Concentration	Soaking time	temperature			
(Song et al., 2010)	Untreated	-	-	-	1245	10,1	Pb^{2+}: 4,446 mg/g
	Modified	10 M H_2O_2	24h	363 K	1062	4,1	Pb^{2+}: 11,501 mg/g
		10 M HNO_3	4h	363 K	1053	3,1	Pb^{2+}: 12,533mg/g
(Shaarani & Hameed, 2011)	Untreated	-	-	-	-	-	2,4-DC[1] :232.56 mg/g
	Modified	10 wt % ammonia solution	48h	Room temperature	-	-	2,4-DC: 285.71 mg/g
(Gokce & Aktas, 2014)	Untreated	-	-	-	1417	-	MB[2]: 428,6 mg/g
	Modified	HNO_3 20% (v/v)	Till no gas produced	90 °C	644	-	MB: 587.6 mg/g
		HNO_3 40% (v/v)		90 °C	524	-	MB: 683 mg/g
		HNO_3 80% (v/v)		90 °C	49	-	MB: 480.4 mg/g
(Machida et al., 2015)	Untreated	-	-	-	1380	-	Pb^{2+}: 2,2 mmol/g

	Modified	2M APS in 1M H_2SO_4	10 days	20 °C	6.5	-	Pb^{2+}:2,2 mmol/g
		2M APS in 1M H_2SO_4	4 days	30 °C	5.5	-	Pb^{2+}:2,2 mmol/g
(Han et al., 2015)	Untreated	-	-	-	2323	-	N-LCO[3]:0.4 mmol/g
	Modified	APS 15wt. % in 1M H_2SO_4	1.5 h	Mild	1829	-	N-LCO:0.47 mmol/g
		APS saturated in 1M H_2SO_4	6 h	Mild	897	-	N-LCO: 0.22 mmol/g
(Yao et al., 2016)	Untreated	-	-	-	1719,32	-	Pb^{2+}: 60,5 mg/g
	Modified	HNO_3 8 M	15 min	130 °C	375,96	-	Pb^{2+}: 93,5 mg/g
(Bhadra et al., 2016)	Untreated	-	-	-	-	-	D-Na[4]: 60 mg/g
	Modified	1M APS in 1M H_2SO_4	3h	60 °C	-	-	D-Na: 250 mg/g
		2M APS in 1M H_2SO_4	3h	60 °C	-	-	D-Na: 320 mg/g
(Dai et al., 2017)	Untreated	-	-	-	861	10,70	Cu^{2+}: 3,66 mg/g Zn^{2+}: 3,07 mg/g
	Modified	2M APS in 1M H_2SO_4	2 days	Room temperature	564	2,70	Cu^{2+}: 27, 47 mg/g Zn^{2+}: 22,52 mg/g
(Feng et al., 2018)	Untreated	-	-	-	1519,53	-	Cd^{2+}: 116,96 mg/g
	Modified	$KMnO_4$ 0,15M	90 min	Boiling	774,13	-	Cd^{2+}: 217,00 mg/g
(Pam et al., 2018)	Untreated	-	-	-	1559,9	4	Pb^{2+}: 80,6 mg/g

	Modified	EDTA[5]	2h	60 °C	1100,07	3,9	Pb^{2+}: 104 mg/g

Dichlorophenol[1], Methylene Blue[2], Nitrogen light cycled oil[3], Diclofenac Sodium[4], EDTA: ethylenediaminetetraacetic acid[5]

The choice of $(NH_4)_2S_2O_8$ as an oxidant for this project over other common ones (HNO_3, H_2O_2, H_2SO_4) was influenced by a minor change in the surface area of activated carbon during oxidation as also stated by (Ang et al., 2020; Moreno-Castilla et al., 2000).

2.6 Adsorption on carbon based adsorbent

Adsorption is typically characterized as the enhancement of chemical species from a fluid phase on the surface of a liquid or solid, or as a mass transfer of a compound (adsorbate) from a liquid or gas phase onto a solid interface (adsorbent), to which contaminants are attached through physical and/or chemical interactions (Worch, 2012). According to the importance of the adsorption enthalpy, adsorption is classified as physical (physisorption) or chemical (chemisorption). In the first category, adsorption is promoted by Van der Waals forces (induction forces, dispersion forces, dipole-dipole interactions), which are relatively simple interactions. The adsorption enthalpy, in this case, is usually less than 50 kJ/mol, while in the last category, adsorption occurs as a result of chemical reactions between the adsorbate and the surfaces sites with the formation of chemical bonds, and the values of reaction enthalpies exceed 50 kJ/mol (Worch, 2012). Furthermore, physical adsorption is characterized by a decrease in free energy and entropy (De Gisi et al., 2016). Physical and chemical factors influence adsorbate activated carbon interaction. The amount of activated carbon surface area available for adsorption is determined by physical factors, which are correlated to adsorbate molecular dimensions and relative size distributions of carbon pores. Since the majority of activated carbon surface area is made up of fine carbon pores, the easier it is to access surface area, the greater the amount of surface area available (Bandosz, 2006).

Adsorption is divided into 3 stages, which are (Worch, 2012):

i. Mass transfer: adsorptive molecules migrate to the outside of adsorbent granules;

ii. Intraparticle diffusion: molecules move through adsorbent pores;

iii. Physical and/or chemical adsorption.

Adsorption potential is influenced by physical and chemical properties of both the adsorbent and the adsorbate, such as the concentration of the adsorbate in the fluid, the composition of the adsorbate (inorganic or organic, polar or non-polar), experimental conditions such as solution pH (acidity or basicity), temperature, and the amount of time the adsorbate is in contact with the adsorbent (Marsh & Reinoso, 2006).

2.6.1 **Factors affecting batch adsorption**

Effect of contact time

The contact time of an adsorbent-adsorbate system is the expected agitation time for the process to reach equilibrium. Adsorption can be depicted as a series of stages that include mass transfer from the liquid/gas phase to the adsorbent surface through the boundary layer, diffusion within the pores, and sorption on the surface (Hadi et al., 2015). Due to adsorbate migration within the pores of the particles inward to their internal surfaces and further surface diffusion toward deeper internal pores, mesoporous activated reached equilibrium faster than microporous activated (Hadi et al., 2015; Smith et al., 2009).

Effect of initial pollutants concentration

The initial dye concentration has a strong effect on the amount of adsorption for dye absorption, which is related to the relationship between the pollutant concentration and the site accessible on the adsorbent surface. In general, an increase in the initial dye concentration has a negative impact on the percentage of dye removal due to the unavailability (saturation) of adsorption sites on the sorbent surface, while an increase in the initial dye concentration has a positive impact on the adsorbent's adsorption capacity. This may be because the higher initial dye concentration induces a higher driving force for mass transfer (Yagub et al., 2014). Jung et al.(2019) increased the adsorption potential of SBAC by adjusting the initial concentration of acid orange from 10 mg/l to 2000 mg/l. The highest initial concentration (2000 mg/l) resulted in 1017 mg/g. Liadi et al. (2018) investigated the adsorption of methyl tert-butyl ether (MBTE) with SBAC. Due to saturation of the binding site, adsorbent efficiency decreased as the concentration of solute increased; the highest removal percentage was 51 percent

with an initial MBTE concentration of 0,5 ppm and 17 percent with an MBTE concentration of 20 ppm.

Effect of adsorbent dosages

The increase in pollutants removal with the inclusion of adsorbent in the solution is due to the enhancement of adsorption sites as well as surface functionalities, but when the optimal dose is exceeded, the percentage of pollutants removed does not improve significantly because pollutants deficiency in the solution induces an unsaturation binding situation at adsorption sites (Zhang et al., 2015) or particle aggregate (Devi & Saroha, 2016) . Nitrate batch adsorption was processed with an initial concentration of 40 mg/l and an adsorbent dosage from 1 to 10g/l, the percentage removal increased from 25% to 83 percent, while the adsorption capacity downward from 11 to 3,3 mg/g, beyond 4g/l dosage. There was little difference in the adsorption process (Mazarji et al., 2017); Zhang, et al., (2015) found a similar pattern using an SBAC for Malachite green adsorption with SBAC doses ranging from 3 mg to 18 mg in a volume of 40 ml; they noted that when the dose adsorbent was increased to 12 mg, the percentage of impurities removed increased slightly. The optimum dose of adsorbent should not be exceeded when weighing the efficiency and viability of the operation.

The effect of pH

The pH of the solution is one of the most important factors to consider when determining the surface charge of the adsorbent and the degree of ionization of the mentioned contaminants in the solution. The adsorption mechanism is dependent on the competition between H^+ and OH^- ions as well as the adsorbate. Adsorption of anions is more efficient and occurs at lower pH due to the presence of H^+ ions, while adsorption of cations is preferred at higher pH due to the surplus OH^- ions (Gupta & Garg, 2015; Liadi et al., 2018). The surface chemistry of carbons is closely related to their heteroatom content; dissociation of acidic groups results in a negative surface charge, while the positive charge is more likely due to the presence of electron-rich regions inside graphene layers acting as Lewis basic centres with an affinity for protons from the aqueous solution (Tascón, 2012). The surface charges are influenced by the pH of the solution and electrostatic interactions; the more hydrophobic the surface, the greater the hydrophobic interaction with hydrophobic solutes due to uptake augmentation and evading the preferential bonding of water molecules by H-bonds,

which reduces the carbon surface's adsorption ability (Worch, 2012) . With acidic oxidation, the concentration of acidic oxygen groups on the sorbent surface increases, causing polarity to increase while pH_{pzc} decreases. Furthermore, acidic oxygen functional groups may serve as an ion exchange centre, maintaining metallic compounds while releasing protons into aqueous solution, facilitating the presence of metal-ligand surface complexes (Rivera-Utrilla et al., 2011). The charge of the adsorbent's surface is connected to the pH above or below the point of zero charge (section 2.4.2), which may provide additional information about the adsorbent's efficiency in the determined conditions and the existence of the targeted anionic or cationic contaminants in terms of adsorbent-adsorbate interaction and functional group dissociation (Tascón, 2012). Adsorption of organic compounds (polar and non-polar) dissolved in aqueous solution is more closely linked to electrostatic and dispersive interactions, and in the case of polar molecules, the hydrogen bond also plays a role (Bansal & Goyal, 2005) . The adsorption of nitrate with activated carbon changed with NaOH and CTAB (cethyl trimethyl ammonium bromide:$C_{13}H_{42}NBr$) as a cationic surfactant was not affected by pH variation because at pH = 2 mild diminution of nitrate uptake was due to competition with Cl^- ions, and at higher pH, the adsorbent was negatively charged which negatively impacted nitrate due to electrostatic repulsion (Mazarji et al., 2017).

Methyl red removal was dependent on adsorbent pHpzc; at 2< pH< 5,1 (methyl red pKa = 5.1), there was an increase in methyl red (MR) removal due to deprotonation of the adsorbent surface, which induced electrostatic attraction between the surface and the positive dye in the considered range (Khan et al., 2018) ; similarly, methylene blue adsorption was higher in acidic to neutral conditions (2<pH<6) and declined significantly with pH augmentation (Gokce & Aktas, 2014). Adsorption of the negative dye AO7 (acid orange 7: C_{16} H_{11} N_2 NaO_4S) was also affected by pH change; when the solution pH increased from 3.0 to 7.0, the adsorption decreased from 70,86 to 39,55 mg/g. The trend was attributed to the electrostatic repulsion force between the split dye molecules (pKa_1 : 11.4, pKa_2 : 1.0) and the deprotonated adsorbent surface (Jung et al., 2019).

Effect of temperature

Temperature is an important factor in the adsorption process because it can increase or decrease adsorption capability. As the viscosity of the solution decreases with temperature, the rate of diffusion of the adsorbate molecules through the external boundary layer and the internal pores of the adsorbent increases (Hadi et al., 2015). The value of free energy (G), entropy (S), and enthalpy () as described by the equation below are used to measure the effect of temperature:

$K_c = \frac{C_0 - C_e}{C_e}$ (2.5)

$\Delta G = -RTlnK_c$ (2.6)

$\Delta G = \Delta H - \Delta TS$ (2.7)

where R is the molar gas constant, 8.314 J/(mol.K) and T is the solution temperature (K)

ΔG is Gibbs free energy, which negative value implies a simultaneity and feasibility of the adsorption process, the nature of the adsorption process physical or chemical can be assessed by the amplitude of ΔH (Gupta & Garg, 2015). In the review pertaining to dyes removal from aqueous solution by adsorption, Yagub et al., (2014) ascribed endothermic process to impurities mobility as well as adsorption active site augmentation with the amount of adsorption as temperature increase while in exothermic process temperature rise influences negatively the amount of adsorption due to lowering adsorptive force between the pollutant and the active site on the sorbent surface. Methyl red adsorption was characterized to be endothermic ΔH°> 0 kJ/mol, feasible, spontaneous and physical as -20 kJ/mol < ΔG° < 0 Kj/mol and the positive value of the entropy implies that oddness progress at the solid/solution interface (Khan et al., 2018). Methyl blue adsorption increased with temperatures, which may be associated with activation of the adsorbent surface and the widening of pore size (Shi et al., 2014). With the value of ΔG= -10 kJ/mol, the adsorption of nitrate was deemed to be physical, feasible, and spontaneous (Mazarji et al., 2017).

2.6.2 **Kinetics**

Three kinetics models are widely applied to elucidate adsorption process of pollutants with activated carbon namely the first and second-order models, and the interparticle diffusion model (Smith et al., 2009; Worch, 2012).

Pseudo first and second order

Adsorption kinetics can be described using the assumption that adsorbate removals follow a first-order rate low:

$$\frac{dq}{dt} = k_1(q_e - q_t) \quad (2.8)$$

where qt and qe are the amount of pollutants adsorbed per mass of adsorbent (mg/g) at the targeted time and equilibrium respectively and k_1 is the constant rate (min^{-1}). After integration with conditions that q_e =0 when t = 0, the equation (2.8) becomes:

$$ln\left(\frac{q_e - q_t}{q_e}\right) = -K_1 t \quad (2.9)$$

Alternatively, equation (2.9) can be written as:

$$Log(q_e - q_t) = Log q_e - \frac{K_1}{2.203} t \text{ or } ln(q_e - q_t) = ln\, q_e - K_1 t \quad (2.10)$$

The straight line plot of log (qe - qt) against t implies that log (qe) as slope and intercept equal to k_1/2.303. therefore the quantity of solute adsorbed per gram of sorbent at equilibrium (qe) and the first order sorption rate constant (k_1) can be evaluated from the slope and the intercept (Tao et al., 2015).

The first pseudo kinetics equation is considered unsuitable because qe it is a dependent variable and fitting parameter (Worch, 2012) . In order to minimize the error, Asuquo et al.(2017) suggested to adopt a non-linear equation for prediction of physisorption of Cd^{2+} and Pb^{2+} with a commercial activated carbon:

$$q_t = q_e(1 - e^{-K_1 t}) \quad (2.11)$$

The second pseudo order kinetics is described by the equation:

$$\frac{dq}{dt} = k_2\,(q_e - q_t)^2 \quad (2.12)$$

where k_2 is the second order rate constant, integration of equation (2.12) with initial conditions when t = 0, q_e =0, gives the equation:

$$\frac{t}{q_t} = \frac{1}{K_2\, q_e^2} + \frac{t}{q_e} \quad (2.13)$$

The rate constant is calculated via regression. If q_e it is determined from the isotherm, it is recommended to carry out the linear regression with t/q_e as independent variable with a slope equal to 1 (Worch, 2012).

The initial adsorption rate is defined as:

$$h = K_2\, q_e^2 \quad (2.14)$$

where k^2 is the second order constant rate (Acheampong, 2020).

Intraparticle diffusion

The intraparticle diffusion model is a practical means to explain the diffusion mechanism and probe whether intraparticle diffusion is the rate limiting step in the adsorption process. The intraparticle model diffusion is represented by equation (2.15) (Zhang et al., 2015) :

$$q_t = K_{int}\, t^{1/2} + C \quad (2.15)$$

Where K_{int} is the intraparticle diffusion rate constant (mg g^{-1} $min^{-1/2}$) and C is the intercept that reflects the boundary layer effect. The greater the C value, the more the surface sorption will contribute to the rate-controlling phase (Zhang et al., 2015). In general, the plotted intraparticle model has 3 phases, which are distinguished by changes in slope. Intraparticle diffusion is considered to be the only rate-controlling stage for the adsorption process if the straight line crosses the axis origin (Yao et al., 2016; Zhang et al., 2015); additionally, in multi-linear diagrams, there are various phases in the adsorption process such as intraparticle diffusion, film diffusion, and so on (Yao et al., 2016). Zhang, et al. (2015) plotted experimental data for Malachite Green adsorption with SBAC, where the first region showed a sharp significant rise attributed to a rapid attachment of pollutants to the external surface of the adsorbent, the second linear zone was the steady adsorption stage with intraparticle diffusion as the rate limiting step, and finally due to the low concentration of pollutants, the last region is the final equilibrium stage where the pollutants diffusion was tardy, similar trends were reported by Yao, et al.(2016) for Pb^{2+} adsorption with activated carbon.

2.6.3 **Isotherm models**

The amount of adsorbate extracted from the solution by the adsorbent is correlated to adsorbent dose in the solution using different adsorption isotherm models (Hadi et al., 2015; Singh et al., 2018), which are summarized in Table 2.4, for practicability purposes to determine quantity of contaminants removed at equilibrium stage. Langmuir and Freundlich isotherms are the most commonly used equilibrium adsorption isotherms. The first's theories are based on the fact that adsorption occurs at homogeneous sites with uniform energy levels, while the second identified heterogeneous systems with non-similar adsorption sites, meaning that each adsorbate compound could only be adsorbed on a single adsorption site (Hadi et al., 2015). According to the Temkin isotherm model, the heat of adsorption decreases as the coverage increases due to the contact between the adsorbate and the adsorbent (Singh et al., 2018). The Flory-Huggins model is applied to evaluate the number of adsorbate occupying adsorption sites (Singh et al., 2018).

Table 2.4 Equilibrium adsorption Isotherms (Singh et al., 2018)

Isotherm	Equation	
	Generalized Form	Linearized Form(s)
Langmuir	$q_e = \frac{q_m K_L C_e}{1 + K_L C_e}$	$\frac{C_L}{q_e} = \frac{1}{K_L q_m} + \frac{C_e}{q_m}$
Freundlich	$q_e = K_F . C_e^{1/n}$	$lnq_e = lnK_F + \frac{1}{n} lnC_e$
Temkin	$q_e = \frac{RT}{b_T}(lnK_{Te}C_e)$	$q_e = \frac{RT}{b_T} lnK_T + \frac{RT}{b_T} lnC_e$
Flory-Huggins	$C_0 = \frac{\theta}{K_{FH}(1-\theta)^n}$	$ln\frac{\theta}{C_0} = lnK_{FH} + n\, ln(1-\theta)$

Where:

- C_0 (mg L^{-1}) and Ce (mg L^{-1}) are the solute concentrations of impurities at initial and equilibrium, respectively, V (L) is the volume of the solution, and W (g) is the mass of adsorbent used, then q_e can be deducted from equation below (Singh et al., 2018):

  $q_e = \frac{(C_0 - C_e) * V}{W}$ (2.16)

- K_L is the Langmuir constant and C_0 is the initial concentration of the pollutants.

  $R_L = \frac{1}{1 + K_L C_o}$ (2.17)

  The value of the separation factor R_L reveals crucial information related to the nature of adsorption. If The value of R_L ranges between 0 and 1, adsorption is favourable, while $R_L > 1$ represents unfavourable adsorption and $R_L = 1$ represents linear adsorption. The adsorption process is considered irreversible if $R_L = 0$ (Acheampong, 2020).

- q_m (mg g^{-1}) is the maximum adsorption capacity corresponding to complete monolayer coverage and K_f (mg g^{-1}) and n are the Freundlich adsorption constants, and n is a measure of the adsorption intensity, respectively, a value of n ranges between 2 and 10 indicates that the adsorption can be easily proceeded, relatively, when it is less than 0,5 the aptitude for adsorption will be too mere (Fan et al., 2016).

  The Freundlich isotherm constants K_f and 1/n are evaluated from the intercept and the slope respectively, of the linear plot of ln q_e versus ln C_e (Singh et al., 2018).

- In the Flory-Huggins model the degree of coverage (θ) can be formulated as:

  $\theta = (1 - Ce/C_0)$ (2.18)

  where n is the number of pollutants occupying sorption sites and K_{FH} is the equilibrium constant of adsorption, n and K_{FH} can be deducted from the slope and the intercept of the straight line plotted log (θ/C_0) versus log (1-θ).

  The Gibbs free energy of adsorption is derived from the equation below(Singh et al., 2018):

  $\Delta G = -RTlnK_{FH}$ (2.19)

- K_t (L g^{-1}) is the Temkin isotherm constant, b_t (J mol-1) is a constant pertaining to

  the heat of sorption and R (8.314 J mol^{-1}. K^{-1}) is the gas constant. K_t and b_T can

be estimated from the slope and the intercept of the straight line plotted from q_e versus ln (C_e) (Singh et al., 2018).

2.7 Synthesis of adsorbent from sewage sludge by chemical activation

Chemical activation was preferred over thermal activation to manufacture activated carbon from sewage sludge in early discussion because it is lead to a creation of an adsorbent with a more evolved porosity at a lower temperature (Devi & Saroha, 2016; Hadi et al., 2015). Hadi et al. (2015) further observed that the disparity in surface area (S_{BET}) of activated carbon from sludge may be attributed to the origin of the raw material (water content and composition).

2.7.1 **Experimental Factors**

Pyrolysis temperature, Heating rate and dwell time

The surface area and porosity of SBAC augment with rising in temperature and the activation time due to the facilitation conditions to achieve an efficient and fully achieved reaction. However, after certain point of time/temperature, there are no longer advantages to proceed further because the surface area and porosity decline due to the contraction of micropores and pore inaccessibility for pollutants, which diminishes adsorption capacity (Devi & Saroha, 2017; Xu et al., 2015). Generally, the effects are likely to be more severe at higher temperatures and high activator concentrations (Devi & Saroha, 2016). It has been observed from the literature that the SS pyrolyzed at low temperature for longer period of time give similar results as the adsorbent pyrolyzed at a higher temperature for a shorter period of time (Devi & Saroha, 2016) and the surface area is likely to be more developed at lower heating rate due to longer residence time of pyrolysis while in the close range of time the surface does not vary significantly (Xu et al., 2015), for instance, Al-Malack & Dauda, (2017) produced SBAC from SS activated adsorbent with a 5M $ZnCl_2$ solution, heated at a rate of 10 °C and pyrolyzed at 700 °C for 60 and 120 minutes, the S_{BET} was merely different 319,4 m^2/g and 314,4 m^2/g. The pyrolysis temperature impact surface chemistry properties when it increases the acidic surface functional groups decrease conversely the basic groups rise therefore the pH of the surface of the SBAC follows the trend. It has been assumed that this phenomenon is generated by the disintegration of carboxyl groups and change of organic nitrogen into pyridine-similar structures (Devi & Saroha, 2016; Hadi et al., 2015).

Activators reagents

Precursors treated with KOH have higher surface areas than those treated with $ZnCl_2$, H_2SO_4, or H_3PO_4 (Devi & Saroha, 2016; Xu et al., 2015), despite the fact that when KOH is used as an activator, activated carbons are mainly microporous in comparison to those activated with $ZnCl_2$ or H_3PO_4, which restricts macro-pollutant absorption in air and water (Hui & Zaini, 2015). For the reasons mentioned above, KOH was chosen as the activating agent in this study. Equations (2.20 - 2.22) may be used to define the mechanism of KOH activation. At higher temperatures, KOH splits into K_2O, which is then reduced to metallic K atoms by intercalation with carbon inward, resulting in gasification, steam emission, and CO_2 production. CO_2 vapours also contribute to porosity by forming cavities in the carbonaceous layers (Devi & Saroha, 2016; Xu et al., 2015)

$$2KOH\ (s,l) \rightarrow\ K_2O\ (\mathrm{s}) + H_2O\ (g) \quad (2.20)$$

$$2\mathrm{K_2O} + \mathrm{C\ (s)}\ \rightarrow 4\mathrm{K\ (l)} + \mathrm{CO_2}\ (g) \quad (2.21)$$

$$K_2O\ (s) + H_2(g) \rightarrow 2K\ (l) + H_2O\ (g) \quad (2.22)$$

Due to the occurrence of side reactions, the temperature begins to negatively affect the surface area and porosity of the adsorbent after a certain stage, particularly at higher temperatures and high reagent concentrations. An increase in the pyrolysis temperature causes the adsorbent's micropore to widen, rendering the pore unavailable for contaminant removal, resulting in lower adsorption ability (Devi & Saroha, 2016, 2017; Hadi et al., 2015; Xu et al., 2015). It's crucial to think about the quantity of triggering reagent you'll need for economic purposes. Surface area increases with reagent quantity and decreases when the latter is in excess due to hyper-activation and microporosity destruction (Hadi et al., 2015; Xu et al., 2015). A similar statement holds true for mixtures such as sewage sludge and rich carbon compound as shown by Zeng et al. (2018) who recorded a significant increase in S_{BET} of SBAC (30% sludge and 70% corn straw) enabled with 2g/L KOH at 750 °C for 60 min, whereas S_{BET} without KOH was 33.245 m^2/g, with a KOH to the raw material ratio of 6:1. With a ratio of 10, the S_{BET} fell from 689, 924 m^2/g to 420 m^2/g.

Addition of carbonaceous feedstock

Blending sewage sludge with rich carbonaceous feedstock including waste coconut shell (Liang et al., 2020; Yang et al., 2019), coal (Li et al., 2016), corn straw (Zeng et al., 2018), corn stalk (Li et al., 2016), sugarcane bagasse (Tao et al., 2015) or cake from Polyetherol production (Velghe et al., 2012) aims to increase the porosity of the adsorbent because sewage sludge contains a small fraction of fixed carbon and a non-negligible proportion of ash on the one hand and the addition provides a higher fixed carbon content than sewage sludge and contribute to increase surface area (J. Li et al., 2018). When 25 percent corn stalk was applied to SBAC pyrolyzed at 600 °C for 1 hour and enabled with a solution of 4M $ZnCl_2$, the S_{BET} was 769.0 m^2/g, compared to 475.0 m^2/g when sewage sludge was the sole precursor (Li et al., 2016).

Table 2.5 SBAC synthesis conditions and adsorption capacity

Activating Reagent	Weight ratio: sludge/reagent	Temperature ° C	holding Time (min)	Iodine Number	Surface Aream^2/g	Sorbents uptake	References
KOH	3	750	30	-	1832	330 mg/g of 4-chlorophenol	(Monsalvo et al., 2011)
$ZnCl_2$	2	-	60	-	377	Cu (II): 10.50 mg/g	(Wang et al., 2011)
KOH: 3M	6	600	60	127	629	Dibenzothiophene(14.12 mg/g) with KOH	(Nunthaprechachan et al., 2013)
$ZnCl_2$: 3M	3	600	60	178	172		
HNO_3 :3M	4	600	60	0	9.26		
$ZnCl_2$: 5M	1	500	120	-	721.2	Pb^{2+} 1.25 mg/g	(Gong, 2013)
H_3PO_4	1.5	600	60	-	296	Toluene 280 mg/g	(Boualem et al., 2014)
KOH: 3M (with 1/3 bagasse)	3	800	30	107	806.57	Pb^{2+} : 48 mg/g	(Tao et al., 2015)
KOH	3	600	120	-	515	Phenol: 4.2 mg/g	(Gupta & Garg, 2015)
$ZnCl_2$	2.5	600	120	-	510.80	Phenol: 4.15 mg/g	
$Zncl_2$:4 M (with 25% corn stalk)	2	600	60	-	792	Dye 144 mg/g	(Li et al., 2016)
$ZnCl_2$	2	500	15		679.3	Diclofenac:157.4 mg/g	(dos Reis, Mahbub, et al., 2016)
						Nimesulide:66.45 mg/g	
KOH	1	550	60	-	186	Cu^{2+}: 31.85 mg/g	(dos Reis, Adebayo, et al., 2016)
$Zncl_2$	1	550	60		192	Cu^{2+}: 19.79 mg/g	
$Zncl_2$: 5M	2	500	60	-	700	Hydrophobic organic compound: fluorene (769 ug/g)	(Björklund & Li, 2017)
$Zncl_2$ (6M)-H_2SO_4 (35%): ratio 4:1	3	550	60	-	218,37	Cu^{2+}: 114.94 mg/g	(Guo et al., 2017)
						Methylene Blue : 125 mg/g	
$Zncl_2$: 5M	1	700	60	-	318,5	Cd^{2+}: 17.04 mg/g	(Al-Malack & Dauda, 2017)
						Phenol: 12.06 mg/g	
$ZnCl_2$	2	700	90	-	385	methyl tert-butyl ether 0.7ppm	(Liadi et al., 2018)
KOH: 10 g/l (with 57 % of corn stalk)	2	750	60	-	689.624	H_2S: 12.38 mg/g	(Zeng et al., 2018)
H_3PO_4 (85%)	2.5	450	120	-	511	Cr (VI): 95.54 mg/g	(Aliakbari et al., 2018)

KOH	2.3	680	80	-	1795	Acid Orange (AO7): 1410 mg/g	(Jung et al., 2019)
KOH	1:2 g	700	60	-	907	Pb^{2+}: 57,48 mg/g	(Zhang et al., 2019)
CH3-COOK	1:2 g				611	Pb^{2+}: 47,59 mg/g	

Washing

The benefits of acid washing followed by water washing as a post-treatment method of SBAC manufacturing were highlighted in peer reviews (Devi & Saroha, 2016, 2017; Hadi et al., 2015; Smith et al., 2009), not only to remove useless organic compounds and triggering reagent to provide unobstructed pores while increasing surface area, but also to increase cations exchangeability since H^+ ion issued from acid substitute exchangeable cations of SBAC, which exhibited high metal uptake.

2.7.2 **Aqueous surfaces Modifications**

Surface modification research aims to achieve the goals outlined in section 2.5, especially to improve SBAC's performance in terms of pollutant removal, both inorganic (J. Li et al., 2018; Li et al., 2019; Tao et al., 2015) and organic (Björklund & Li, 2017; Zhang et al., 2015). As shown in Table 2.6, SBAC modification increases adsorption potential by enhancing surface functionalities, implying that chemical bonds predominate in the process but that surface area is reduced due to micropore volume reduction (Björklund & Li, 2017; Li et al., 2019; Zhang et al., 2019). Although the S_{BET} (86 m^2/g) was lower than the unmodified SBAC, Bjokrlund & Li (2017) observed a sharp decrease in S_{BET} from 721, 2 m^2/g before modification with nitric acid to 86 m^2/g after the procedure, the equilibrium adsorption of capacity was 5,6 times higher than the unmodified SBAC (0,5 mg/g). Li, et al.(2018) made a sewage sludge coal blended adsorbent with a thio-functional group, with Pb^{2+} and Cu^{2+} adsorption capacities of 238,1 mg/g and 87,7 mg/g, respectively. According to Li et al.(2019), the unmodified SBAC had a Pb^{2+} adsorptive potential of 1,25 mg/g and a time and a half (4,05 mg/g) higher after nitric acid alteration, while the S_{BET} was reduced from 721,2 m^2/g to 86,12 m^2/g.

Table 2.6 Aqueous phase modified SBAC and adsorption capacity

References	SBAC State	Modification Conditions			S_{BET} (m^2/g)	pH_{PZC}	Adsorption
		Oxidant Concentration	Soaking time	Temperature			
(Zhang et al., 2015)	Unmodified	-	-	-	1003,8	4,02	Malachite Green: 269,54 mg/g
	Modified (2 stages: 1 and 2)	1: 2M HNO_3	1: 3h	1: 60 °C	838,3	3,78	Malachite Green: 303,03 mg/g
		2:-	3h	2: 300 °C			
		1: 2M H_2SO_4	1: 3h	1: 60 °C	960	3,66	Malachite Green: 284,90 mg/g
		2:-	3h	2: 300 °C			
(Tao et al., 2015)	Unmodified (bagasse/sludge: 1/2)	-	-	-	804,57	-	Pb^{2+}:-
	Modified (bagasse/sludge: 1/2)	60% HNO_3	6h	90 °C	69,19	-	Pb^{2+}: 51,3 mg/g
(Björklund & Li, 2017)	Unmodified	-	-	-	721	-	Fluorene: 0,5 mg/g
	Modified	10 M HNO_3 1g:10 ml	4h	90 °C	86,1	-	Fluorene: 2,8 mg/g
(Li et al., 2019)	Unmodified	-	-	-	721,2	-	Pb^{2+}: 1,25 mg/g
	Modified	10 M HNO_3 1g:4 ml	4h	20 °C	674,7	-	Pb^{2+}: 3,04 mg/g
		10 M HNO_3 1g:10 ml	4h	90 °C	86,12	-	Pb^{2+}: 4,05 mg/g

2.7.3 **Environmental consideration for manufacturing and disaposal of SBAC**

Heavy metals remain in the char after pyrolysis because there are not eliminate by evaporation or sublimation , except for a small and manageable gas emission during

sewage sludge pyrolysis (J. Li et al., 2018). Since a TCLP (Toxicity Characteristic Leaching Procedure) test concluded that metal leaching during water treatment poses a low risk of toxicity, pyrolysis is an efficient means of stabilizing inorganic compounds found in SBAC (Xu et al., 2015). Exhausted sewage sludge adsorbent has raised concerns due to encapsulated contaminants being released; however, cement and lime have demonstrated their effectiveness in reducing pollutants. The spent sludge base adsorbent formed from metal uptake application has been immobilised by binding cement based method, the calcium silicate binds the metal ions and prevents their release from the solid cement module, similar to leaching due to the formation of sodium arsenate (Devi & Saroha, 2017). The lower the H/C ratio, the higher the aromaticity; SBAC pyrolyzed at higher temperatures have higher aromaticity and are resistant to decomposition, allowing them to survive for several years in the soil (Huang et al., 2017; Z. Li et al., 2018).

Leachability test

Since SBAC is extracted from wastewater discharge, it is recommended that a leachability test be performed to determine the risk of metal found in the adsorbent being released during the adsorption phase in soil or solution in reviews published on the use of SBAC for waste water treatment (Devi & Saroha, 2016; Xu et al., 2015). In general, the procedure for a leachability test is dictated by a normalized standard. Rio et al.(2005) tested metal leachability with demineralized water modified to pH 5 using the AFNOR X31-210 procedure. The results showed that the metal was stable and that the concentration in the solution did not exceed 2%. The metals found in the low-cost adsorbent were stable and insoluble under the conditions ascribed by the standard, according to Li, et al., (2016) who used the horizontal vibration process (HJ 557-2009) for sewage sludge mixed with 25% cornstalk. When 1g of the sorbent was placed in contact with 40 ml of distilled water at pH 3 and agitated for 24 hours, Li et al.(2019) found that metal solubilisation was minimal or non-existent. To determine the ecotoxicology of heavy metals, TCLP was performed by mixing glacial acetic acid (pH=2,8) with biochar in a solid-liquid proportion of 1:20 (Huang et al., 2017; Xue et al., 2019). In the case of sewage sludge-based adsorbent manufactured by electromagnetic induction heating, it was discovered that metal concentrations ranged from 0 mg/l to 1,913 mg/l of Zn, while Cr, Ni, and Cu concentrations did not exceed 0.003 mg/L, 0.024 mg/L, and 0.017 mg/L,respectively (Xue et al., 2019).

CHAPTER 3: MATERIALS AND METHODOLOGIES

3.1 Samples and chemicals

Two types of sewage (Figure 3.1) were collected at ERWAT wastewater treatment plant located in Midvaal: the first was an overflow stream from the dissolved air Flotation stage of the secondary sewage sludge labelled as “D”, the second was the digested and dewatered sludge ready for disposal referred as “S”, the collection points are indicated in Appendix A.



Figure 3.1 (a) Dissolved Air Flotation and (b) Final Sludge.

It is hypothesized in this study that, blending sewage sludge with discard coal prior to the pyrolysis stage would increase the surface area of the pyrolyzed product (as mentioned in section 2.7.1) since discard coal has higher carbon content compared to sewage sludge. Letter C will be added to indicate sorbent mixed with discard coal: “DC” for D or “SC” in the case of S. Discard coal (100% passing 150 µm), were provided by the Sustainable Energy and Environment Research Unit (SEERU). The nitrogen (N_2) gases baseline 99 % were purchased at Afrox, South Africa.

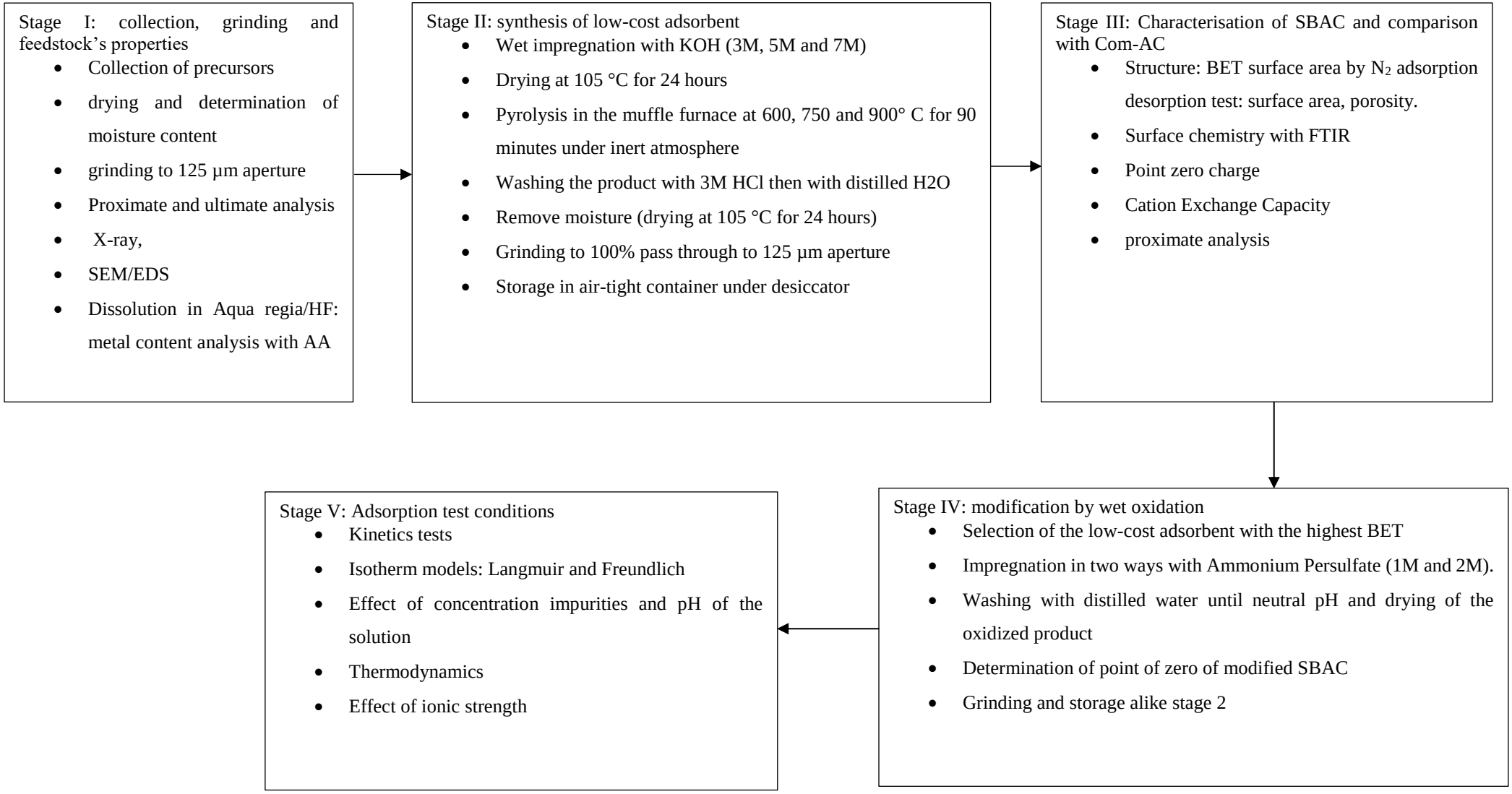


Figure 3.2 Resume of principal practical research activities

KOH, HCl (32%), NaCl, H_2SO_4 were purchased from Associate Chemical Enterprises, activated charcoal (C3014-500G) and Lanthanum chloride hexahydrate (211605-500G) were acquired from Sigma Aldrich and all reagents were branded analytic grade

3.2 Raw materials processing

3.2.1 Drying and precursors analysis

To assess moisture content, a representative sample of each sludge was dried in the oven for 24 hours at 105°C immediately after collection. Devi & Saroha (2016) identified 2 methods for drying sewage sludge: sun drying, also known as air-drying, and oven drying, the latter of which is considered the best. Lin, et al., (2012) and Li et al., (2018) air-dried sewage sludge for 7 days before extracting the final moisture in the oven for 24 hours at 105 °C before further treatment and characterization. In this study, the sludge was air-dried on the roof of The Richard Ward building, as seen in Figure 3.3. it's worth to mention that the time was favourable for the experiment as it was a sunny season in Johannesburg (Braamfontein) and the sun drying process spanned from August 19 to September 6, 2019.



Figure 3.3 Photography of the sewage air-dried, D in the plastic cylinder and S laid on the bash

Moisture content in sundried sludge was first determined by macroscopic observation and then determined by oven drying using the procedure stated above before the final

drying (as discussed above). The dried sludge was crushed with a vibrating pulverizer to a final product that passed 100 percent through 125 µm aperture sieves in Peter King Laboratories. For characterization, 5 g of each dried sludge is properly ground to a pulverized condition. In order to perform SEM and EDS analysis, a ZEISS SIGMA FESEM 03- 39 apparatus is used to analysed coated samples on a carbon tape support using Gold-Palladium techniques. TGA was performed with a nitrogen flow rate of 20 ml/min and a heating temperature of 10 °C after calibration with the Pioneer (SDT-Q500) equipment. Samples weighing 10 mg were mounted in the crucibles and heated to 1000 °C. TGA analysis also tests the selection of pyrolysis temperature based on the unvarying weight loss of sewage sludge with temperature as a measure of thermal stability of the dried sludge (dos Reis, Adebayo, et al., 2016; Liadi et al., 2018). After calibrating the instrument, proximate analysis of sewage was performed using a PerkinElmer STA 6000 simultaneous thermal analyser. For this reason, 10 mg of the precursor were placed in the refractory container and the protocol as published was followed (Donahue & Rais, 2009). FT-IR revealed functional surface groups of dried sewage sludge, discard gas, SBAC, and Com-AC using PerkinElmer FT-IR Spectrometer Spectrum Two. With the thermoscientific flash 2000, an ultimate analysis test was conducted to show the composition of C, H, N, and S. XRD study using a Bruker 2D phaser instrument with CuKα1 radiation at a wavelength of 1.54060 cm^{-1} and a 2θ angle ranging from 10° to 90° was used to detect the crystalline phase.

3.3 synthesis and characterization of Sludge based activated carbon

Dried and crushed sewage sludge was impregnated with KOH solution with concentrations of 3,5 and 7, and a ratio of activating reagent to the sludge of 1,5:1. After impregnation, the mixture was dried for 24 hours at 105°C. The dried impregnated precursors were crushed to 100 percent passing through 150 µm, then placed in a crucible and pyrolyzed in an inert atmosphere for 90 minutes in a muffle furnace connected to a nitrogen bottle with a flowrate of 50 ml/min. The furnace regulator was turned off when the dwell time was reached, and the pyrolyzed SS was cooled to room temperature in the furnace before the washing stage. The washing stage consists of 2 steps: acidic and water. The former was carried out with a 3M HCl solution to remove excess activating reagent and laden soluble ash (Devi & Saroha, 2016), while the latter was carried out with distilled water until the filtrate reached a neutral pH value of 6 to 7. SBAC was washed and dried in an oven at 105°C for 24

hours, then crushed and sieved to 125 m before being stored in an airtight container in the desiccator for further testing. The properties of SBAC were compared to those of commercial activated carbon for the purposes of performance comparison. From the characterization of N_2 adsorption at 77K, the surface and pore volume were deducted. The NH_4OAC method (Sheldrick, 1984) was used to determine cations exchange capacity (Björklund & Li, 2017; Gong, 2013; Li et al., 2019). In a 100 ml Erlenmeyer flask, a solution of 15 ml of 1M ammonium acetate solution adjusted to pH 7 with ammonium hydroxide or acetic acid and 0,3 g of SBAC was added to the ammonium acetate solution, the mixture was agitated for 30 minutes prior to solid-liquid separation with a 0.45 um syringe filter, and the filtrate recovered was diluted 20 times with deionized water The AA test was used to determine the concentration of extractable cations (Mg^{2+}, Ca^{2+}, K^+, and Na^+) in the diluted filtrate.Exchange cations in meq/100 g were calculated by the formula below:

$$\frac{\mu g/ml\ measured}{equivalent\ weight\ of\ cation \times 1000} \times \frac{100 \times vol\ of\ extractant(ml) \times dilution}{weight\ of\ SBAC(g)} \quad (3.1)$$

The equivalent weight of Mg^{2+}, Ca^{2+}, K^+ and Na^+ are 20,039 g/mol, 24,305 g/mol, 39,083g/mol and 22,989 g/mol respectively.

$$CEC = Exchangeable\ Mg + Exchangeable\ Ca + Exchangeable\ K + Exchangeable\ Na \quad (3.2)$$

Boehm titration was used to determine the acidity of SBAC (Boehm, 2002). For acidic functional group determination, 0,1 g of SBAC was placed in a sealed bottle in 40 ml of 0,01 M solution of $NaHCO_2$, Na_2CO_3, or NaOH agitated for 48hrs, whereas for basicity determination, 0,1 g of SBAC was placed in contact with 0,01 M HCl and then titrated with 0,01 M NaOH. Titration with 0,01 M HCl in case of basicity or 0,01 M NaOH in case of acidity revealed the acidity or basicity of the filtrate. All titration tests were run in duplicate with an aliquot of 10 ml and methyl red as pH indicator. The pH point of zero charge was determined using the procedure established by (Leng et al., 2015): 0.05 g of SBAC was poured into a vial filled with 40 ml of a 0.01 M NaCl solution with a pH range of 2 to 12 with a 1 increment, and the pH solution was adjusted with 0,1 N HCl or 0,1 N NaOH solution after the vials were shaken for 24 hours at 200 rpm in an incubator shaker. The pH point of zero charge was defined as the point at which the initial pH equaled the final pH, and the difference (ΔpH) between them was zero.

The toxicity contaminant leaching procedure was carried out as described by (Huang et al., 2017; Xue et al., 2019), and the element concentrations were determined using Atomic Adsorption (AA).

3.4 Use of the experimental design for adsorbent synthesis

The use of RSM in design experiments has been applied in previous studies (Table3.1) Aside from optimizing SBAC's performance and properties, it also reveals, if possible, interactions between the factors involved in the synthesis process.

Table 3.1 previous research of SBAC preparation using RSM

Feedsotck	Factors	Responses	References
Aerobically digested sludge dewatered by centrifugation	Activation temperature (600 °C-700 °C), holding time (60 min-220 min) and impregnation ratio (0.5–1.5 g H_2SO_4 per gram of sludge)	mass yield (%), SBET (m^2/ g), mesopore volume (cm3/g), micropore volume (cm3/g), surface pH, functional groups (meq/g): acidic, basic,,adsorption (mg/g); of copper phenol; basic Violet 4; Acid Red 18; acetone; toluene	(Rio et al., 2005)
Biological sludge	Pyrolysis temperature (300 °C- 700 °C), binding agent:0 g to 20/100 g of sludge. Types of binding agent: humic matter, phenolic resins, or clayey soil, NaOH (0,5g-100g/100g of sludge)	Textural properties (surface area: m^2/g) Adsorption capacity (mg/g) of: Tetracycline, Cd (II), dichlorophenol, methylene blue	(Gómez-Pacheco et al., 2012)
Digested anaerobically and dewatered sludge	Pyrolysis temperature (300°C - 600 °C), holding time (30 min-90 min) and activator concentration	Iodine value (mg/g), specific surface area (S_{BET}:m^2/g), micropore volume (cm^3/g) and pH	(Sheha et al., 2013)
-	Microwave: Power radiation (700W-980W), holding time, holding time (8 min-12 min), ratio $ZnCl_2$/Sludge (0,5-1,5)	Surface area (S_{BET}:m^2/g)	(dos Reis, Wilhelm, et al., 2016)
	Conventional furnace: Pyrolysis temperature (500 °C-800 °C), holding time (8-12 min), ratio $ZnCl_2$/Sludge (0,5-1,5)	Surface area (S_{BET})	
-	Carbonizing temperature (400 °C-600 °C) and time (0,5h-2h), impregnation ratio (KOH/ g of SS:1-3,5), activation	Adsorption capacity of Azo dye	(Jung et al., 2019)

	temperature (600 °C-800 °C) and time (0,5h-2h)		
Dehydrated municipal sludge mixed with coconut shell in a ratio of 1:1	Carbonization temperature (750 °C -850 °C) and time (45min-75 min), activator concentration KOH (2M-3M)	Iodine Number (mg/g)	(Liang et al., 2020)
Raw sewage sludge	Activation temperature (500 °C -800 °C), contact time (60 min-180 min) chemical activation ratio(KOH) (w/w):0,5-1,5	Surface area (m^2/g)	(Almahbashi et al., 2020)

As shown in Figure 3.4, optimal (custom) design with surface response methodology was used to configure the activation conditions of SBAC synthesis. Design Expert software version 12 was used for this purpose.

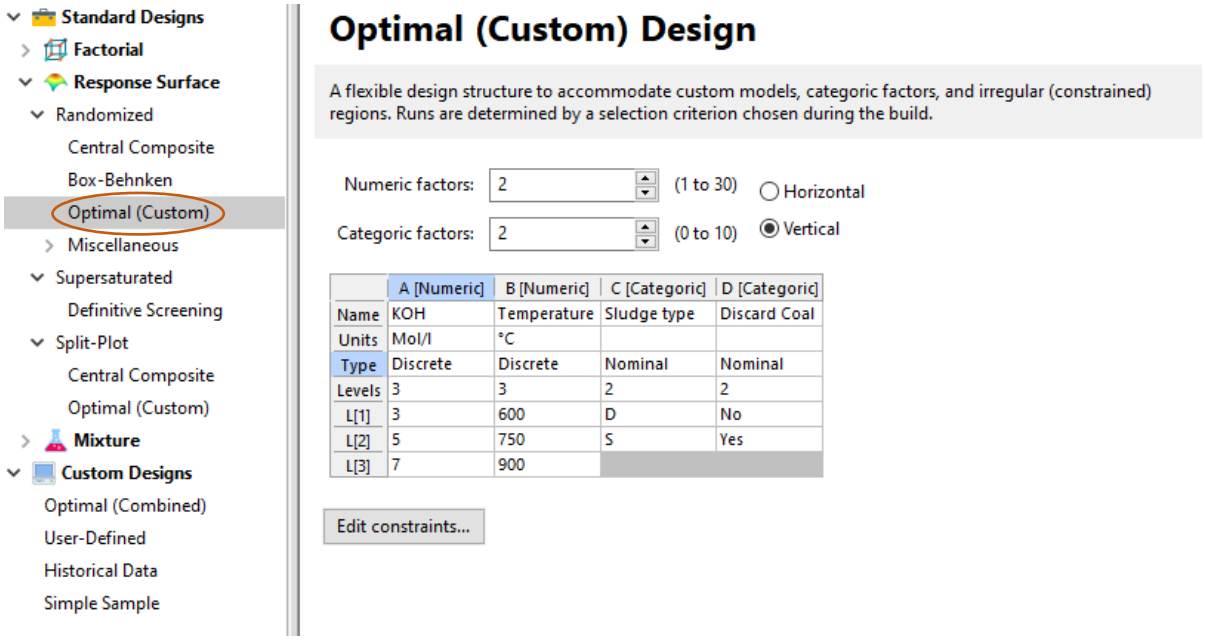


Figure 3.4 Screenshot of the factors with their levels

The factors were categorized into 2 categories: numerical (pyrolysis temperature and activating agent concentration) and categorical (types of SS and discard coal mixture NO: 0% or Yes: 50%). The tests are listed in Table 3.2.

Table 3.2 Experiments generated by Design Expect 12.0

	Factors			
	Numerical		Categorical	
Run	KOH: Mol/l	Temperature (°C)	Sludge types	Discard coal
1	3	900	S	Yes
2	7	900	S	No
3	5	600	D	No
4	3	600	S	Yes
5	3	900	S	No
6	5	900	D	No
7	3	600	S	No
8	5	750	D	Yes
9	7	750	S	Yes
10	7	900	D	Yes
11	7	600	D	No
12	7	600	S	Yes
13	3	600	S	Yes
14	7	900	S	No
15	7	600	D	No
16	5	600	S	No
17	5	600	D	Yes
18	3	600	D	No
19	7	900	D	Yes
20	3	900	D	Yes
21	5	900	S	Yes
22	3	750	D	No
23	3	900	D	Yes

Apart from the alphabetical order (D, DC, S, and SC), the experiments were rearranged (Table 3.3) in ascending order, beginning with reagent concentration and ending with temperature.

Table 3.3 Rearranged experiment

			Factors			
			Categorical		Numerical	
Sample	Run	Name	Sludge	discard coal	KOH: mol/l	Temperature (°C)
1	18	D-3-600	D	No	3	600
2	22	D-3-750	D	No	3	750
3	3	D-5-600	D	No	5	600
4	6	D-5-900	D	No	5	900
5	11&15	D-7-600	D	No	7	600
6	20&23	DC-3-900	D	Yes	3	900
7	17	DC-5-600	D	Yes	5	600
8	8	DC-5-750	D	Yes	5	750
9	10&19	DC-7-900	D	Yes	7	900
10	7	S-3-600	S	No	3	600
11	5	S-3-900	S	No	3	900
12	16	S-5-600	S	No	5	600
13	14&2	S-7-900	S	No	7	600
14	13&4	SC-3-600	S	No	3	900
15	1	SC-3-900	S	Yes	3	900
16	21	SC-5-900	S	Yes	5	900
17	12	SC-7-600	S	Yes	7	600
18	9	SC-7-750	S	Yes	7	750

The porosity development (surface area and porosity), chemical properties (cations exchange capacity, pHPzc, acidity and basicity), and organic content ratio (H/C and N/C) will be considered as primary inherent characteristics of SBAC.

3.5 modifications with Ammonium Persulfate

Surface modification was carried out with the APS in the conditions summarized in Table 3.4 on 2 of each (D or S) SBAC with the highest surface. Adsorbents with more developed structures are more likely to acquire more functional groups through wet oxidation, so the selection was not limited only to surface area but also to microporosity and pore volume growth (Daud & Houshamnd, 2010).

Table 3.4 wet oxidation conditions

Conditions	Temperature	SBAC wt (g)/ vol of APS (ml)	Time (min)	APS concentration (mol/L) in 1 M H_2SO_4
1	60 °C	1/25	240	1
2				2

3.6 adsorption test

Batch adsorption tests were performed in an incubator shaker at 250 rpm with a sorbent dosage of 0,5 (5 mg of adsorbent/10 ml of solution) to select the best SBAC for further studies, beginning with an evaluation adsorption efficiency test. Nitrate and methyl red uptake were measured in a single solution using the IC Dionex-120 ionic chromatography system and the U-vis Shimadzu 1800 system at a maximum wavelength of 522 nm for the former and the U-vis Shimadzu 1800 system for the latter. The best oxidized and unmodified SBAC were chosen based on preliminary evaluation tests performed at a constant temperature of 303 K for 180 and 360 min with an initial concentration of 50 mg/l of nitrate, 90 min and 180 min for MR with 75 ppm as an initial concentration and an initial pH of 2 for nitrate and 4 for methyl red. The initial pH of 2 in the case of nitrate was chosen based on the hypothesis that adsorbent surfaces become positively charged as pH decreases, preventing competition with hydroxyl anions (Mazarji et al., 2017) and pH 4 in the case of methyl red to avoid competition with H^+ cations while attempting to keep the surface deprotonated (below the pHpzc for the modified adsorbent) as MR pKa = 5,1 (Khan et al., 2018). Table 3.5 summarizes the adsorption conditions. As explained in section 2.6.2, the effect of time was investigated to elucidate kinetics order and intraparticle diffusion model, the isotherms were plotted from data issued from different concentrations as described in section 2.6.3. Variation of pH helped to gauge the impact of sorbate-sorbent interaction under different conditions (acidity or basicity). The pH of the solution was adjusted to the desired value with 0,1 N HCl or 0,1N NaOH.

Table 3.5 Adsorption test conditions

sorbate	Effect of time (min)	Effect of initial concentration (mg/l)	Effect of pH	Effect of ionic strength	Effect of temperature (°K)
Nitrate	30, 60,90, 120, 150 and 180 with 50 mg/l as initial concentration.	10, 30, 50, 70 and 90 agitated for 120 min	2, 4,6,8 and 10 agitated for 180 min with 50 mg/l as initial concentration	-	303, 318 and 333 agitated for 120 min with 50 mg/l as initial concentration.
Methyl Red	30, 60, 90, 120, 150, 180 with 75 mg/l as initial concentration.	25,50,75, 100 and 125 agitated for 240 min	2, 4,6,8 and 10 agitated for 180 min with 75 mg/l as initial concentration	0,001 M and 0,005 M of NaCl agitated for 240 min with 75 mg/l as initial concentration	303, 318 and 333 agitated for 240 min with 75 mg/l as initial concentration

CHAPTER 4: SYNTHESIS AND CHARACTERIZATION OF SBAC

4.1 precursors pre-treatment and preliminary characterizations

4.1.1 Moisture content

Before advanced stages of processing, the precursors were sun dried, and the moisture content of the sample was determined by mass losses after oven drying at 105 °C for 24 hours. Table 4.1 summarizes the findings of the moisture content test.

Table 4.1 Moisture content of non-dried and sun dried sample

Types of sludge	Non-dried sample Moisture (%)	Moisture content After sun drying (%)
D	96,28	6,285
S	85,33	7,0.37

4.1.2 Elemental, Proximate Analysis and inorganic composition

The elemental analysis (Table 4.2) reveals that there is only a minor difference between the 2 samples, indicating that digestion has no effect on the organic content of sewage sludge, despite the volatile solid content being slightly different. Sludge D had a content of 2,161 percent and sludge S had a content of 1,216 percent, both of which were similar to the discard coal content (1,474%).

Sludge D and S contain more volatile than discard coal (16,28 percent), 66,7%, and 59,16 percent, respectively, with less fixed carbon (4,15 percent: D, 4,86 percent: S, and 15,76 percent: discard coal) and ash, according to proximate analysis calculated on a dry basis (29,15 percent: D,35,98 percent: S and 67,96 percent: discard coal).

However, although the surface area of sludge from D was approximately 1.5 m^2/g, the surface area of sludge S could not be determined, possibly due to a lack of porosity in the precursor materials.

Table 4.2 Precursors properties

	Precursors		
	D	S	Discard coal
Elemental analysis			
C (%)	36.511	36,640	43,133
H (%)	5,526	5,215	2,424
N (%)	5,020	2,681	0
S (%)	2,002	2,225	2,429
H/C	0,151	0,142	0,056
N/C	0,137	0,073	0
Proximate analysis			
Fixed carbon (%)	4,15	4,86	15,76
Ash (%)	29,15	35,98	67,96
Volatile (%)	66,7	59,16	16,28
Volatile solid	2,161	1,216	1,474
Surface properties			
S_{BET} (m^2/g)	1,411	-	3,848
Pore volume	0,011	-	0,014
Pore size (nm)	30,72	-	15,11

4.1.3 Thermogravimetric Analysis

Figure 4.1 TGA curve of dried sludge shows that between 30 °C and 190 °C, there is a slight mass loss, and the mass of both sludges was roughly 5%, possibly due to adsorbed water (dos Reis, Adebayo, et al., 2016; Liadi et al., 2018). The most mass loss occurred between 200 and 600 ° C, with mass loss of D and S increasing from about 5% at 200 ° C to about two-thirds (64%) and half (46%) at 600 ° C, respectively. De Filippis et al.(2013) attributed the mass loss to the decomposition of compounds based on temperature ranges of 100 °C to 350 °C for carbohydrates and 350 °C to 500 °C for proteins, whereas Dos Reis et al. (2016) broaden mass loss to a temperature range of 180 °C to 550 °C for numerous compounds

volatilization/decomposition such as biodegradable materials, semi-volatile compounds, despite the fact that the mass loss from 600 °C to 1000 °C is not negligible in comparison to the previous gap, it is less intense for both sludge with 17 and 13 % for D and S respectively. As a result, 600 °C was chosen as the minimum temperature for pyrolysis. S appears to be slightly more stable than D based on the TGA curves; this may be due to the process treatment, as S is mixed with the primary sludge and the dissolved air flotation sludge before digestion, followed by dewatering on a band filter before disposal. This situation may result in an inorganic compound enrichment of the final sludge (S) resulting from the primary stage settling operation.

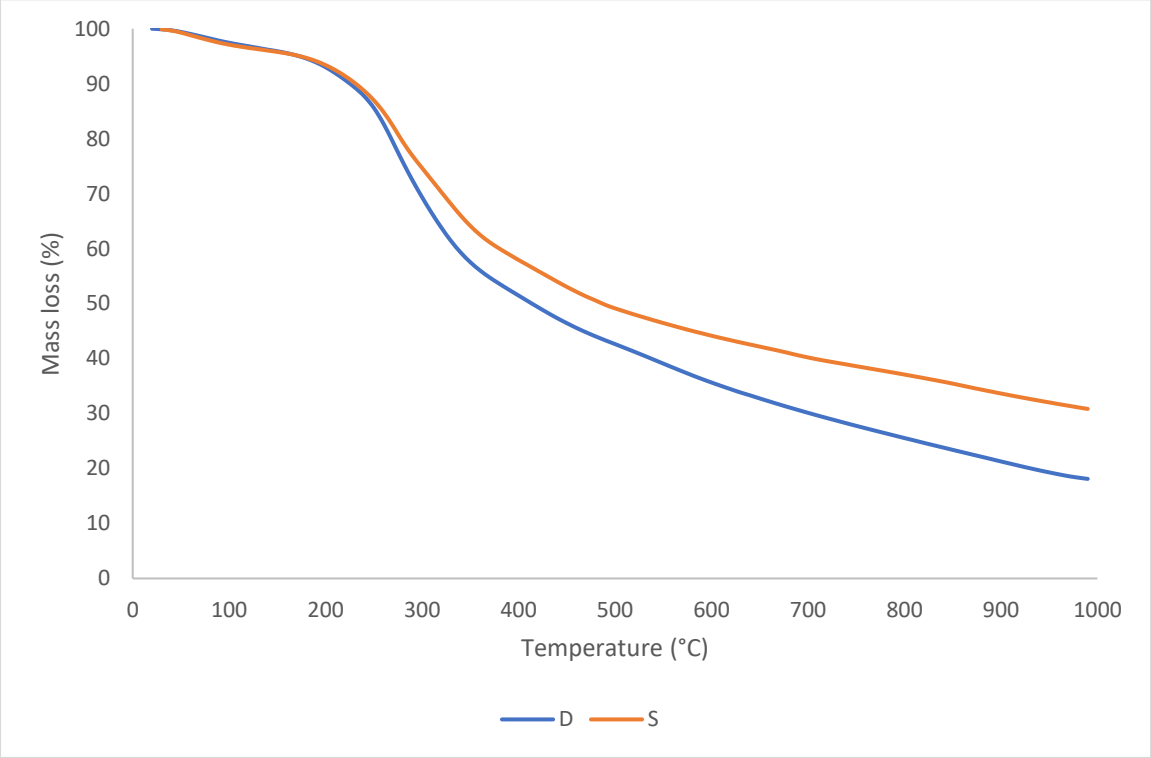


Figure 4.1 Thermogravimetric curves of Sludge precursor

4.2 precursors and sludge based adsorbent analysis

Precursors, as well as synthesized adsorbents were, further subjected to SEM, EDS, FT-IR, and XRD analysis in addition to the previous preliminary characterizations.

4.2.1 **Morphology**

Both samples D and S show heterogeneous morphology and composition as revealed by microscopic examination of precursors revealed by SEM techniques. Figures 4.2 (a, b), (c, d), and (e, f). According to qualitative EDS analysis (Figure 4.3a and b), the sponge-like form shown in Figure 4.2b can be attributed to an organic water-repellent compound that adhered to

the bubbles during the dissolved air flotation process. The main elements were carbon and oxygen, with Silica and Aluminium at trace concentrations. Carbon analysis by EDS for many particles was not considered because the sample was coated on a carbon tape, which could produce bias results; it was only used when concentrating on a single particle.

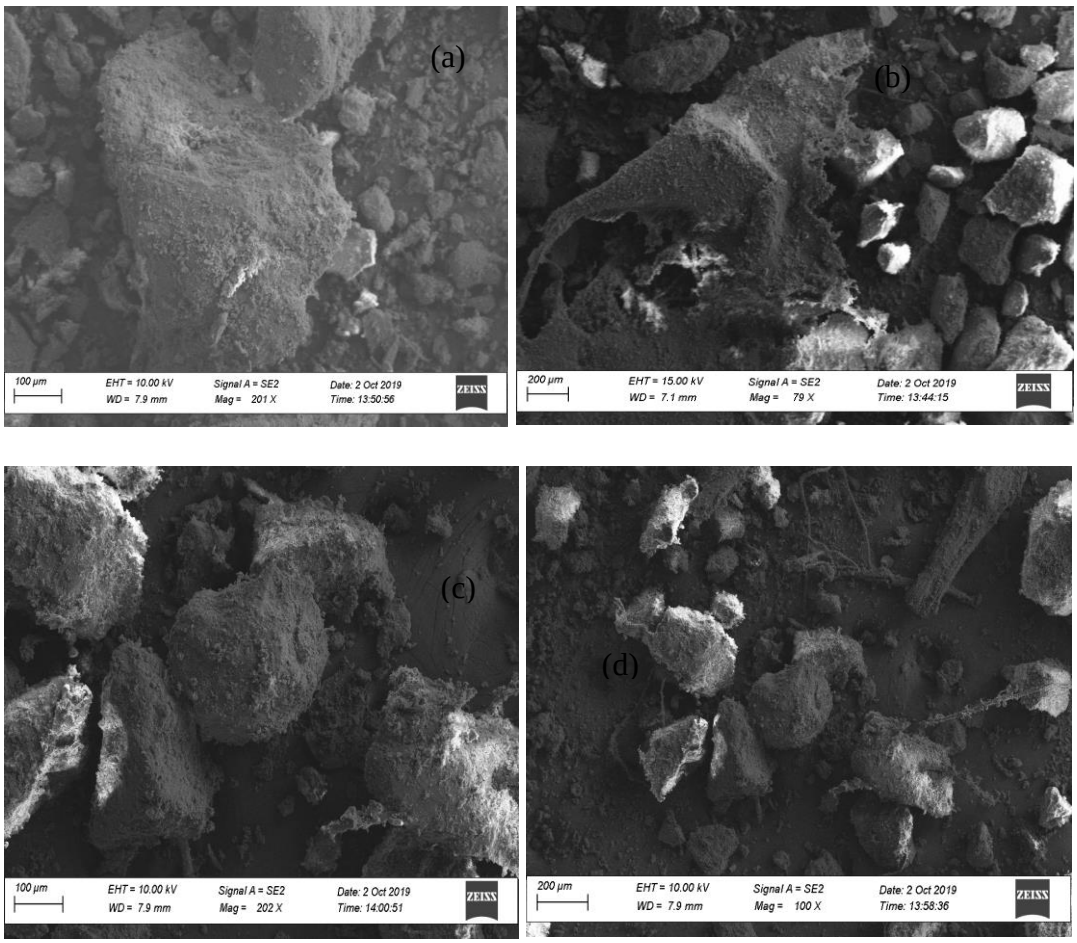
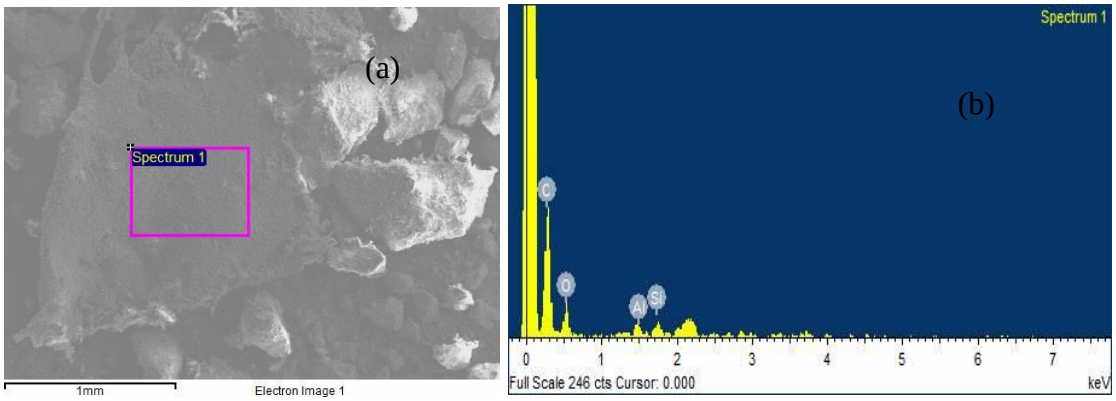


Figure 4.2 microscopic observation of sewage sludge precursor D: (a) and (b), S: (c) and (d).



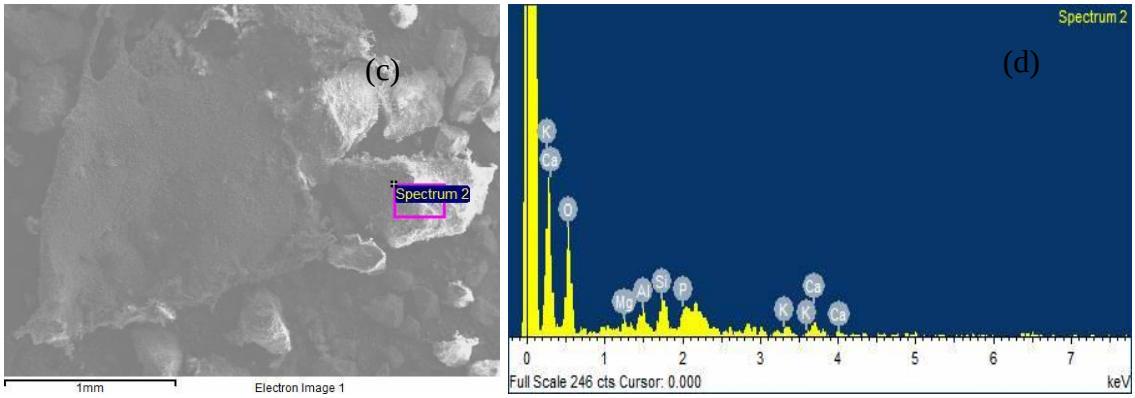


Figure 4.3 Elemental analysis of D precursors particles by EDS

In comparison to D particle (Figure 4.4 b and d), the qualitative analysis of particle (Figure 4.4 a and c) from S sample by EDX revealed an advanced inorganic character in composition, possibly sourced from domestic wastewater particles settled during decantation or solid-liquid separation process.

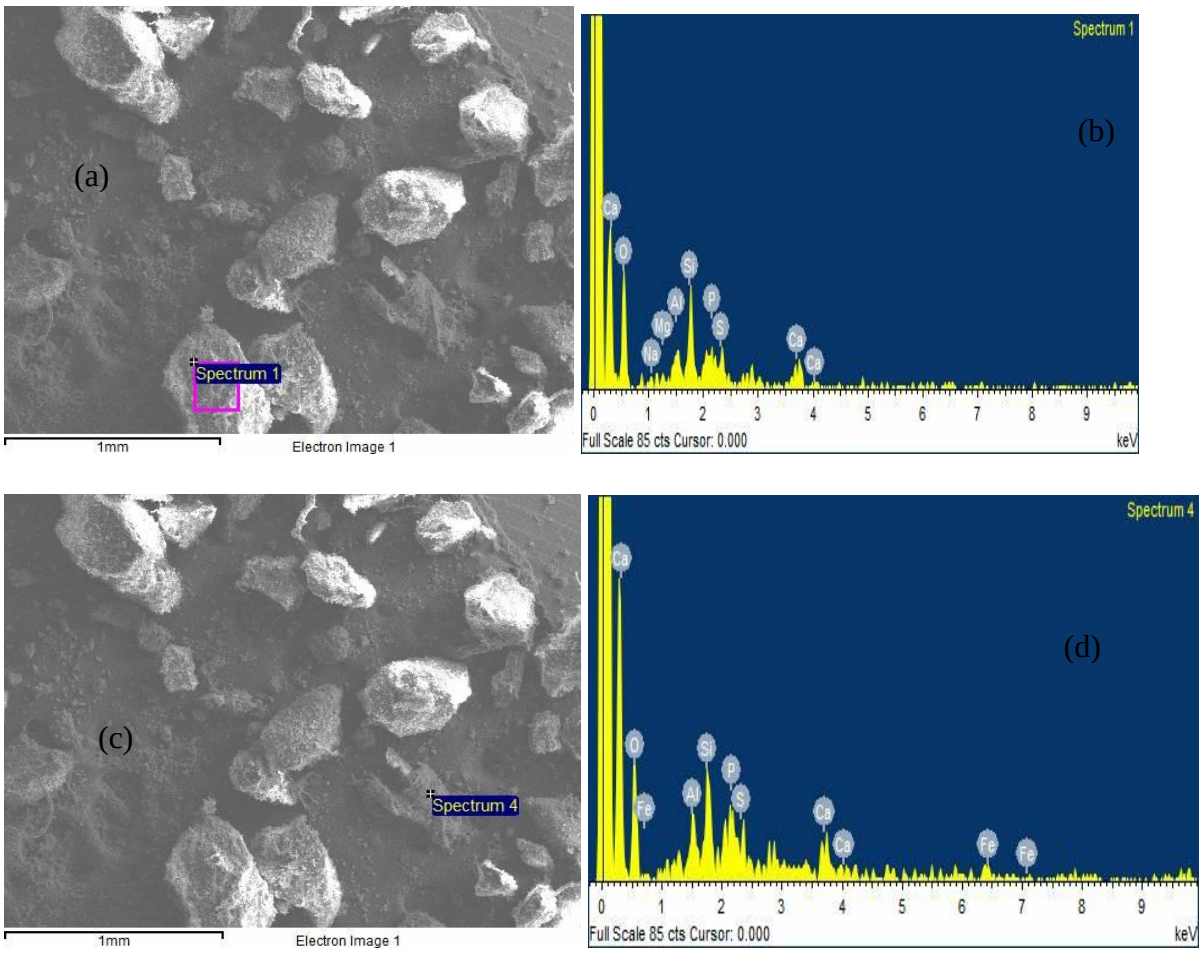


Figure 4.4 Elemental EDS analysis of S sample

Figure 4.5.a shows the microscopic examination of the sorbent after activation. Pyrolysis and washing stages may have facilitated cavity formation of highly formed cavities due to the remarkable depletion of inorganic and organic components (Gupta & Garg, 2015). Furthermore, some particles (Figure 4.5a and 4.5b) lack or have insignificant cavities, which may be attributable to a lack of volatile and decomposed matter escaping to facilitate porosity (J. Li et al., 2018). The EDS qualitative analysis (Figure 4.5.c) of the local particle (4.5.b) revealed inorganic characteristics as well as the presence of K and Cl from activation and washing, respectively.

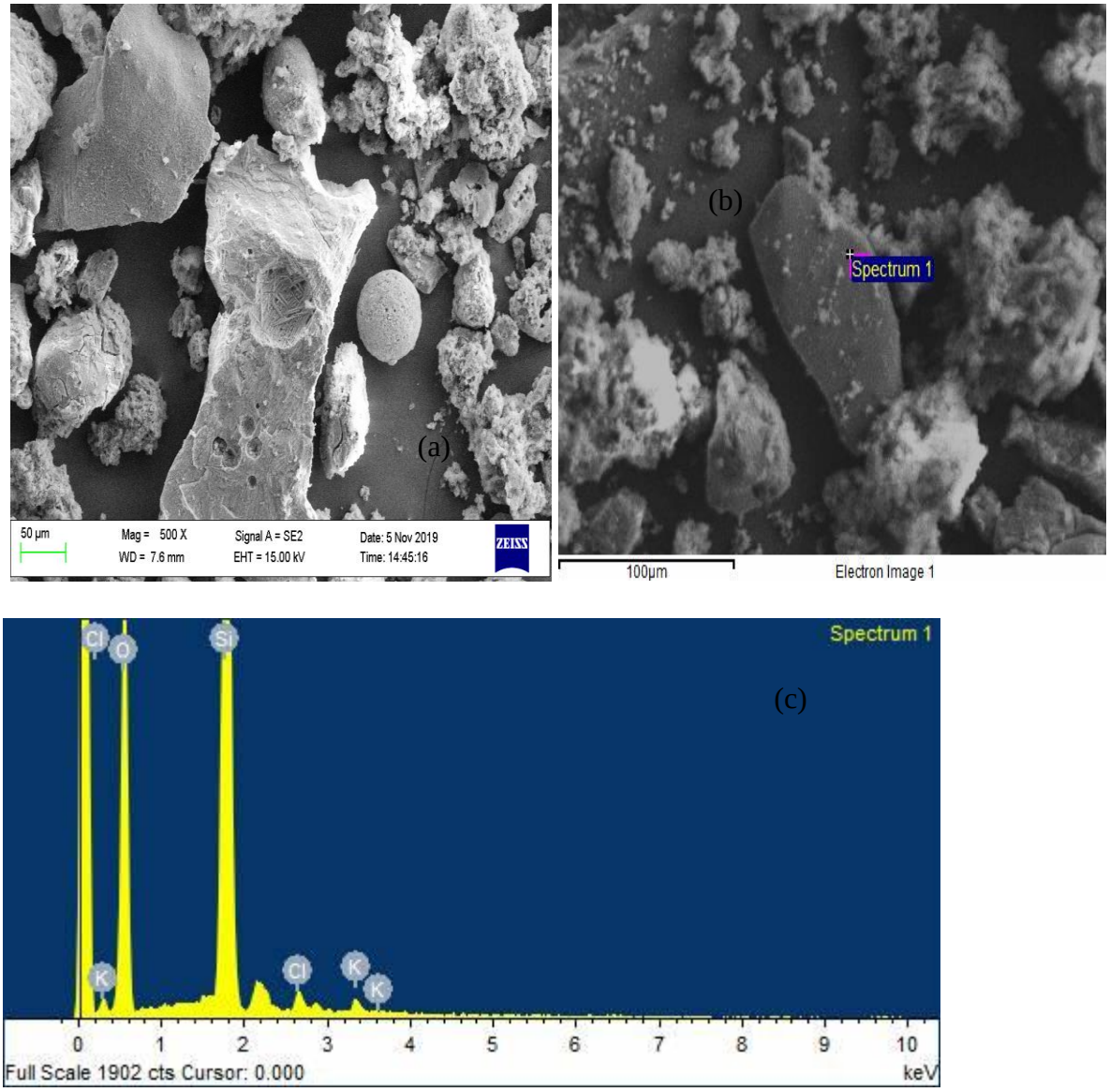


Figure 4.5 SEM microscopic analysis of SBAC, (a) multiple particle (b) focus on particle without cavity after activation and (c) qualitative analysis of the targeted particle

4.2.2 **Functional group**

Figure 4.6 shows the FT-IR spectra of raw material with wavenumbers ranging from 450 cm^{-1} to 4000 cm^{-1}. Sludge feedstock exhibited similar spectra shape with the lowest transmittance in the fingerprint field, as S has lower transmittance than D, implying that the former contains more functional classes. Reading the peaks spectra wavelengths from left to right, the peak observed at 3688-3619 cm^{-1} is attributed to OH-kaolinite and gibbsite lattice stretching(Diffo et al., 2015; Reig et al., 2002), 2988-2901 cm^{-1} to -C-H group vibration (Fan et al., 2016; Yang et al., 2019), 1631 cm^{-1} and 1538 cm^{-1} to sulphur and nitrogen functional groups, respectively (Fan et al., 2016). The shape of the shoulder peaks at 1050-1090 cm^{-1} was attributed to Si-C or Si-O-Si bands (Liang et al., 2020), C-O-C vibration (Fan et al., 2016), and finally, under 1000

cm^{-1}, the peaks at 749 cm^{-1}, 535 cm^{-1}, and 467 cm^{-1} were attributed to silica or calcium carbonate stretching (Al-Malack & Dauda, 2017; Reig et al., 2002). Discard coal has a lower transmittance from 1498 cm^{-1} peaks than FT-IR spectra sludge.1007 cm^{-1}, 1030 cm^{-1}, implying that waste coal contains more mineral elements.

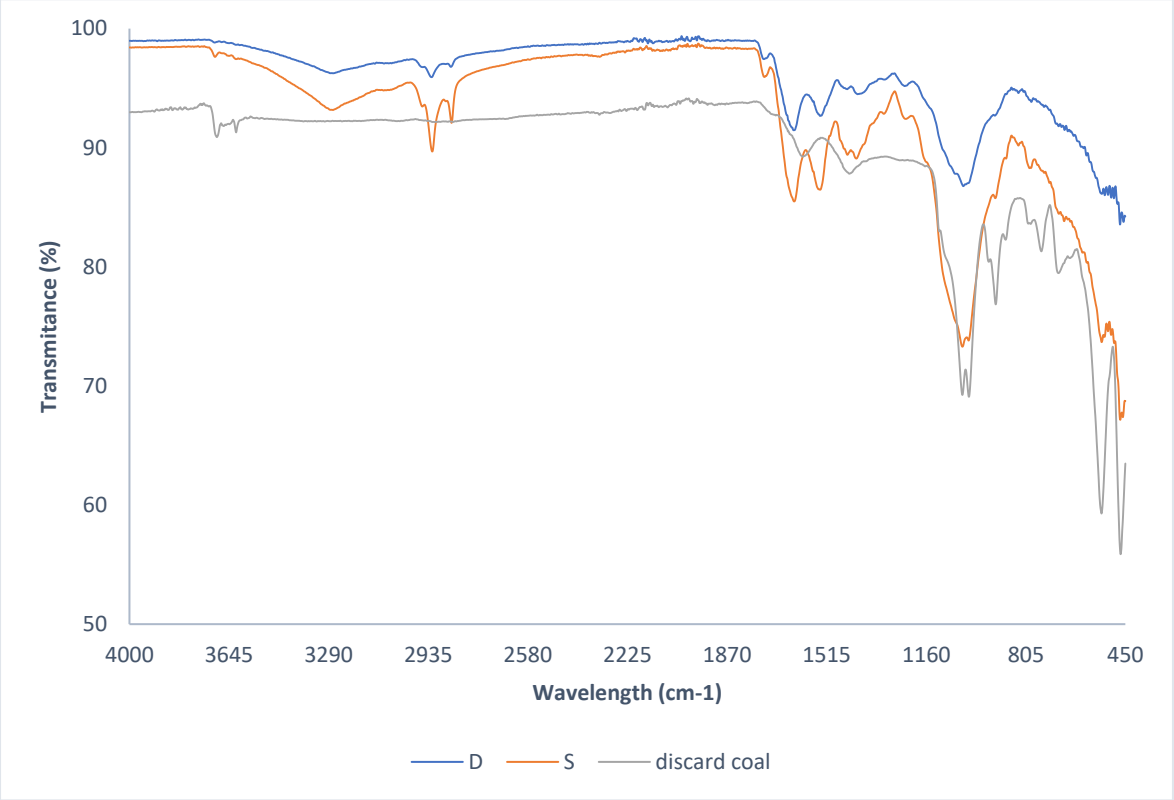


Figure 4.6 FT-IR spectra for precursors

The FT-IR spectrum of the SBAC exhibited almost identical shapes and peaks with different intensities regardless of the parameter involved in the synthesis process, as shown in Figures 4.7 and 4.8. The spectra have 6 main peaks, which are 3676 cm^{-1}, 2901-2998 cm^{-1}, 1394 cm^{-1}, 1225 cm^{-1}, and 892 cm^{-1} in all SBAC samples.

In comparison to feedstock spectra, the disappearance of the wavelength peak at 470 cm^{-1} and 500 cm^{-1} in SBAC could be due to inorganic matter solubilisation during the acid washing phase (Devi & Saroha, 2016; Hadi et al., 2015; Xu et al., 2015), while 798 cm^{-1} could be due to dehydrogenation reactions (J. Li et al., 2018) , 1631 cm^{-1} and 1538 cm^{-1} could be due to thermal degradation of protein for nitrogen related compound or sulphur (Fan et al., 2016).

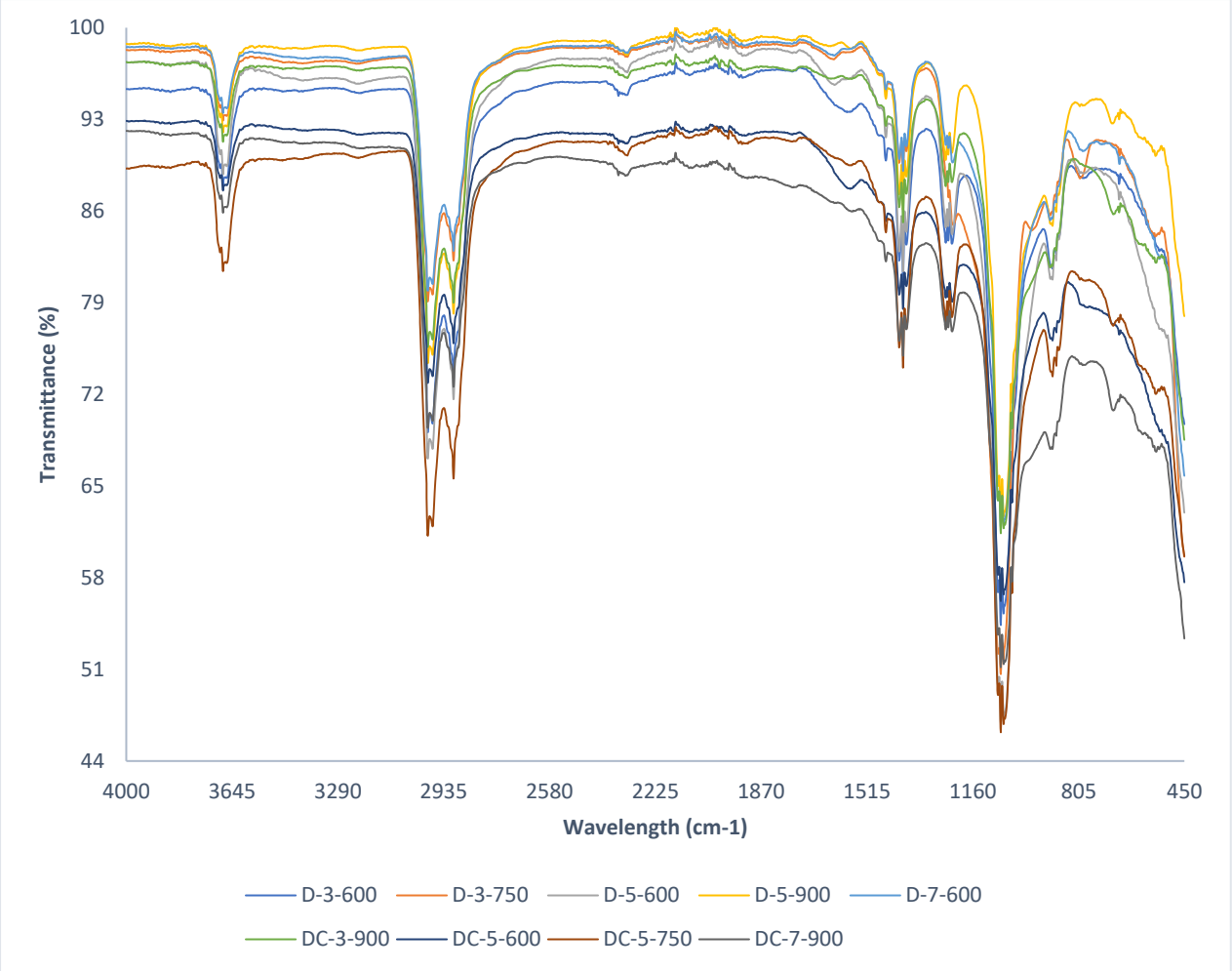


Figure 4.7 FT-IR spectra of SBAC with sludge D as precursor

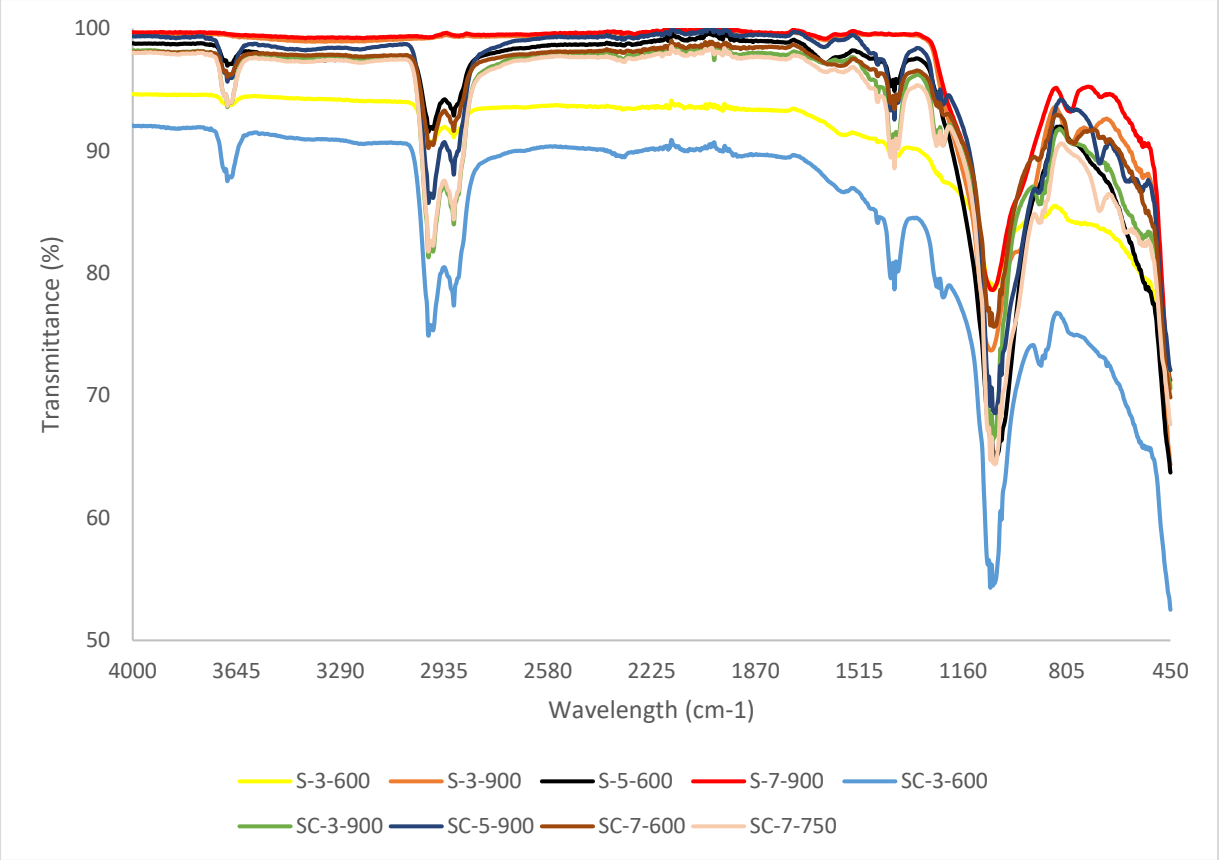


Figure 4.8 FT-IR spectra of SBAC with sludge S as precursor

The peaks associated with C-H group stretching not only shifted slightly from 2859-2922 cm^{-1} in feedstock to a higher value (2901-2988 cm^{-1}) in SBAC, which can be related to the presence of saturated group (Tao et al., 2015) but also transmittance decreased after activation for all samples, which is in contrast to some literature (Fan et al., 2016; Huang et al., 2017; Yang et al., 2019) in which it was argued that the disappearance of the peaks was due to the decomposition of fatty organic matter and dehydration (Yang et al., 2019). The organometallic formation may be a possible explanation for the decreased transmittance of SBAC pyrolyzed at lower temperatures followed by depletion as temperature rises; for example, the abundance of functional groups (hydroxyl, carboxyl) on the biochar surface synthesized from sewage sludge pyrolyzed at 300 °C reduced extractable cations due to the formation of organometallic compounds (Lee et al., 2018; Lu et al., 2013). The functional groups present in SBAC can be summarized as O-H, C=C, C=O, aliphatic C-H, Si-C, Si-O-Si, phosphate, and carbonate, based on the observations. FT-IR spectra of SBAC synthesized under analogous conditions can be overlaid (Figure 4.9, 4.10, 4.11 and 4.12) to demonstrate the effect of factors involved in pyrolysis conditions on functional groups:

a. D-5-600 and DC-5-600

Due to the higher content in silica and the decomposition or formation of -CH bonding such as organometallic compound, the effect of discard coal addition on SBAC functionalities is visible in the gap peaks ranging from 1000 cm^{-1} to 1100 cm^{-1} and 2800 cm^{-1} to 3000 cm^{-1} in Figure 4.9.

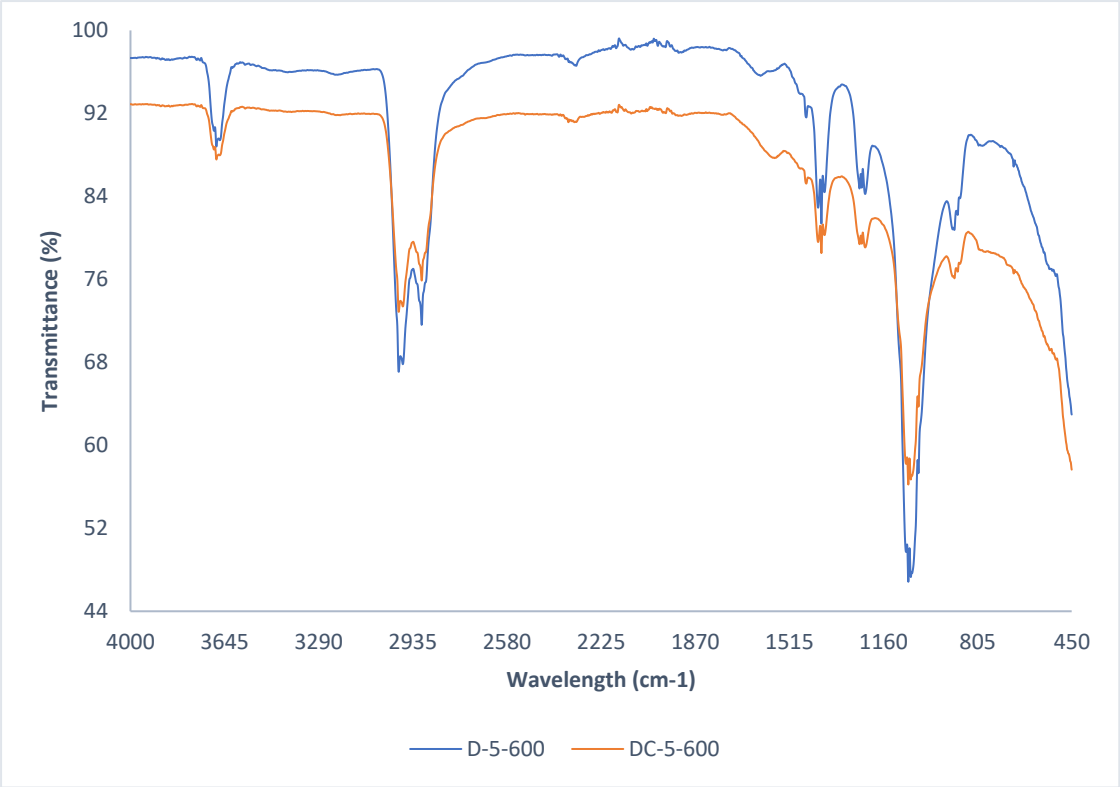


Figure 4.9 FT-IR spectra of D-5-600 and D C-5-600

b. S-3-600 and SC-3-600

In contrast to SBAC sourced from D (Figure 4.9), SBAC without discard coal had higher transmittance across the wavelength spectrum than SBAC blended with discard coal. This may be due to the consistency of Sludge S, as shown by the TGA curve (Figure 4.1), which may have caused lower sludge decomposition.

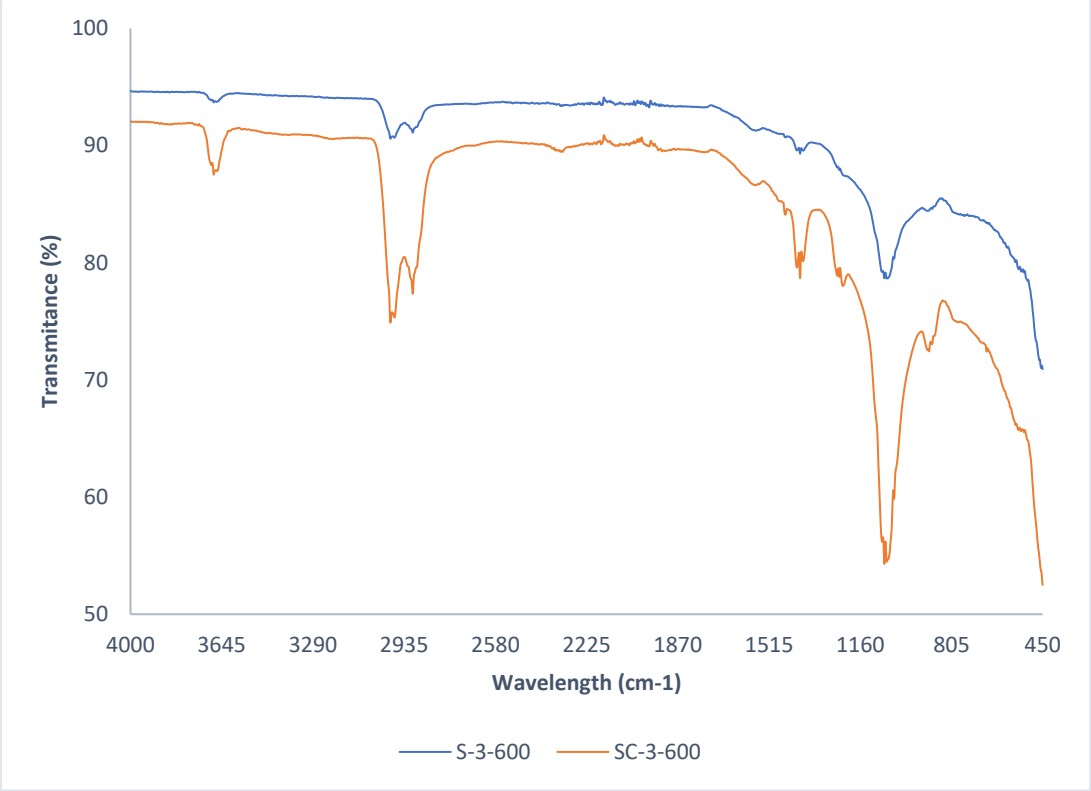


Figure 4.10 FT-IR spectra of S-3-600 and SC-3-600

c. SC-3-600 and SC-3-900

The influence of temperature can be seen in the FT-IR peak (Figure 4.11) of SC-3-600 and SC-3-900, where the SC-3-900 transmittance intensity outperforms SC-3-600 due to the decomposition of acidic functional groups at higher temperatures (Devi & Saroha, 2016). One may also argue that as part of this work, the compound associates to (-C-H) bonding to 2800 cm^{-1} and 3000 cm^{-1} underwent also thermal decomposition.

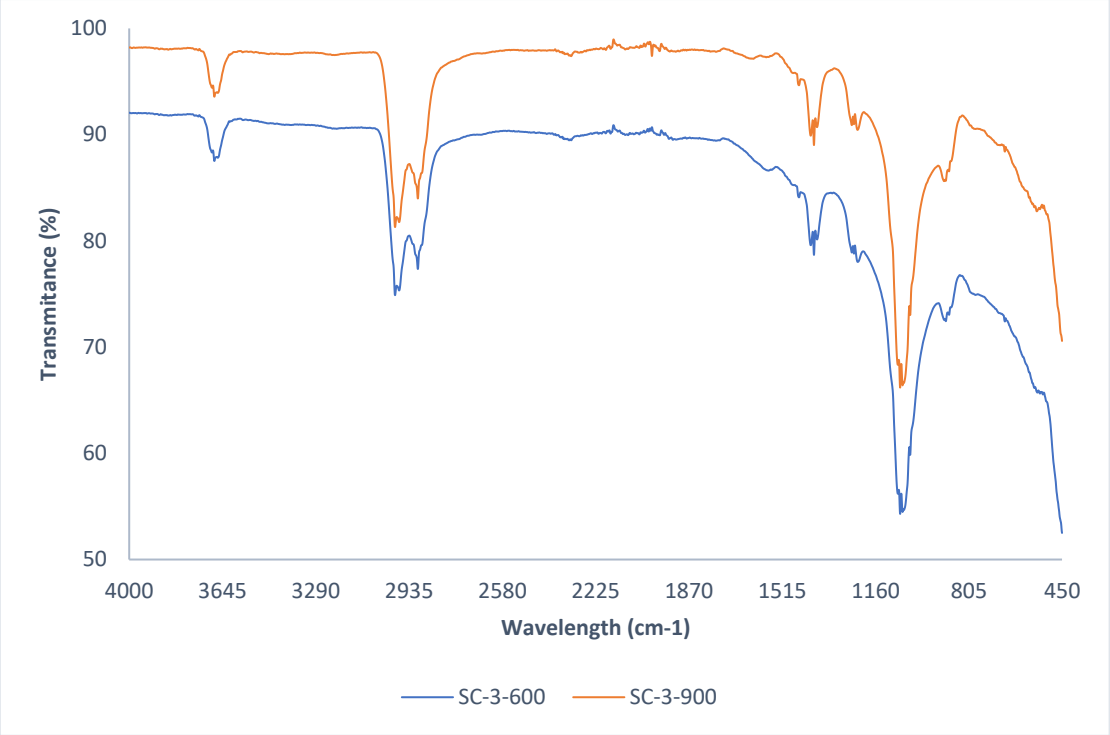


Figure 4.11 FT-IR spectra of SC-3-600 and SC-3-900

d. D-3-600 vs S-3-600

The FT-IR spectra of SBAC Pyrolyzed at 600 °C with a KOH concentration of 3M from sludge D and S (Figure 4.12) showed a difference in transmittance intensity, which could be due to: i) relative stability of sludge S versus D as per TGA curve (Figure 4.1), which leads to further decomposition of the former than the latter; (ii) formation of organometallic compounds, which could induce the presence of -C-H vibrations bonding in both SBAC, especially more in the one from sludge D as it is less thermal stable than S.

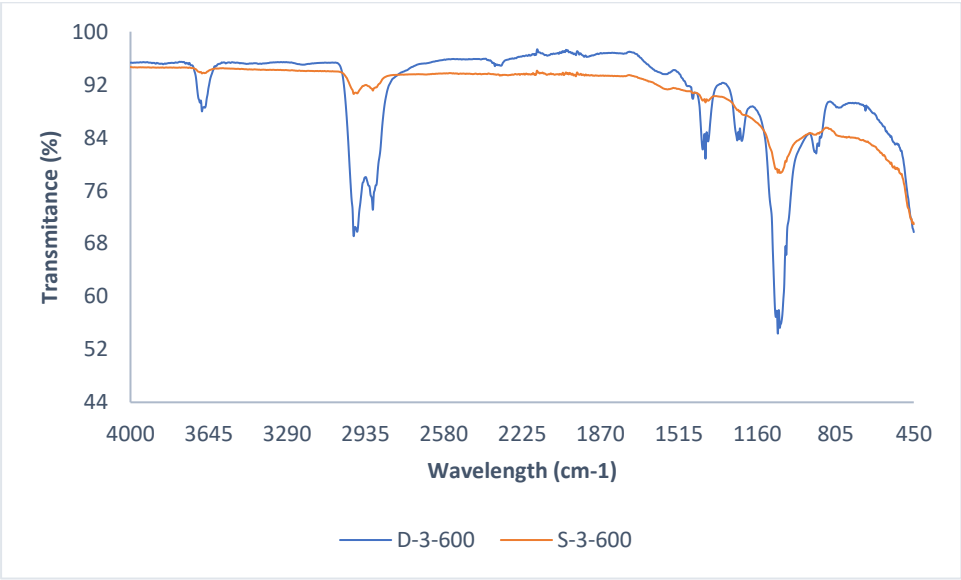
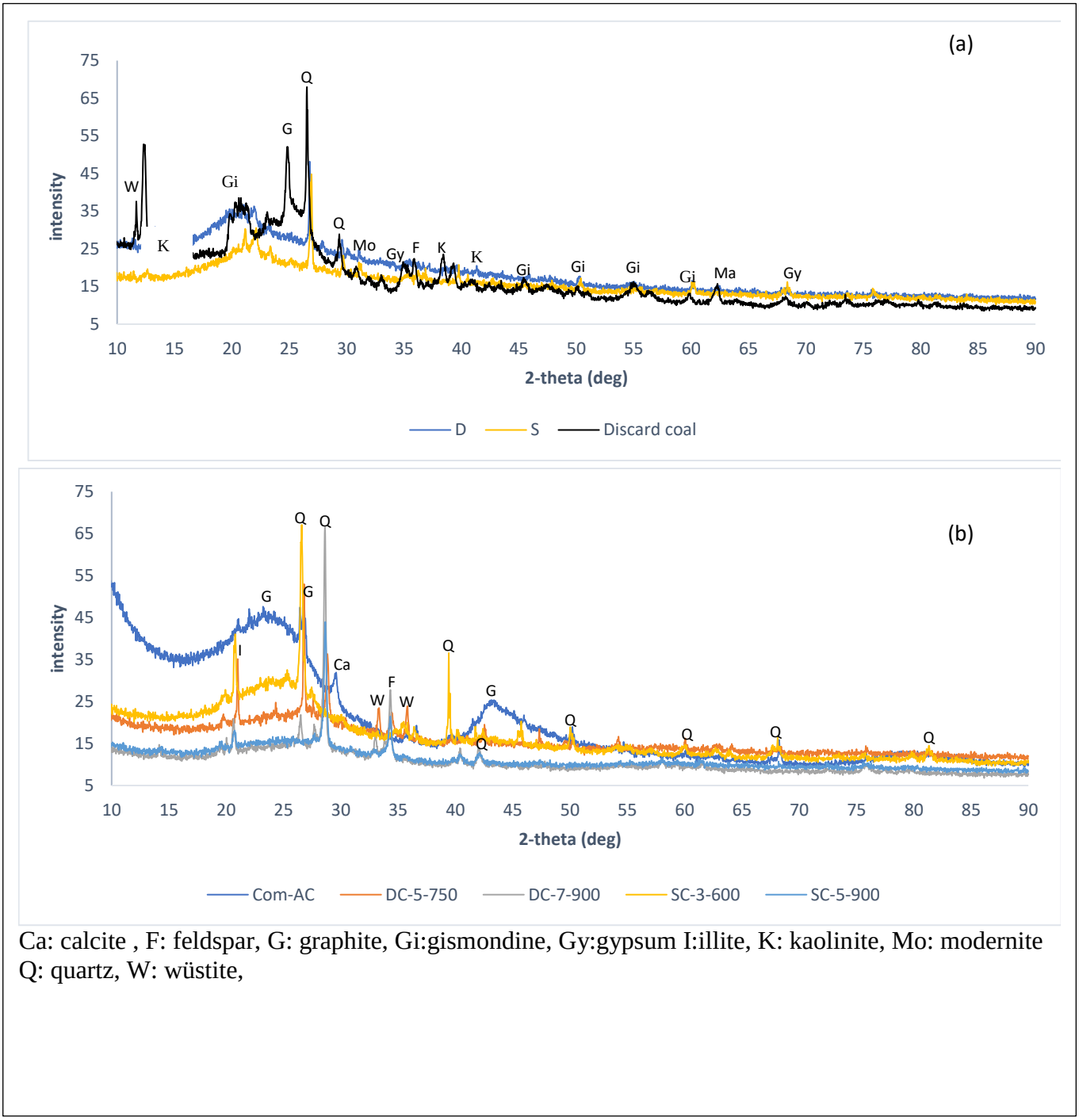


Figure 4.12 FT-IR spectra of D-3-600 and S-3-600

4.2.3 **Crystalline phase composition**

Com-AC has broad peaks ($2\theta = 25{,}3°$ and $2\theta = 44{,}6°$) linked to its amorphous phases, while the XRD pattern (Figure 4.13a and b) demonstrated mineral phases transformation from broad peak in the precursors to sharp in the manufactured absorbent, which clarified transition from amorphous to crystalline phase due to pyrolysis. XRD verified the existence of minerals such as wustite, quarts, illite, and feldspars in SBAC. It is worth noting that the presence of alkaline earth elements in the minerals (feldspars and illite) led to magnesium, calcium, and iron being classified as exchangeable cations (Gupta & Garg, 2015).



Ca: calcite , F: feldspar, G: graphite, Gi:gismondine, Gy:gypsum I:illite, K: kaolinite, Mo: modernite Q: quartz, W: wüstite,

Figure 4.13 XRD graph of feedstock (a), SBAC and Com-AC (b)

4.3 design Responses

The parameters were coded as follow: A= Reagent concentration, B= Temperature, C= sample type, D= discard coal.

4.3.1 **Porosity development**

Response 1: surface area

The surface area response analysis of variance (Table 4.3) with p-value 0,0196 indicates that the model is significant, with D, AB, and B^2 being the significant variables. The actual equation is summarized in Table 4.4.

Table 4.3 Analysis of variance (ANOVA) of surface area response

Source	Sum of Squares	Df	Mean Square	F-value	p-value	
Model	1,982E+05	12	16514,12	3,89	0,0196	significant
A-KOH	15459,83	1	15459,83	3,64	0,0853	
B-Temperature	4281,02	1	4281,02	1,01	0,3388	
C-Sludge type	1909,92	1	1909,92	0,4502	0,5174	
D-Discard Coal	32076,31	1	32076,31	7,56	0,0205	
AB	26570,55	1	26570,55	6,26	0,0313	
AC	6933,65	1	6933,65	1,63	0,2300	
AD	11133,36	1	11133,36	2,62	0,1363	
BC	6042,19	1	6042,19	1,42	0,2602	
BD	1477,85	1	1477,85	0,3484	0,5681	
CD	1109,94	1	1109,94	0,2616	0,6201	
A^2	545,99	1	545,99	0,1287	0,7272	
B^2	73335,56	1	73335,56	17,29	0,0020	
Residual	301,9168	5	60,3834		0,1825	Not significant
Lack of Fit	122,3169	5	24,4634			
Pure Error	2,406E+04	22				
Cor Total	301,9168	17	60,3834			

Table 4.4 Actual equation of microporosity percentage response

Microporosity	=
Sludge type	D
Discard coal	No
+84,24646	

-2,14643	KOH
-0,062446	Temperature
Sludge type	D
Discard coal	Yes
+109,74339	
-2,14643	KOH
-0,062446	Temperature
Sludge type	S
Discard coal	No
+64,87262	
-2,14643	KOH
-0,062446	Temperature
Sludge type	S
Discard coal	Yes
+90,36954	
-2,14643	KOH
-0,062446	Temperature

The addition of discard coal increased surface area significantly in S-3-600 (54,39 m^2/g) and SC-3-600 (281,72 m^2/g), which represents a 5-fold rise, and similarly in D-5-600 (76,03 m^2/g) and DC-5-600 (149,35 m^2/g); this pattern is consistent with previous studies as detailed in section (2.7.1). This upward trend in surface may be attributed to discard coal's lower ash content as compared to sludge precursor. From Figure 4.14 to 4.17, the surface area increases with temperature and activating reagent concentration regardless of the presence of discard coal; however, above 800 °C, the surface area decreases; this trend is consistent with previous studies in which, was reported that temperature allows the reactions to be potent and complete, but that at higher temperatures, the merging of current pores reduces (Devi & Saroha, 2016). Excessively high reagent concentrations have a negative effect on the porosity of the SBAC, causing micropores to expand into macropores due to over-activation, and salt crystals released as temperature grew could block the pore (Liang et al., 2020), as well as because hyper-activation causes the pore wall to collapse, resulting in partial demolition of microporosity (Xu

et al., 2015).The surface area decreased by more than 6 times and half from 281,72 m^2/g (SC-3-600) to 43,29 m^2/g (SC-3-900), encapsulating the situation.

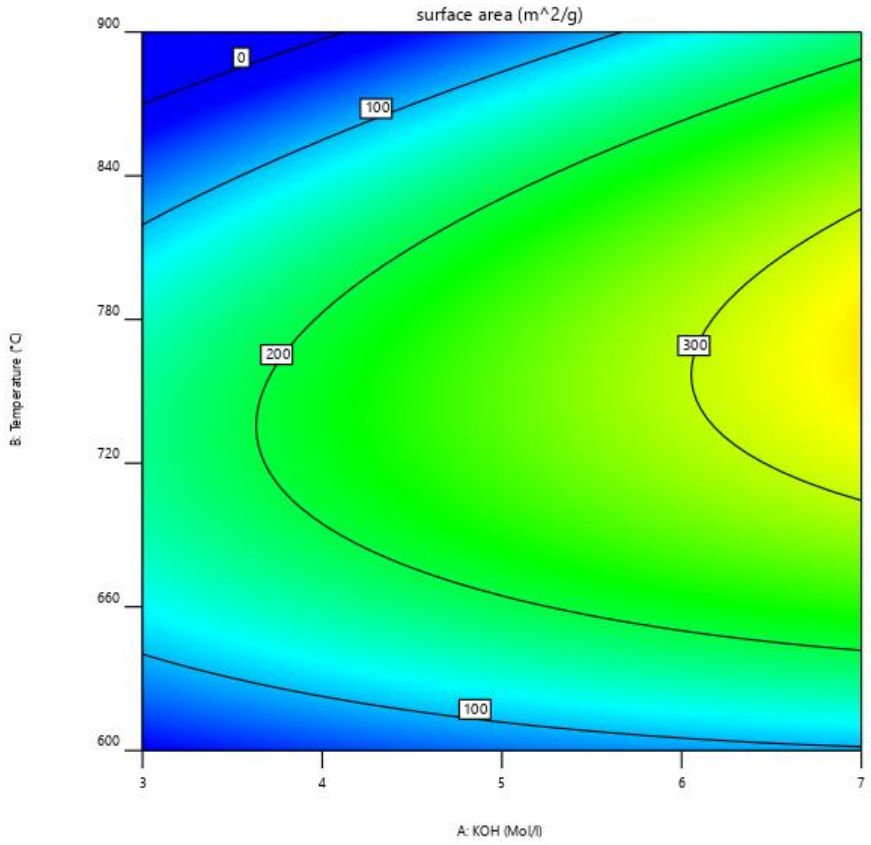


Figure 4.14 graphic of SBAC surface area from Sludge D without discard coal

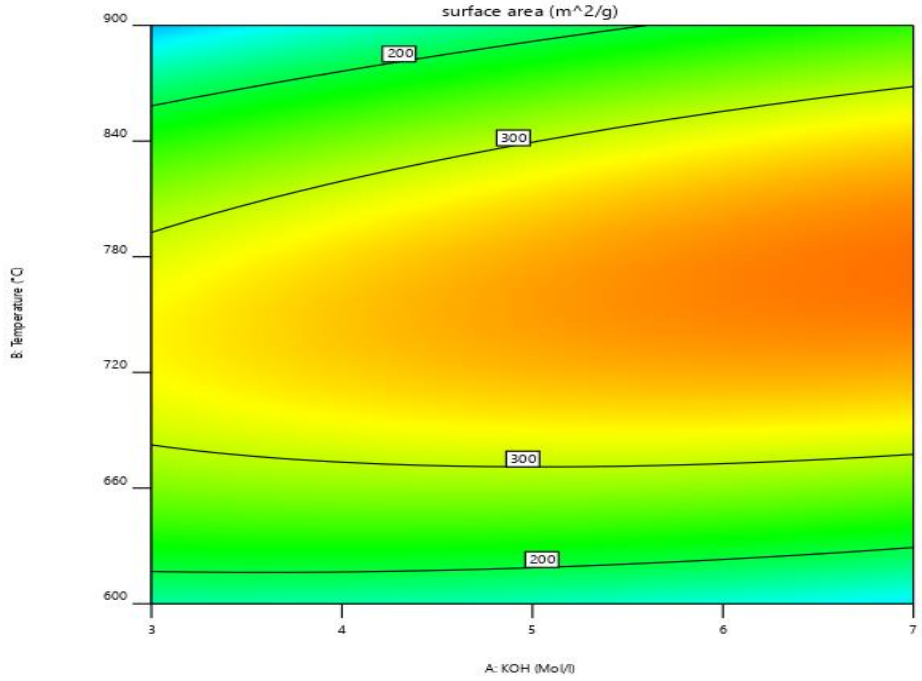


Figure 4.15 graphic of surface area from Sludge D mixed with discard coal

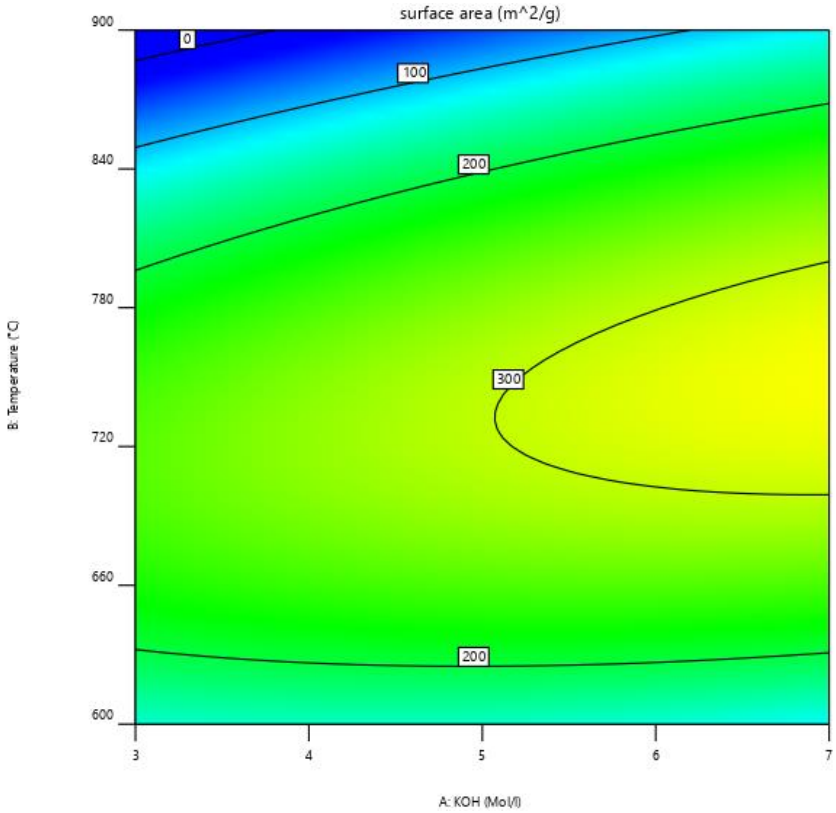


Figure 4.16 graphic of SBAC surface area from Sludge S without discard coal

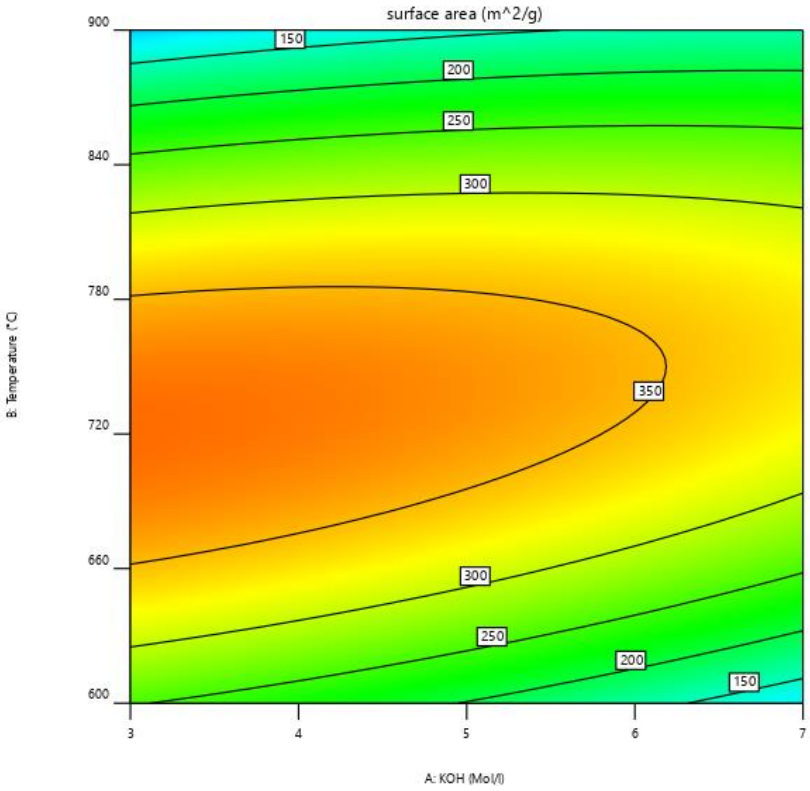


Figure 4.17 graphic of SBAC surface area from Sludge S with discard coal

Response 2: micropore area proportion

The micropore area percentage response analysis of variance (Table 4.5) with a p-value of 0,0007 indicates that the model is important, with B, C, and D being the significant factors since their p-values are less than 0,05 and the actual equation is found in Table 4.6.

The temperature augmentation decreased the fraction of micropore surface area in SC-3-600 and SC-3-900 from 56,17 percent to 9,80 percent, respectively, due to micropore wall collapse with temperature (Abdulsalam et al., 2019; G. Xu et al., 2015), as compared to S-3-900, which has no micropore surface area.

Secondly, as compared to D-3-600, the addition of coal discard increased the microporosity percentage, with about half of the surface (55,55%) being micropore versus 79,98% for DC-3-600. S-3-600 reported a fraction of 12 percent micropore surface area when discard coal was added, compared to 56 percent for SC-3-600. This may be due to a reduction in inorganic elements; the discard coal mixture reduces inorganic content and compensates by increasing carbon content, which is thought to be more conducive to cavity formation during activation (Gupta & Garg, 2015; Hadi et al., 2015). Finally, relative to sludge S, the D-type sludge has a

higher proportion of micropore surface area. The sludge based activated carbon (SBAC) from D has 55 percent of its surface area as micropore compared to 12 percent for S at the same temperature (600 °C), KOH concentration (3M), and without discard coal blending. The fact that sludge with low polymerisation has a higher proportion of micropore surface area may explain this result (Smith et al., 2009). This study suggests that sludge D has a lower polymerisation ratio than sludge S, resulting in a greater fraction of micropore surface in the adsorbent derived from the former.

Table 4.5 Analysis of variance (ANOVA) of Microporosity percentage response

Source	Sum of Squares	df	Mean Square	F-value	p-value	
Model	6837,68	4	1709,42	7,92	0,0007	Significant
A-KOH	309,67	1	309,67	1,43	0,2467	
B-Temperature	1686,51	1	1686,51	7,81	0,0120	
C-Sludge type	2144,10	1	2144,10	9,93	0,0055	
D-Discard Coal	3581,38	1	3581,38	16,58	0,0007	
Residual	38,8714	8	4,8585			
Lack of Fit	25,8740	3	8,6246		0,1256	Not Significant
Pure Error	13,01740	5	2,6034			
Cor Total	6876,5514	12				

Table 4.6 Actual equation of microporosity percentage response

Microporosity	=
Sludge type	D
Discard coal	No
+84,24646	
-2,14643	KOH
-0,062446	Temperature
Sludge type	D
Discard coal	Yes
+109,74339	
-2,14643	KOH

-0,062446	Temperature
Sludge type	S
Discard coal	No
+64,87262	
-2,14643	KOH
-0,062446	Temperature
Sludge type	S
Discard coal	Yes
+90,36954	
-2,14643	KOH
-0,062446	Temperature

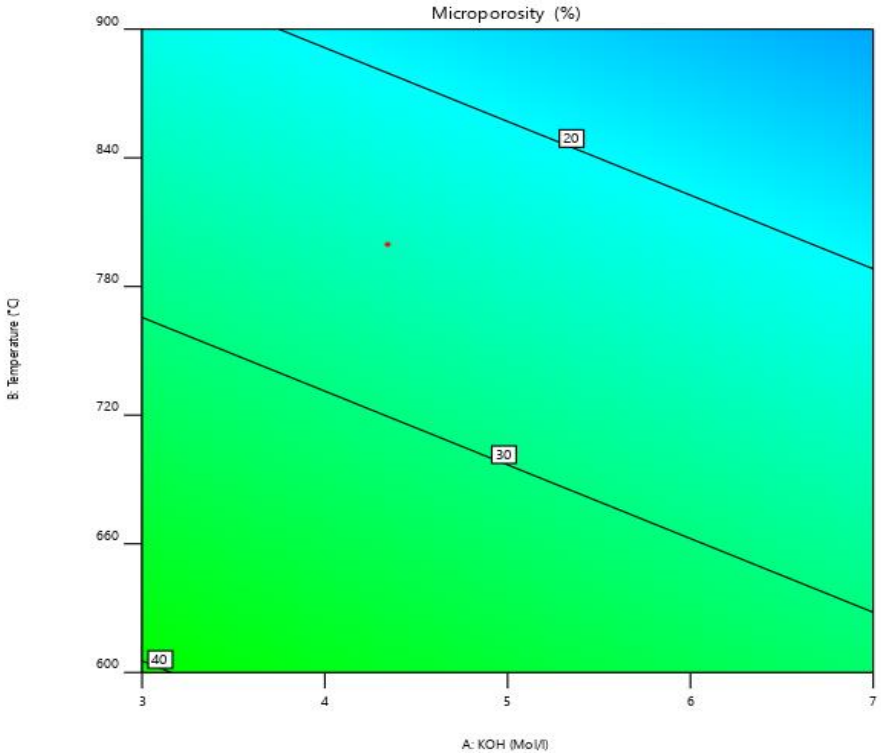


Figure 4.18 Graphic of SBAC microporosity from sludge D without Discard coal

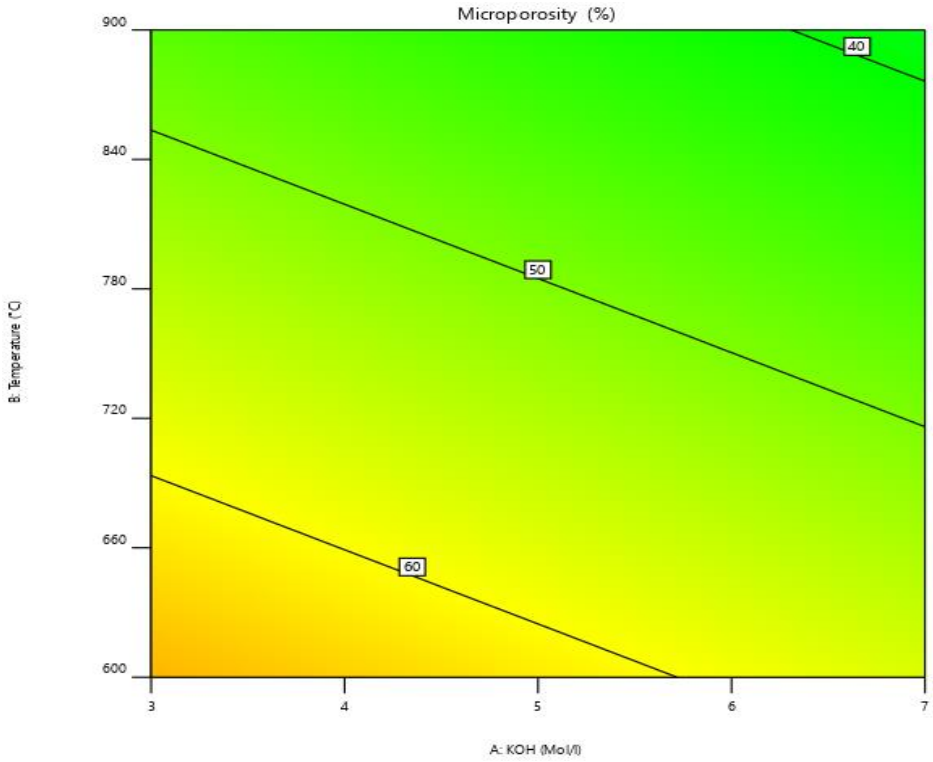


Figure 4.19 Graphic of SBAC microporosity from sludge D with Discard coal

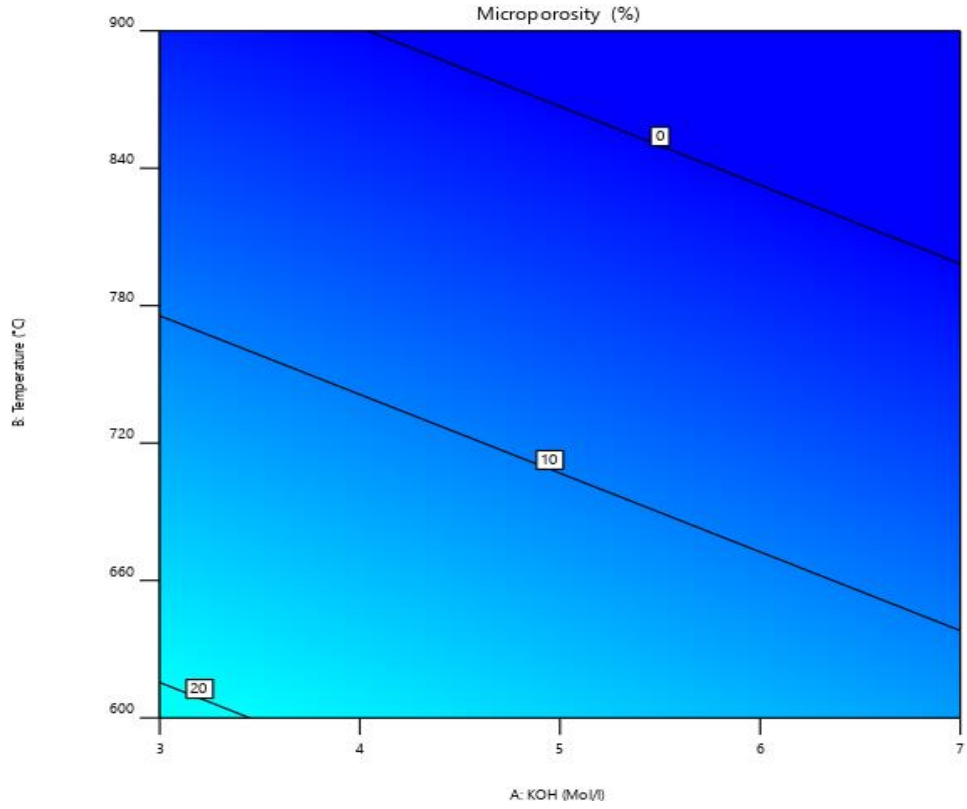


Figure 4.20 Graphic of SBAC microporosity from S-sludge without discard coal

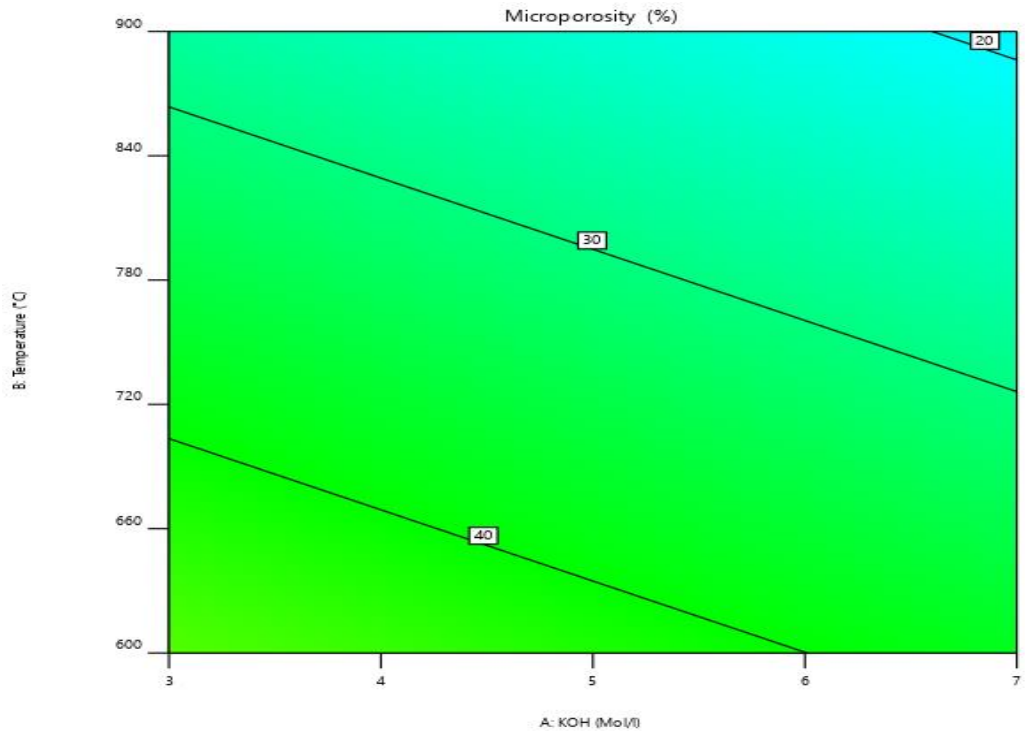


Figure 4.21 Graphic of SBAC microporosity from Sludge S with discard coal

After activation, the sorbent had a higher porosity than the initial material, despite having a marginal surface area (Table 4.2). Although the addition of discard coal improved the structure properties of SBAC, as shown in Table 4.7, the values obtained in this study are lower than those obtained by previous researchers. This trend may be explained by the lower carbon content of the sorbent and its higher inorganic composition, where cavities are unlikely to be fostered (J. Li et al., 2018), as well as XRD analysis (Figure 4.13.b).

Table 4.7 Comparison of structural properties of chemically activated SBAC from literature

		Activation conditions			Physical properties						
Sludge type	Feedstock Added	Time (min)	Temp (°C)	(Sludge/activating) Ratio	S_{Tot} (m^2/g)	S_{micro} (m^2/g)	V_{tot} (cm^3/g)	V_{micro} (cm^3/g)	C (%)	H/C	Reference
Thermally Dried (spherical aggregate)	-	60	700	5g NaOH:5g sludge	179	46,3	0,253	0,0085	-	-	(de Andrés et al., 2013)
Primary	-	60	600	w/w($ZnCl_2$): 1:3	505,65	-	0,288	-	64,75	0,043	(Gupta & Garg, 2015)

Dewatered	Bagasse (w/w) 50%	30	800	[sludge-bagasse/KOH (3M)]:1/3	806,57	-	0,678	-	44,82	0,14	(Tao et al., 2015)
-	-	60		KOH, w/w 1:1	550	-	0,112	-	16,7	0.052	(dos Reis, Adebayo, et al., 2016)
-	-	90	700	5 M $ZnCl_2$, w/w:1:2	385	213	0,36	0,01	-	-	(Liadi et al., 2018)
-	-	120	700	400g/l KOH and 100 g sludge	127,6	13,23	0,231	0,005	6,87	0.091	(Z. Li et al., 2018)
-	Coconut shell (w/w) 50%	60	800	[Sludge/2,5 M KOH] 1:1,5	680,34	-	0,73	0,49	-	-	(Liang et al., 2020)
Digested dewatered	Discard coal 50 %	90	600	3M KOH for 3/2 sludge (v:w)	281,72	158,49	0,342	0,075	45,23	0,0164	This work
			900	5M KOH for 3/2 sludge (v:w)	422,09	111,15	0,453	0,05	2,01	0,000	
Primary dissolved air flotation		90	750	5M KOH for 3/2 sludge (v:w)	312,79	188,65	0,366	0,089	23,612	0,0192	
			900	7M KOH for 3/2 sludge (v:w)	247,57	71,97	0,264	0,032	15,460	0,000	

The sorbents in Table 4.7 are mesoporous, as seen by the pore size distribution curve (Figure 4.22), which shows that all of the sorbents have a peak around 4.1nm, and the isotherm N_2 adsorption-desorption curves (Figure 4.23), which can be assimilated to type IV isotherm with a hysteresis loop associated with capillary condensation involved in the mesopores of the sorbent (Huang et al., 2017), this observation is in agreement with previous studies from which SBAC chemically activated with KOH presented a prevalence mesoporous characteristic(Z. Li et al., 2018; Liang et al., 2020; Yang et al., 2019; Zhang et al., 2019).

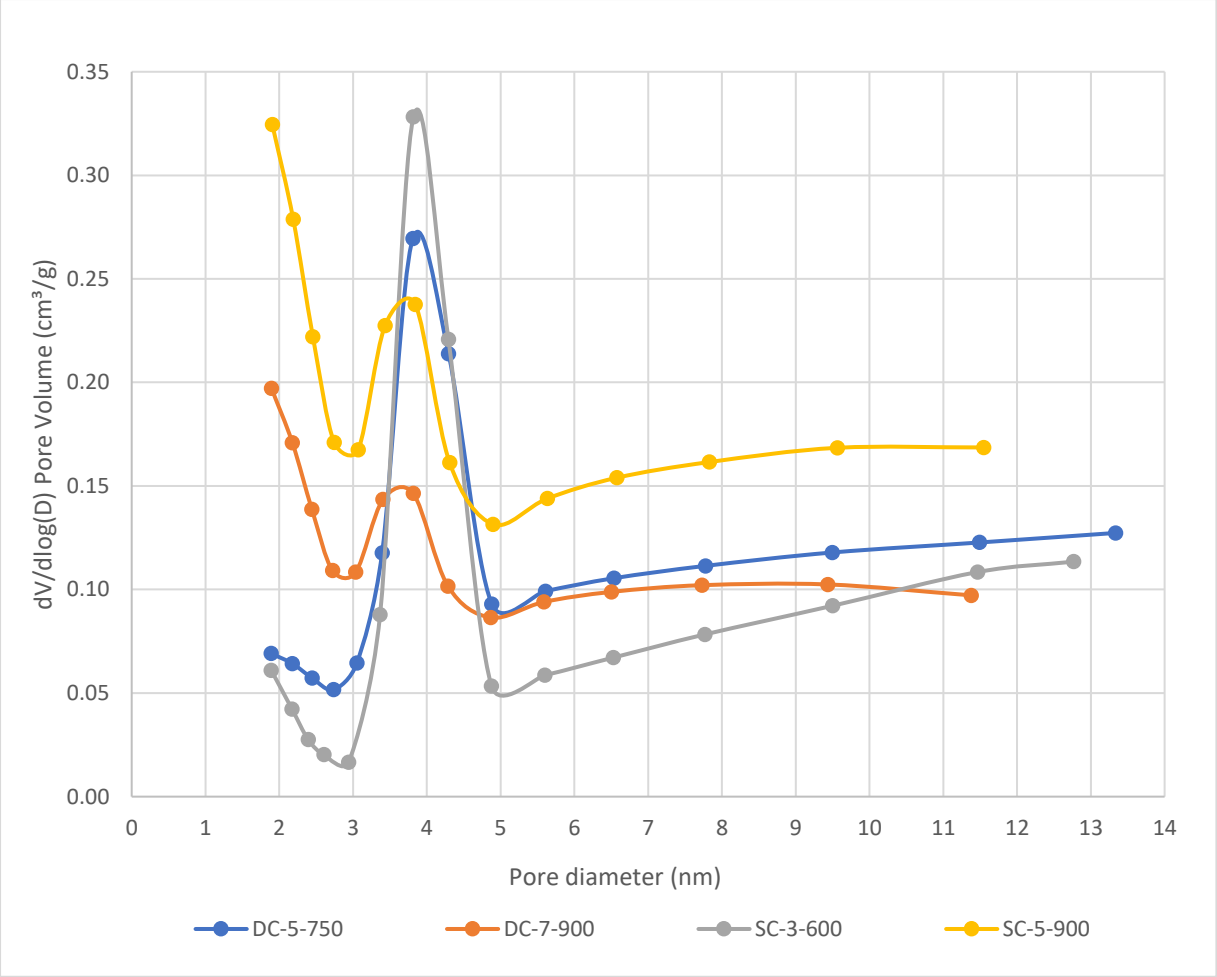


Figure 4.22 pore size distribution of adsorbents

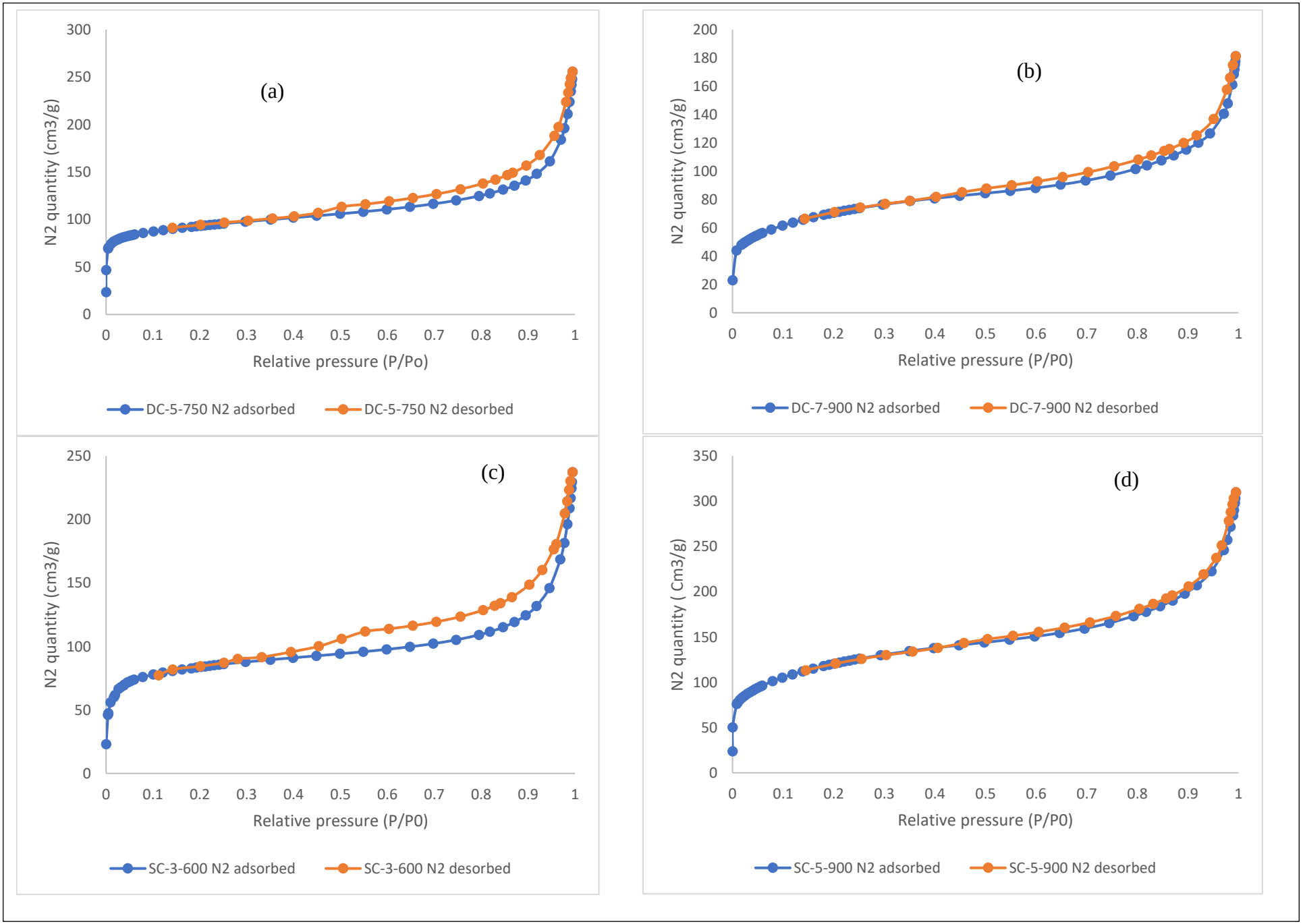


Figure 4.23 N2 adsorption-desorption isotherm (a) DC-5-750 , (b) DC-7-900, (c) SC-3-600 and (d) SC-5-900

Table 4.8 Summary of experimental design responses

		Activation conditions				Responses							
Run	Experiments	C1	C2	C3	C4	*R1*	R2	R3	R4	R5	R6	R7	R8
1	15	3	900	S	Yes	43,250	9,80	115,363	6,100	0,095	0,335	0,025	0,000
2	22	7	900	S	No	105,930	6,44	171,314	5,900	0,115	0,315	0,300	0,000
3	3	5	600	D	No	76,040	16,97	128,373	4,600	0,3225	0,09	0,000	0,014
4	14	3	600	S	Yes	281,720	56,17	117,247	4,400	0,915	0,335	0,000	0,016
5	11	3	900	S	No	27,230	0,00	104,745	7,600	0,3025	0,24	0,000	0,000
6	4	5	900	D	No	50,710	12,31	226,163	8,600	0,1925	0,275	0,166	0,000
7	10	3	600	S	No	54,390	12,96	156,758	4,800	0,155	0,26	0,000	0,022
8	8	5	750	D	Yes	312,790	60,31	124,007	6,600	0,17	0,315	0,000	0,019
9	18	7	750	S	Yes	422,110	26,33	137,340	6,600	0,23	0,315	0,038	0,000
10	9	7	900	D	Yes	247,570	29,07	85,667	9,200	0,08	0,72	0,000	0,000
11	5	7	600	D	No	100,510	39,66	146,959	3,800	0,2075	0,28	0,161	0,000
12	17	7	600	S	Yes	46,590	9,39	203,714	4,800	0,14	0,275	0,000	0,052
13	14	3	600	S	Yes	281,720	56,17	117,247	4,400	0,915	0,335	0,000	0,016
14	13	7	900	S	No	105,930	6,44	171,314	5,900	0,115	0,315	0,300	0,000
15	1	7	600	D	No	100,510	39,66	146,959	3,800	0,5175	0,235	0,161	0,000

16	12	5	600	S	No	211,540	6,40	190,858	5,700	0,16	0,27	0,000	0,000
17	7	5	600	D	Yes	149,350	79,98	128,097	3,000	0,21	0,305	0,004	0,026
18	1	3	600	D	No	55,300	55,55	51,624	7,600	0,2775	0,385	0,000	0,062
19	9	7	900	D	Yes	247,570	29,07	85,667	9,200	0,2075	0,28	0,000	0,000
20	6	3	900	D	Yes	115,090	45,80	158,586	7,700	0,18	0,245	0,000	0,000
21	16	5	900	S	Yes	134,980	47,55	224,103	7,500	0,115	0,31	0,207	0,000
22	2	3	750	D	No	126,860	18,96	139,586	6,700	0,2775	0,17	0,140	0,000
23	6	3	900	D	Yes	115,090	45,80	158,586	7,700	0,18	0,245	0,000	0,000
suggested Model						Quadratic	Linear	Quadratic	2FI	2FI	Linear	2FI	Quadratic
p-value						0,01958	0,0007	0,0092	< 0.0001	0,0179	0,3560	0,0025	0,0485
Sum of square						1,98E+05	6837,68	1,11E+05	63,21	0,8474	0,0553	0,1882	0,0051
Mean square						16514,124	1709,42	9229,1	6,32	0,0847	0,0138	0,0188	0,0004
R^2						0,8237	0,6375	0,8524	0,9083	0,7547	0,2067	0,8329	0,7793
Adjusted R^2						0,6121	0,5570	0,6753	0,832	0,5504	0,0304	0,6936	0,5144
Predicted R^2						-0,952	0.4003	-0,4448	0,4498	-0,8142	-0,2904	0,3315	-1,1101
Std.dev						65,13	14,70	43,79	0,7291	0,1515	0,1086	0,0561	0,0120
Mean						148,38	30,90	153,06	6,18	0,2624	0,2978	0,0653	0,0099
Adeq precision						8,2085	9,9002	10,9648	10,8927	6,8170	3,2795	9,265	6,3402
Range						27,23 to 422,11	0,0 to 79,98	51,63 to 456,16	3 to 9,2	0,08 to 0,915	0,09 to 0,72	0,0 to 0,3	0,0 to 0,062

Conditions: C1 (KOH concentration 3M,5M and 7M), C2 (Pyrolysis temperature: 600 °C, 750 °C and 900 °C), C3(Type of Sludge: S or D), C4 (Discard Coal: Yes, or NO).

*Responses: R1 (Specific surface area: m^2/g), R2 (Micro porosity or micropore surface area/total surface area*100: %), R3 (CEC: meq/100g), R4 (pHpzc), R5 (Acidity: mmol/g), R6 (Basicity: mmol/g), R7 (N/C ratio) and R8 (H/C ratio)*

The difference between the actual R^2 and predicted should not exceed 0,2 for prediction accuracy.

A negative predicted R^2 implies that the overall mean could be a better tool to foresee the response.

4.3.2 **Chemical properties**

Response 3: Cations Exchange capacity

The concentration value of elements can be found in appendix C the Table of the ANOVA of CEC response as shown in Table 4.9 where B, D, BC, CD, and A^2 are significant factors. Table 4.11 shows the results of CEC determined using a similar protocol (section 3.3). Despite the fact that the feedstocks have about the same value it is worthy mentioning that SBAC and commercial activated carbon (Com-AC) in this study have higher CEC values than those found in previous studies (Gong, 2013). This may be due to i) the accumulation of Na, K, Mg, and Ca fostered by pyrolytic temperature enhancement (Lu et al., 2013) (ii) the presence of minerals elements in CEC causing the disintegration of stable inorganic minerals carbonate from sludge during pyrolysis with increased temperature, resulting in the liberation of fixed metals from the lattice (Z. Li et al., 2018). However, adding waste coal reduced the amount of alkali and alkaline earth in the ash, implying a reduction in empty sites that could be filled by other cations, as reported in the case of carbonaceous rich material: cotton stalks (Wang et al., 2019).

Table.4.9 ANOVA of CEC response

Source	Sum of squares	Df	Mean square	F-value	P-value	
Model	1,107E+05	12	9229,10	4,81	0,0092	Significant
A-KOH	4473,82	1	4473,82	2,33	0,1577	
B-Temperature	23220,81	1	23220,81	12,11	0,0059	
C-Sludge type	377,88	1	377,88	0,1970	0,6666	
D-Discard Coal	24411,53	1	24411,53	12,73	0,0051	
AB	5777,73	1	5777,73	3,01	0,1133	
AC	1248,67	1	1248,67	0,6511	0,4385	
AD	1696,96	1	1696,96	0,8848	0,3690	
BC	38169,91	1	38169,91	19,90	0,0012	
BD	7367,20	1	7367,20	3,84	0,0784	
CD	19708,60	1	19708,60	10,28	0,0094	
A^2	38231,29	1	38231,29	19,93	0,0012	

B^2	2029,32	1	2029,32	1,06	0,3279	
Residual	19178,33	10	1917,83			
Lack of Fit	19178,33	5	3835,67			
Pure Error	0,0000	5	0,0000			
Cor Total	1,299E+05	22				

The actual equation of CEC response is on table 4.10

Table 4.10 Actual equation of CEC response

CEC	=
Sludge type	D
Discard coal	No
-399,91834	
+303,65359	KOH
-1,05375	Temperature
-0,071481	KOH * Temperature
-24,08076	KOH^2
+0,001440	$Temperature^2$
Sludge type	D
Discard coal	Yes
-265,67629	
+292,46900	KOH
-1,34704	Temperature
-0,071481	KOH * Temperature
-24,08076	KOH^2
+0,001440	$Temperature^2$
Sludge type	S
Discard coal	No
+9,21874	
+313,08782	KOH
-1,73921	Temperature

-0,071481	KOH * Temperature
-24,08076	KOH²
+0,001440	Temperature²
Sludge type	S
Discard coal	Yes
+277,32131	
+301,90323	KOH
-2,03251	Temperature
-0,071481	KOH * Temperature
-24,08076	KOH²
+0,001440	Temperature²

Figures of CEC response are shown in (Figure 4.24-4.27).

A large value of CEC has a high benefit in soil amendment application because it enriches the soil with nutrients (K, Ca, Mg) and reduces fertilizer use. Additionally, a high pH provides base cations to mitigate soil neutrality and minimize Al^{3+} toxicity in the land (Wang et al., 2019).

Table 4.11 brief comparison of CEC

Sample type	Synthesis conditions				CEC (meq/100g)	References
	Activating agent	Conc (M)	Time (min)	Temp (°C)		
D	-	-	-	-	84,642	This work
S	-	-	-	-	111,142	
Discard coal	-	-	-	-	107,17	
Raw sludge	-	-	-	-	91,100	(Li et al., 2019)
Com-AC	-	-	-	-	193,88	This work
Zeolite	-	-	-	-	72,982	(Gong, 2013)
SBAC	ZnCl2	5	90	500	2,2	(Li et al., 2019)
D-3-600	KOH	3	90	600	51,624	This work
SC-5-900	KOH	5	90	900	224,102	

S-7-600	KOH	7	90	600	203,713	
DC-3-900	KOH	3	90	900	158,586	

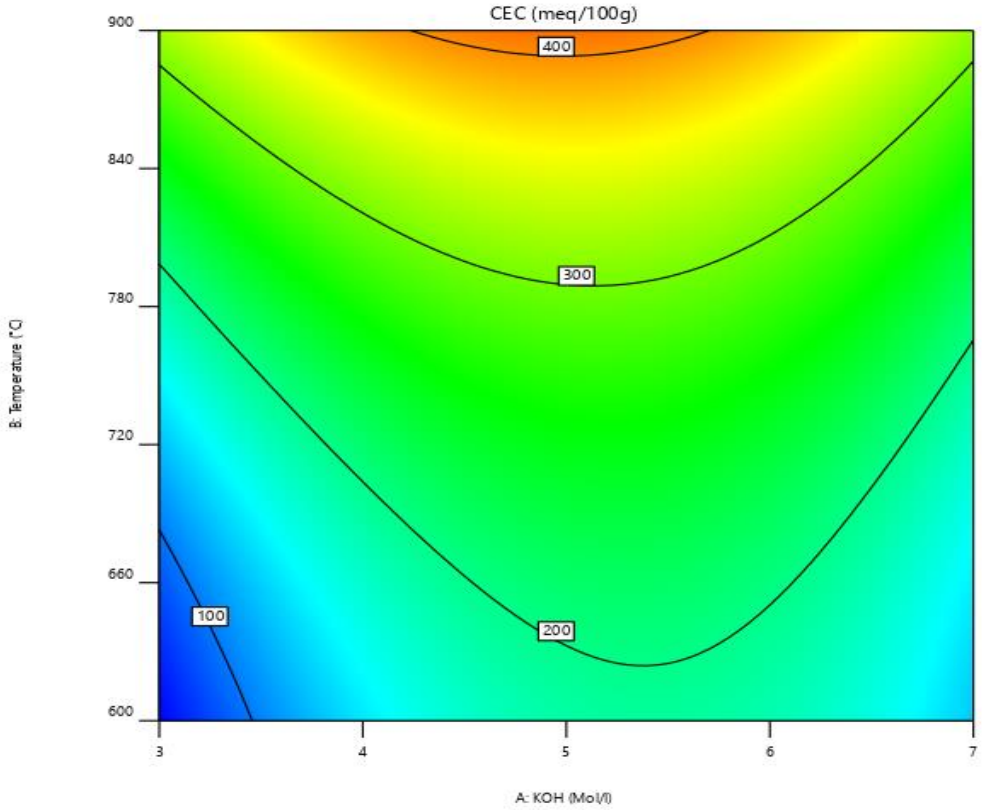


Figure 4.24 graphic of SBAC CEC from sludge D without discard coal

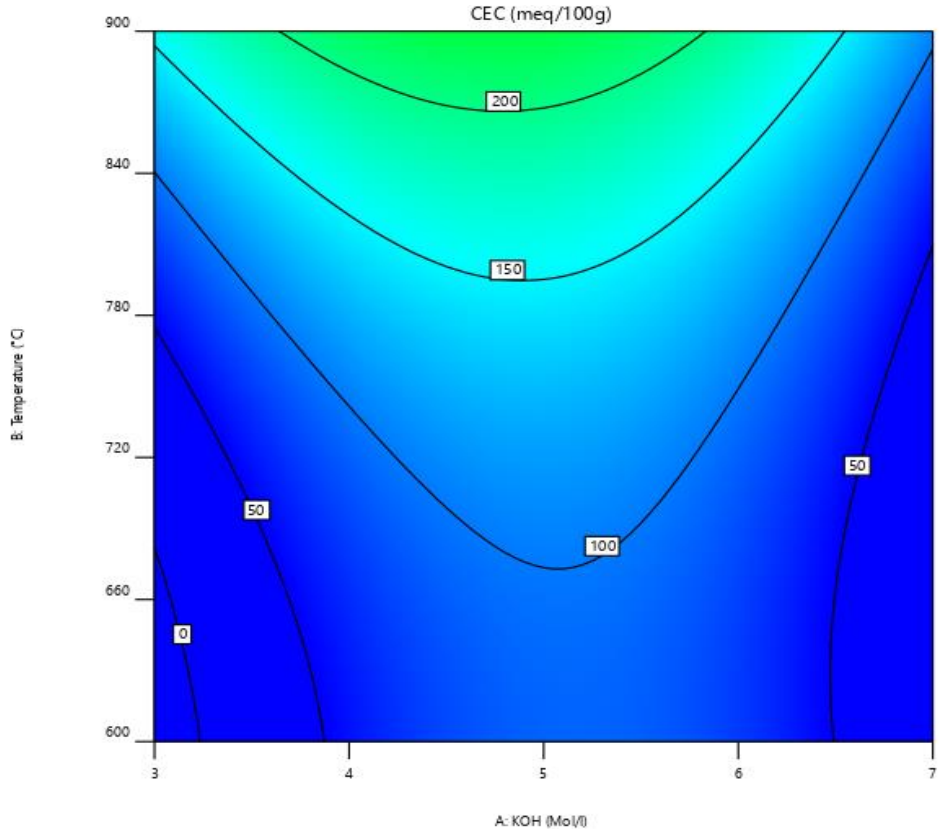


Figure 4.25 graphic of SBAC CEC from sludge D with discard coal

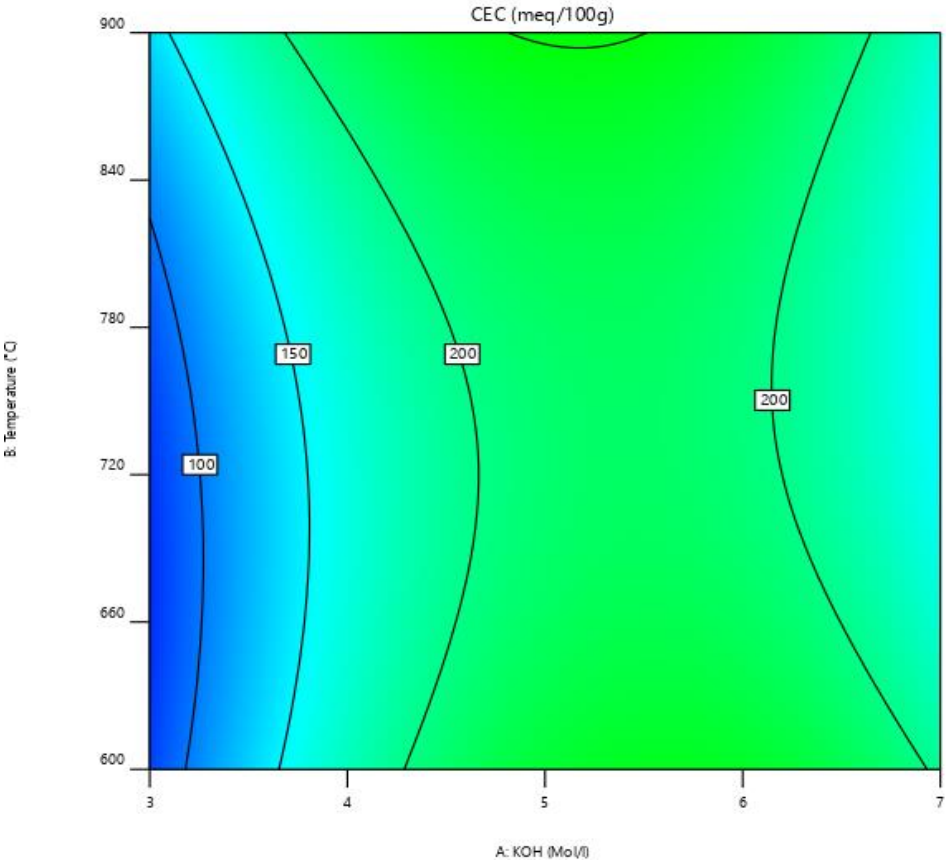


Figure 4.26 graphic of SBAC CEC from sludge S without discard coal

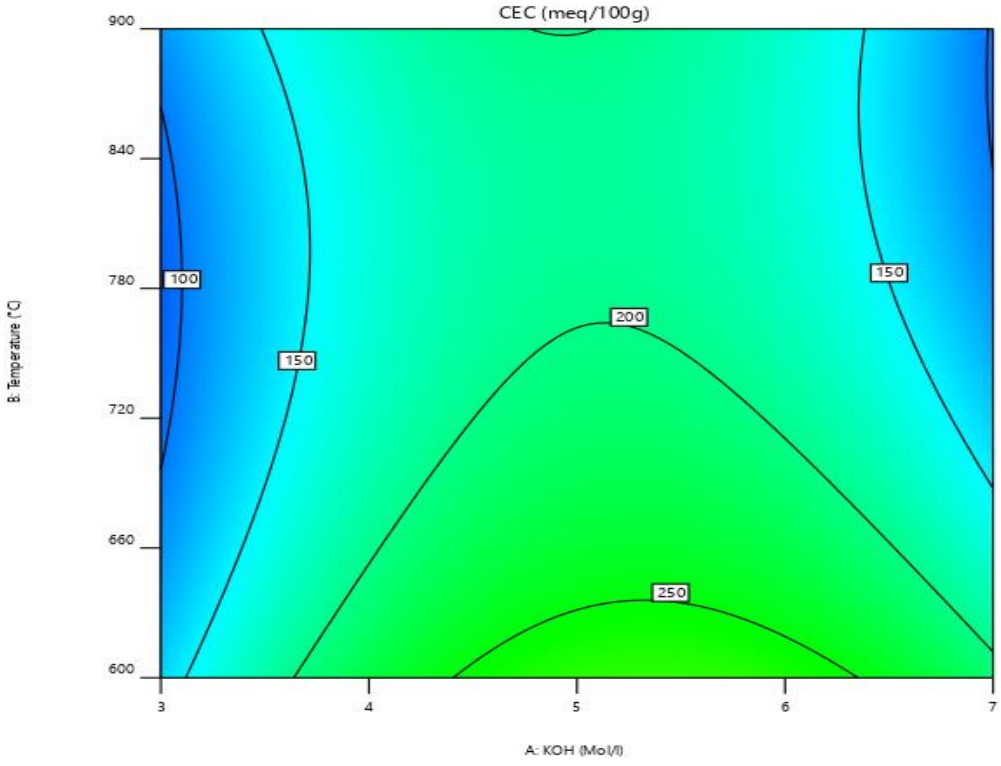


Figure 4.27 graphic of SBAC CEC from sludge S with discard coal

Response 4: Point of zero charge

Table 4.12 shows the analysis of variance of the pHpzc response, with B, AD, and BC as significant variables, with comprehensive details in appendix E. The increase of the response value with temperature is a common pattern in graphics of pHpzc response (Figures 4.28 to 4.31). This can be due to: i) the thermal degradation of acidic functional groups with temperature and creation of basic nitrogen base functional groups (Devi & Saroha, 2016; Lu et al., 2013) (ii) the addition of alkali and alkaline earth metals to ash, causing the adsorbent to become basic (Z. Li et al., 2018; Wang et al., 2019), as well as the formation of basic oxides and the decomposition of organic salt (Devi & Saroha, 2016) according to CEC response. The observation of pHpzc growth from slightly acidic 4,4 (SC-3-600) to neutral 6,1 (SC-3-900) similarly S-3-600 (pHpzc = 4,8) and S-3-900 (pHpzc = 7,6) shows that adsorbent blended to discard had a lower pHpzc than the non-blended, which can be explained by assuming that i) higher carbon content promoted the formation of acidic functional on the carbon surface of the adsorbent and (ii) lower alkali and alkaline earth metal as per CEC results.

Table 4.12 ANOVA of pHpzc Response

Source	Sum of Squares	Df	Mean Square	F-value	p-value	
Model	63,21	10	6,32	11,89	< 0.0001	Significant
A-KOH	0,4381	1	0,4381	0,8241	0,3819	
B-Temperature	39,29	1	39,29	73,92	< 0.0001	
C-Sludge type	1,46	1	1,46	2,75	0,1233	
D-Discard Coal	0,2044	1	0,2044	0,3845	0,5468	
AB	1,24	1	1,24	2,34	0,1522	
AC	0,2375	1	0,2375	0,4467	0,5166	
AD	7,40	1	7,40	13,91	0,0029	
BC	3,11	1	3,11	5,85	0,0325	
BD	1,82	1	1,82	3,43	0,0889	
CD	1,14	1	1,14	2,14	0,1691	
Residual	0,2754	12	0,0229			
Lack of Fit	0,2192	7	0,0313		0,2357	Not significant

Pure Error	0,0562	5	0,0112			
Cor Total	1,12	22				

The actual equation of pH_{PZC} response is contained in Table 4.13

Table 4.13 Actual equation for pHPZC

PHpzc	=
Sludge type	D
Discard coal	No
+4,62694	
-1,27618	KOH
+0,006103	Temperature
+0,001048	KOH * Temperature
Sludge type	D
Discard coal	Yes
-2,97593	
-0,584731	KOH
+0,010679	Temperature
+0,001048	KOH * Temperature
Sludge type	S
Discard coal	No
+7,53314	
-1,15246	KOH
-4,16310E-06	Temperature
+0,001048	KOH * Temperature
Sludge type	S
Discard coal	Yes
+0,933642	
-0,461010	KOH
+0,004572	Temperature
+0,001048	KOH * Temperature

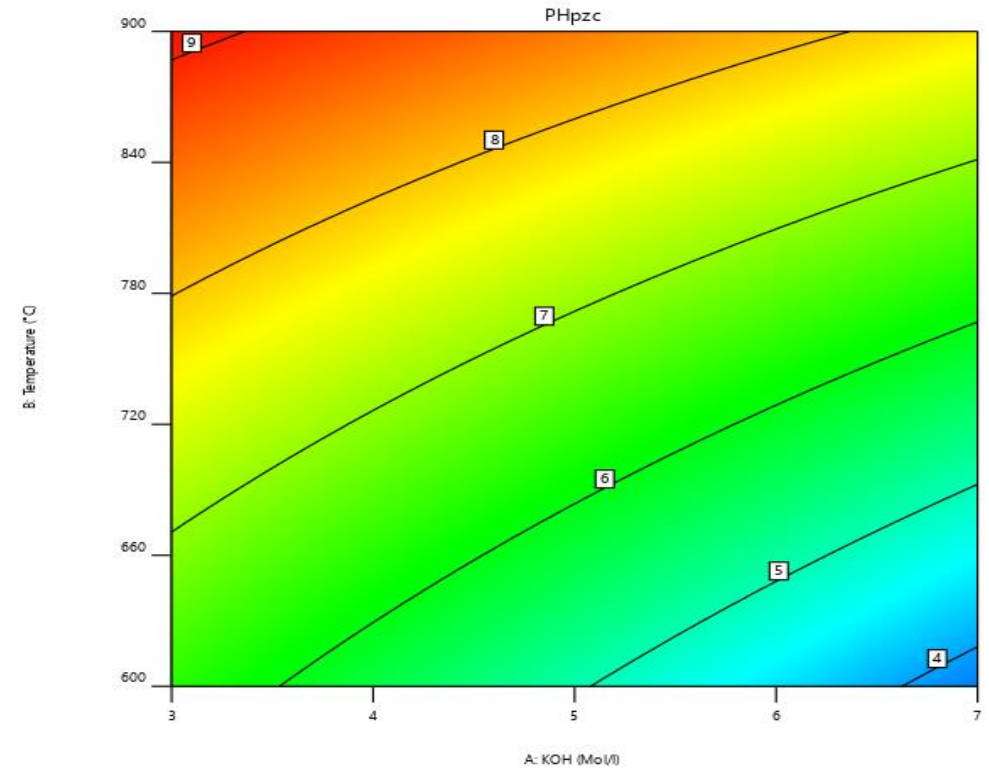


Figure 4.28 Graphic of pHpzc response for SBAC from sludge D without discard coal

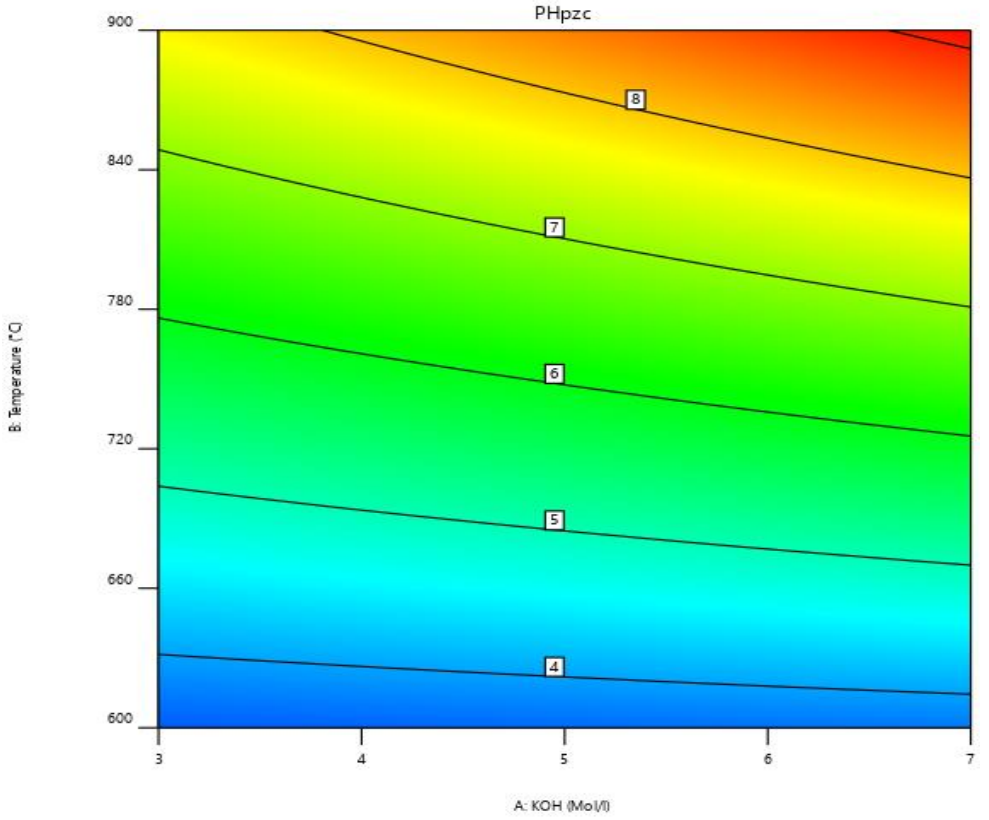


Figure 4.29 Graphic of pHpzc response for SBAC from sludge D with discard coal

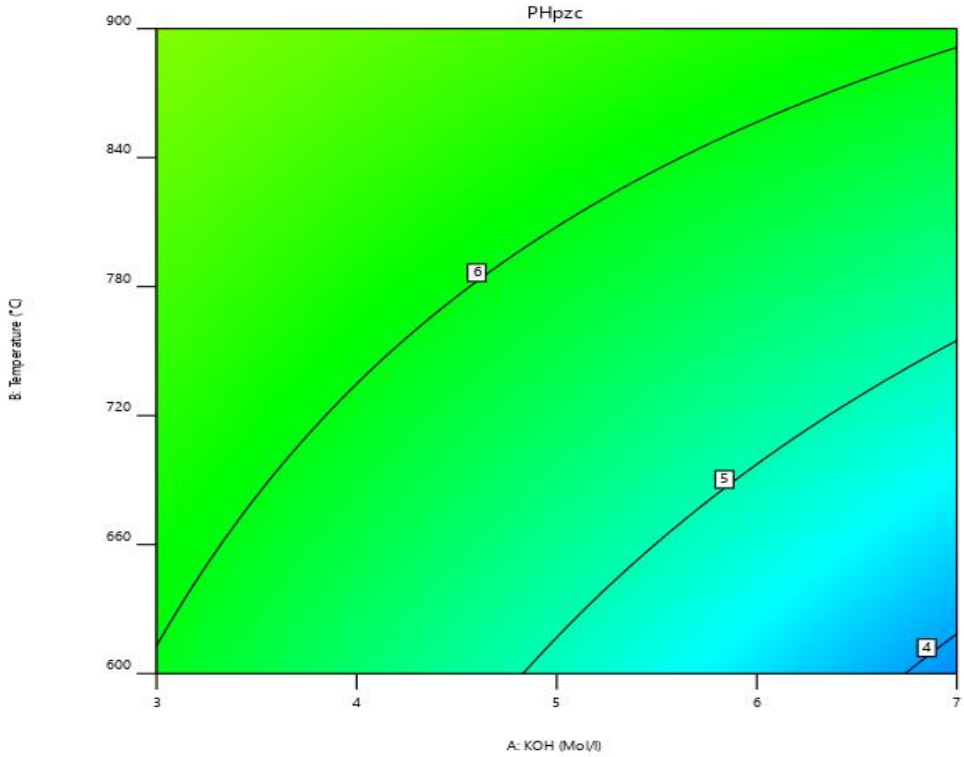


Figure 4.30 Graphic of pHpzc response for SBAC from sludge S without discard coal

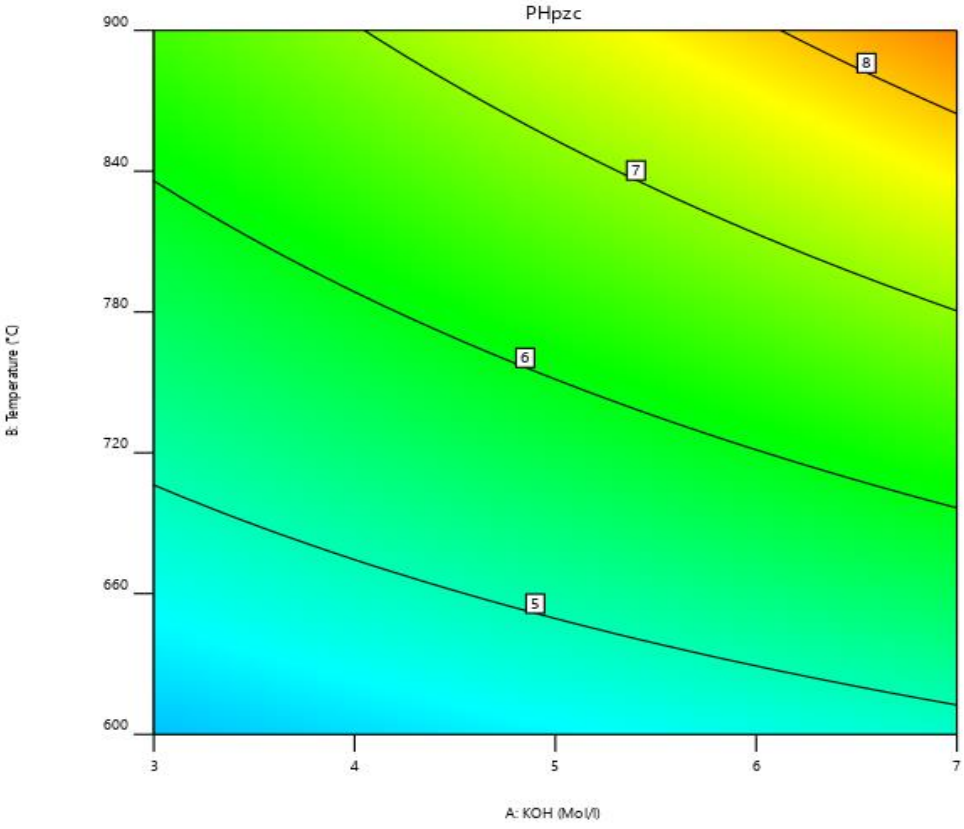


Figure 4.31 Graphic of pHpzc response for SBAC from sludge S with discard coal

Acidity and basicity of SABC are shown in Table 4.14, the calculations are based on data in appendix B

Table 4.14 Acidity and basicity of SBAC

				Functional group				
sample	Run	Labelled	Sludge type	Carbox (1)	Lacton (2)	Phenolic (3)	Acidity: (1)+(2)+(3)	Basicity (4)
1	18	D-3-600	D	0,870	0,000	0,605	1,475	0,615
2	22	D-3-750	D	0,735	0,000	0,115	0,850	0,830
3	3	D-5-600	D	0,805	0,000	0,135	0,940	0,910
4	6	D-5-900	D	1,000	0,000	1,015	2,015	0,725
5	11&15	D-7-600	D	0,960	0,000	0,140	1,100	0,235
6	20&23	DC-3-900	D	0,820	0,015	0,060	0,895	0,755
7	17	DC-5-600	D	0,910	0,000	0,125	1,035	0,695
8	8	DC-5-750	D	0,950	0,000	0,040	0,990	0,685
9	10&19	DC-7-900	D	0,005	0,000	0,075	0,080	0,720
10	7	S-3-600	S	0,970	0,873	0,000	1,843	0,740
11	5	S-3-900	S	0,845	0,000	0,220	1,065	0,760
12	16	S-5-600	S	0,900	0,000	0,040	0,940	0,730
13	14&2	S-7-900	S	1,000	0,000	0,000	1,000	0,685
14	13&4	SC-3-600	S	0,935	0,000	0,000	0,935	0,665
15	1	SC-3-900	S	0,905	0,015	1,010	1,930	0,665
16	21	SC-5-900	S	0,925	0,000	0,035	0,960	0,690
17	12	SC-7-600	S	0,860	0,047	0,535	1,443	0,725
18	9	SC-7-750	S	0,980	0,000	0,000	0,980	0,685
Com-AC				0,05	0,001	0,000	0,051	0,615

Response 5: Acidity

Table 4.15 shows the results of the study of variance of the acidity response, which shows that none of the variables are important. With the exception of Figure 4.32 (Sludge D without discard coal), the graphics of acidity responses are shown in Figures 4.32, 4.33, 4.34, and 4.35. In the 3 remaining cases, acidity tends to decrease with temperature augmentation due to thermal decomposition of acidic functional groups with temperature augmentation (Devi & Saroha, 2016), while the opposite situation (acidity growth with temperature increase) may be due to the release of carbonates in

Boehm solution (Mohamed et al., 2011) or solubilisation of inorganic species (silica and alumina) which contribute to the acidity of the adsorbent without being part of the surface functionalities (Tsechansky & Graber, 2014).

Table 4.15 ANOVA of acidity response

Source	Sum of Squares	Df	Mean Square	F-value	p-value	
Model	0,8474	10	0,0847	3,69	0,0179	significant
A-KOH	0,0744	1	0,0744	3,24	0,0969	
B-Temperature	0,0831	1	0,0831	3,62	0,0813	
C-Sludge type	0,0082	1	0,0082	0,3587	0,5603	
D-Discard Coal	0,0074	1	0,0074	0,3209	0,5815	
AB	0,0560	1	0,0560	2,44	0,1441	
AC	0,0937	1	0,0937	4,08	0,0662	
AD	0,1041	1	0,1041	4,54	0,0546	
BC	0,0201	1	0,0201	0,8749	0,3680	
BD	0,1035	1	0,1035	4,51	0,0551	
CD	0,0926	1	0,0926	4,04	0,0676	
Residual	0,2754	12	0,0229			
Lack of Fit	0,2192	7	0,0313	2,79	0,1385	not significant
Pure Error	0,0562	5	0,0112			
Cor Total	1,12	22				

The actual equation of acidity response is contained in Table 4.16

Table 4.16 Actual equation of Acidity response

Acidity	=
Sludge type	D
Discard coal	No
+0,710409	
-0,121126	KOH
-0,000808	Temperature
+0,000223	KOH * Temperature

Sludge type	D
Discard coal	Yes
+1,83582	
-0,203142	KOH
-0,001899	Temperature
+0,000223	KOH * Temperature
Sludge type	S
Discard coal	No
+1,28241	
-0,198834	KOH
-0,001299	Temperature
+0,000223	KOH * Temperature
Sludge type	S
Discard coal	Yes
+2,69407	
-0,280851	KOH
-0,002390	Temperature
+0,000223	KOH * Temperature

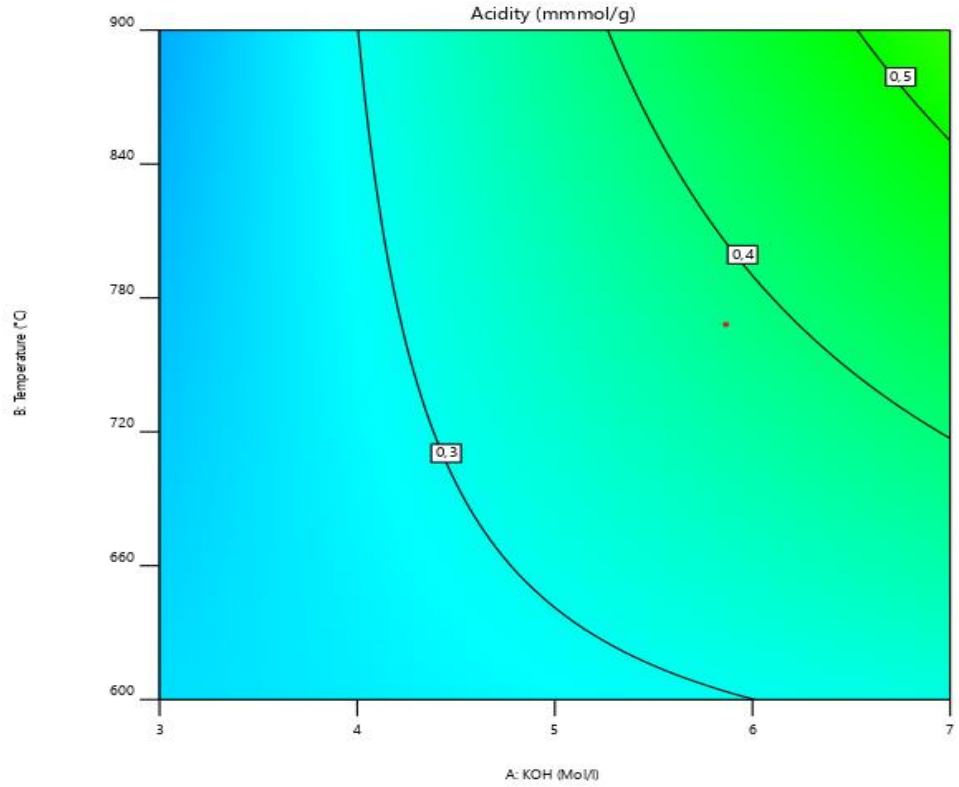


Figure 4.32 graphic of SBAC acidity from sludge D without discard coal

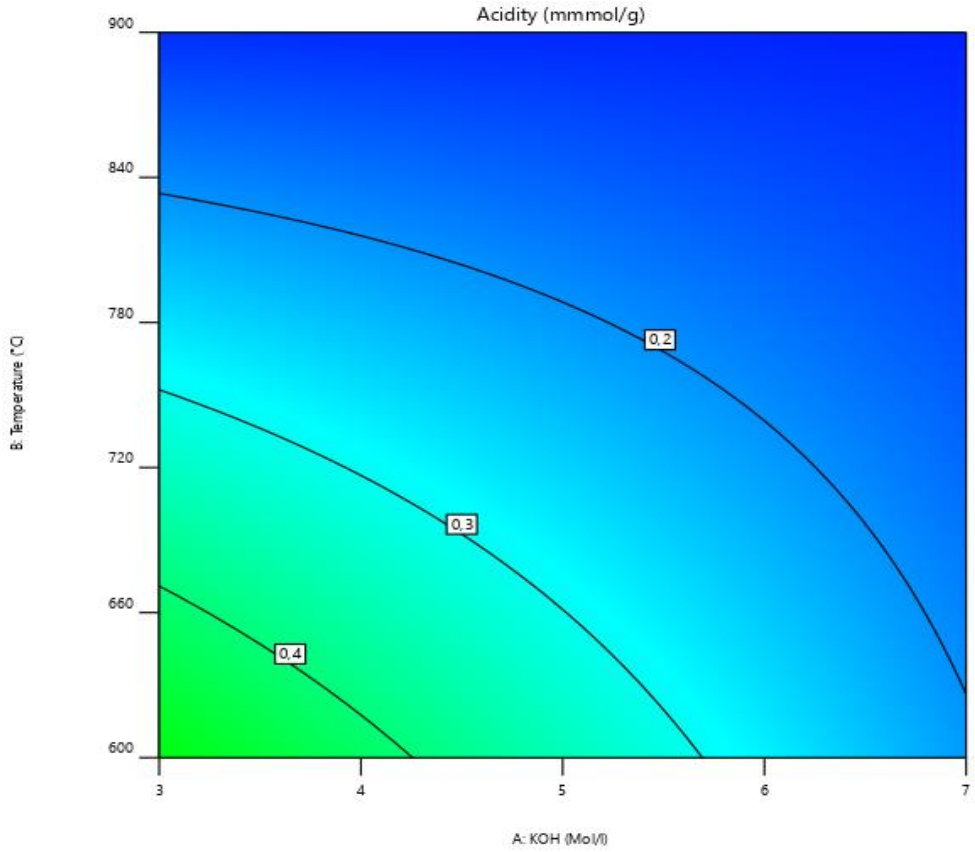


Figure 4.33 graphic of SBAC acidity from sludge D with discard coal

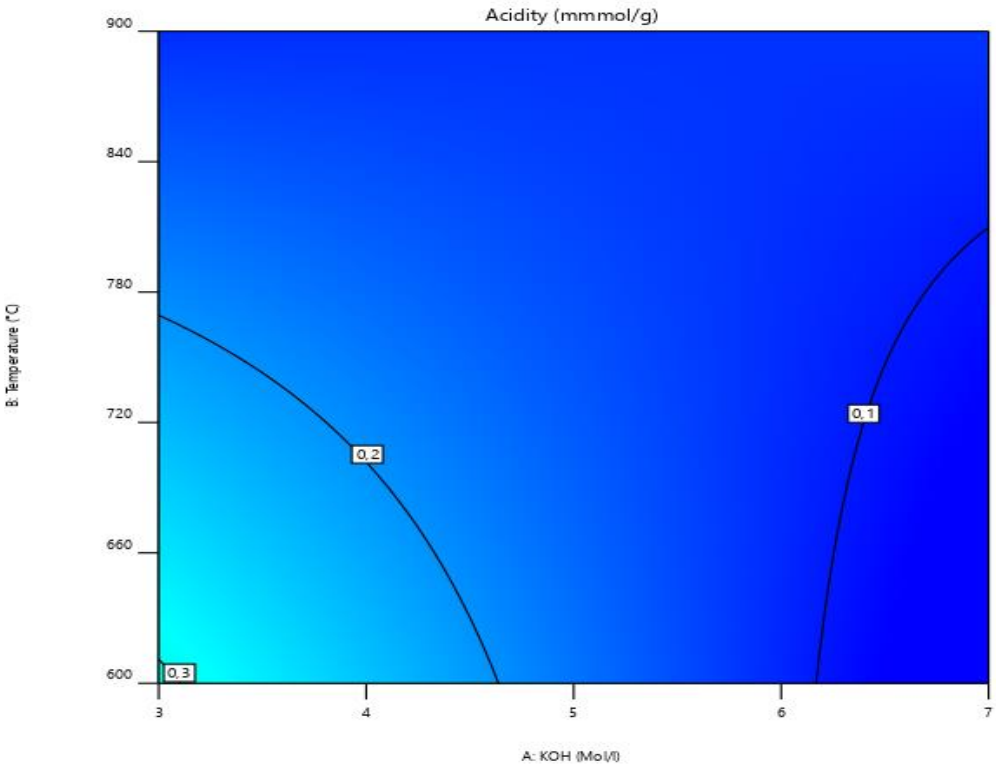


Figure 4.34 graphic of SBAC acidity from sludge S without discard coal

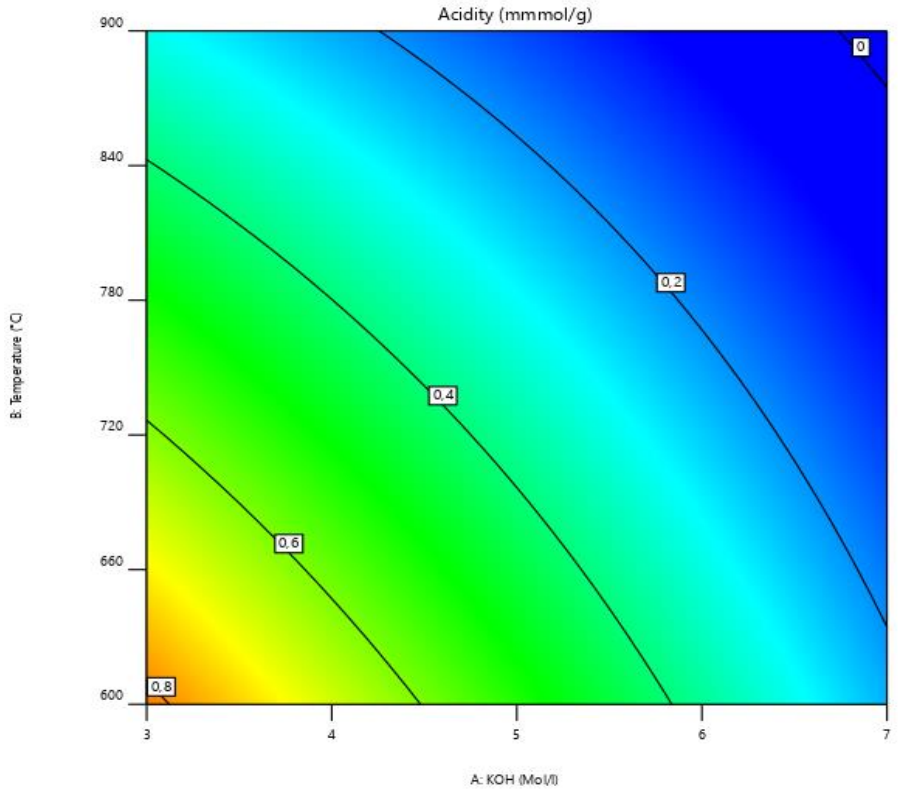


Figure 4.35 graphic of SBAC acidity from sludge S with discard coal

Response 6: Basicity

The response was not significant (table 4.17), probably due to solubilisation of ferric ions in acidic solution (Mohamed et al., 2011) or side effect reactions reaction i.e. equation 4.1 of the adsorption of H^+ ions on the silicon or aluminium oxide groups (Velghe et al., 2012).

$$Si - O^- + 2\,H^+ \rightleftharpoons Si - OH + H^+ \leftrightarrows Si - OH_2^+ \quad (4.1)$$

Table 4.17 ANOVA of basicity response

Source	Sum of Squares	df	Mean Square	F-value	p-value	
Model	0,0553	4	0,0138	1,17	0,3560	not significant
A-KOH	0,0148	1	0,0148	1,26	0,2771	
B-Temperature	0,0054	1	0,0054	0,4536	0,5092	
C-Sludge type	0,0001	1	0,0001	0,0094	0,9239	
D-Discard Coal	0,0296	1	0,0296	2,51	0,1305	
Residual	0,2123	18	0,0118			
Lack of Fit	0,1145	13	0,0088	0,4503	0,8855	not significant
Pure Error	0,0978	5	0,0196			
Cor Total	0,2676	22				

4.3.3 **Organic contents ratio**

Response 7: N/C ratio

Tables 4.18 and 4.19 show the analysis of variance and the actual equation of the N/C ratio response respectively where the significant factors are A, B, D, and AD. Figures 4.36, 4.37, 4.38, and 4.39 show that the prediction of the N/C trend, which increases with pyrolysis temperature, is in conflict with previous conclusions (Devi & Saroha, 2016; Figueiredo et al., 2018; Z. Wang et al., 2019). Despite the fact that nitrogen content in SBAC decreased significantly when compared to precursors (Table 4.2), the fact that the carbon content decreased with temperature i.e. DC-5-600 (57,44 percent C -0,00 percent N) vs. DC-5-750 (23,61 % C- 0,208 % N) and SC-3-600 (45 % C- 0,00 % N) vs SC-3-900 (6,97%C- 0,6890 %N), implies that the augmentation of the N/C ratio was due to diminution of C content linked to volatile mater and maybe also due the formation of basic functional group.

Table 4.18 ANOVA of N/C ratio response

Source	Sum of Squares	Df	Mean Square	F-value	p-value	
Model	0,1882	10	0,0188	5,98	0,0025	Significant
A-KOH	0,0309	1	0,0309	9,82	0,0086	
B-Temperature	0,0335	1	0,0335	10,66	0,0068	
C-Sludge type	0,0013	1	0,0013	0,4119	0,5331	
D-Discard Coal	0,0356	1	0,0356	11,32	0,0056	
AB	0,0073	1	0,0073	2,31	0,1542	
AC	0,0057	1	0,0057	1,80	0,2042	
AD	0,0295	1	0,0295	9,36	0,0099	
BC	0,0040	1	0,0040	1,27	0,2822	
BD	0,0016	1	0,0016	0,5179	0,4855	
CD	0,0111	1	0,0111	3,54	0,0843	
Residual	0,0563	12	0,00469			
Lack of Fit	0,0378	7	0,0054		0,3986	Not Significant
Pure Error	0,0185	5	0,0037			
Cor Total	0,2444	22				

Table 4.19 Actual equation for N/C response

H/C	=
Sludge type	D
Discard coal	No
+0,057605	
-0,025939	KOH
-0,000133	Temperature
+0,000080	KOH * Temperature
Sludge type	D
Discard coal	Yes
+0,240261	
-0,069569	KOH
-0,000270	Temperature
+0,000080	KOH * Temperature
Sludge type	S

Discard coal	No
-0,235297	
-0,006814	KOH
+0,000086	Temperature
+0,000080	KOH * Temperature
Sludge type	S
Discard coal	Yes
+0,046672	
-0,050444	KOH
-0,000051	Temperature
+0,000080	KOH * Temperature

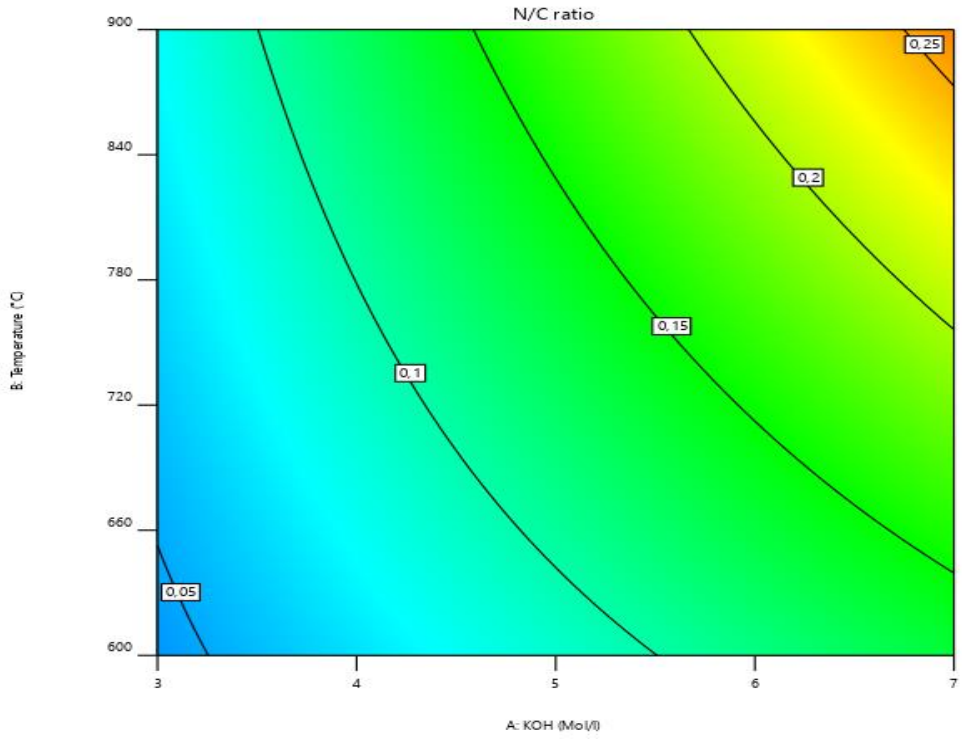


Figure 4.36 graphic of SBAC N/C ratio from Sludge D without discard coal

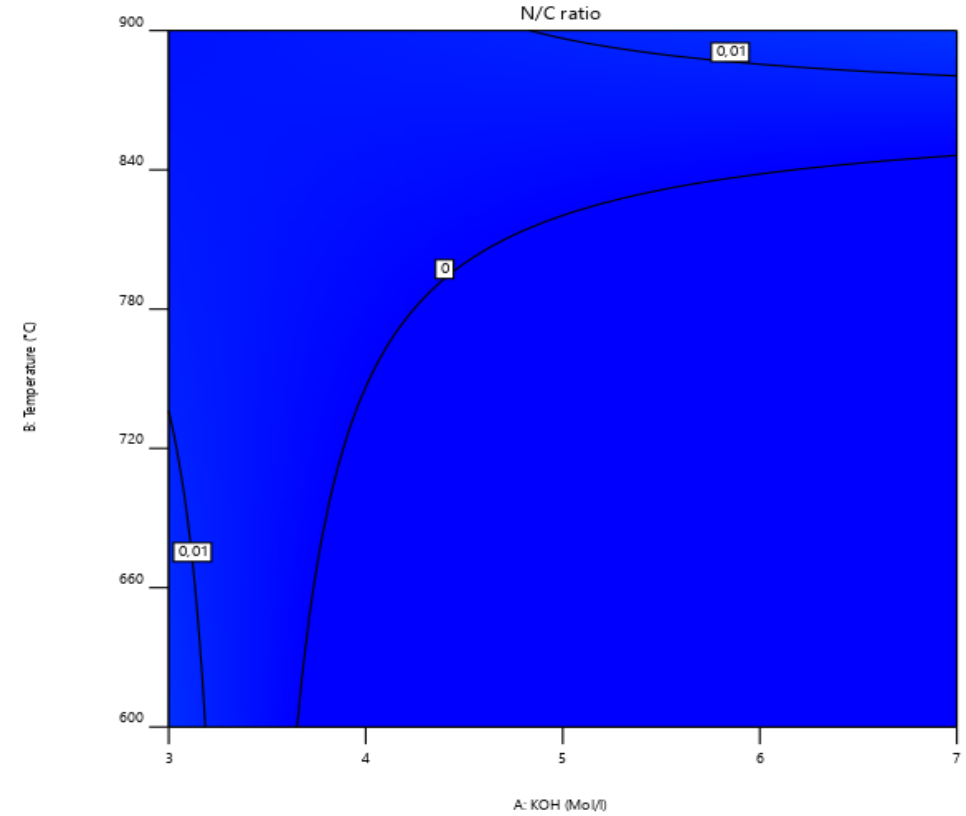


Figure 4.37 graphic of SBAC N/C ratio from Sludge D with discard coal

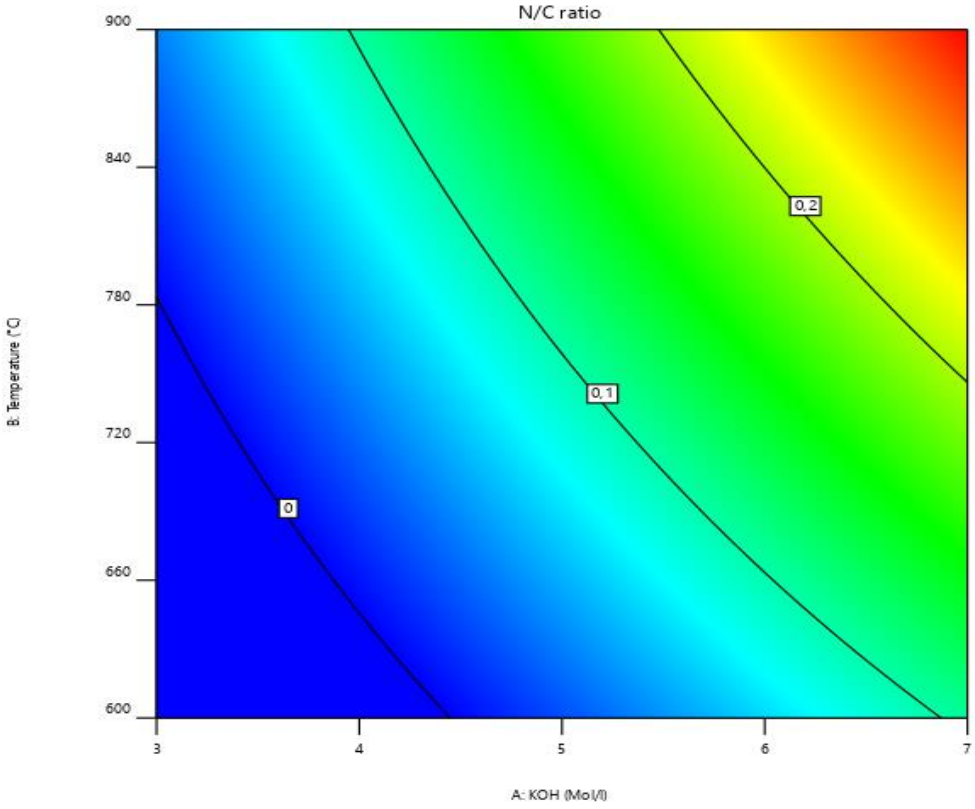


Figure 4.38 graphic of SBAC N/C ratio from sludge S without discard coal

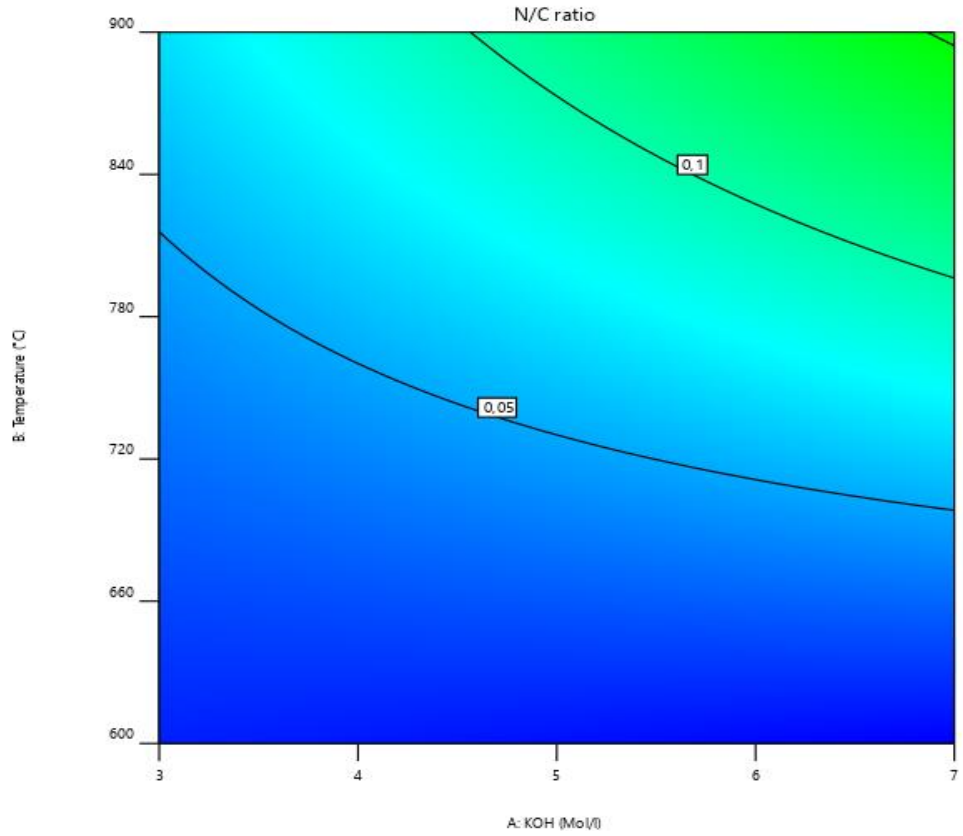


Figure 4.39 graphic of SBAC N/C ratio from sludge S with discard coal

Response 8: H/C ratio

The temperature (B) is the sole non-combined significant factor in the study of variance of H/C ratio (Table 4.20), at 600 °C, SC-3-600 and S-3-600 had a H/C ratio value of 0, 0016 and 0,022 while at 900 °C it was zero due to decomposition of volatile compounds (Devi & Saroha, 2016) as well as hydroxyl (-OH) compound, condensation and dehydration process (Figueiredo et al., 2018) ,and this trend is depicted in figure 4.40-4.43. This conclusion corroborates the FT-IR spectra in Figure 4.11 in which the sorbent pyrolyzed at higher temperature exhibited higher absorbance in comparison to those pyrolyzed at lower temperature. The combined significant factors are AC, AD, and B^2.

Table 4.20 ANOVA of H/C response

Source	Sum of Squares	Df	Mean Square	F-value	p-value	
Model	0,0051	12	0,0004	2,94	0,0485	Significant
A-KOH	0,0003	1	0,0003	1,88	0,1998	
B-Temperature	0,0022	1	0,0022	15,16	0,0030	

C-Sludge type	0,0001	1	0,0001	0,8275	0,3844	
D-Discard Coal	0,0007	1	0,0007	4,59	0,0578	
AB	0,0001	1	0,0001	0,6745	0,4306	
AC	0,0010	1	0,0010	6,65	0,0274	
AD	0,0011	1	0,0011	7,95	0,0182	
BC	0,0003	1	0,0003	1,85	0,2037	
BD	0,0002	1	0,0002	1,21	0,2965	
CD	0,0000	1	0,0000	0,0795	0,7837	
A^2	0,0001	1	0,0001	0,4277	0,5279	
B^2	0,0009	1	0,0009	6,22	0,0318	
Residual	0,0040	10	0,0003			
Lack of Fit	0,0025	5	0,0005		0,0856	Not significant
Pure Error	0,0015	5	0,0003			
Cor Total	0,0091	22				

The actual equation of H/C response is contained in Table 4.21

Table 4.21 Actual equation of H/C response

N/C	=
Sludge type	D
Discard coal	No
+0,702656	
-0,027447	KOH
-0,001570	Temperature
+9,28377E-06	KOH * Temperature
+0,000968	KOH^2
+9,58386E-07	$Temperature^2$
Sludge type	D
Discard coal	Yes
+0,701274	

-0,018245	KOH
-0,001615	Temperature
+9,28377E-06	KOH * Temperature
+0,000968	KOH^2
+9,58386E-07	$Temperature^2$
Sludge type	S
Discard coal	No
+0,611493	
-0,019169	KOH
-0,001512	Temperature
+9,28377E-06	KOH * Temperature
+0,000968	KOH^2
+9,58386E-07	$Temperature^2$
Sludge type	S
Discard coal	Yes
+0,613344	
-0,009967	KOH
-0,001558	Temperature
+9,28377E-06	KOH * Temperature
+0,000968	KOH^2
+9,58386E-07	$Temperature^2$

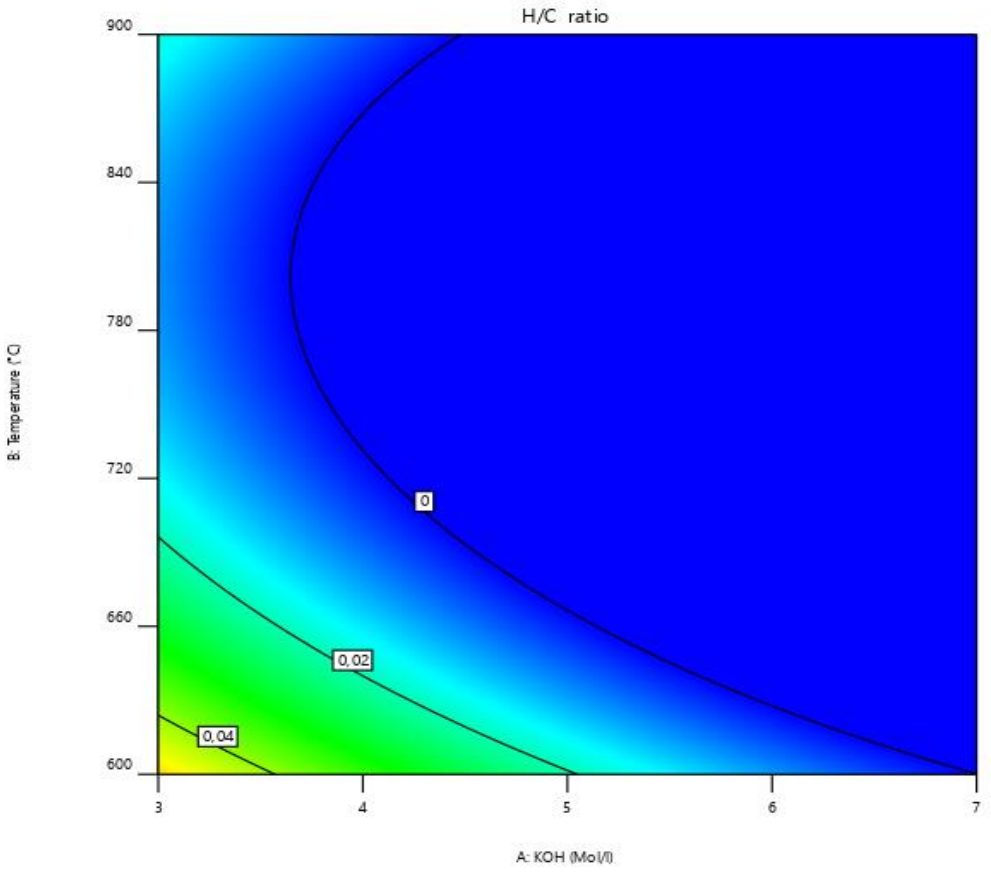


Figure 4.40 graphic of SBAC H/C ratio from sludge D without discard coal

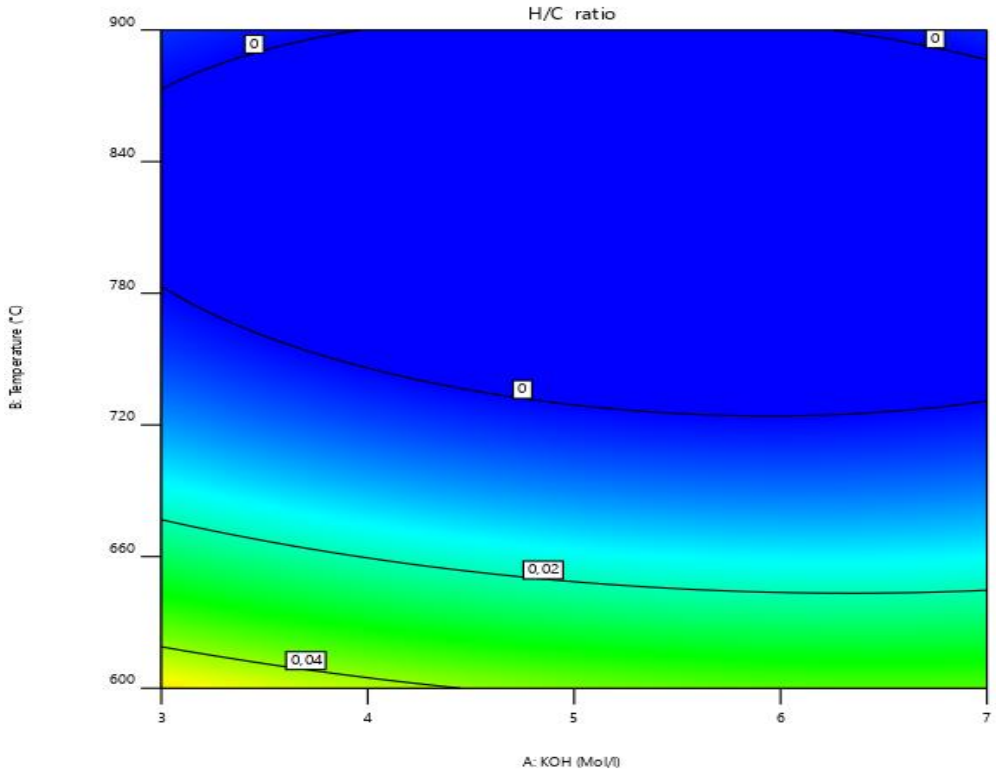


Figure 4.41 graphic of SBAC H/C ratio from sludge D with discard coal

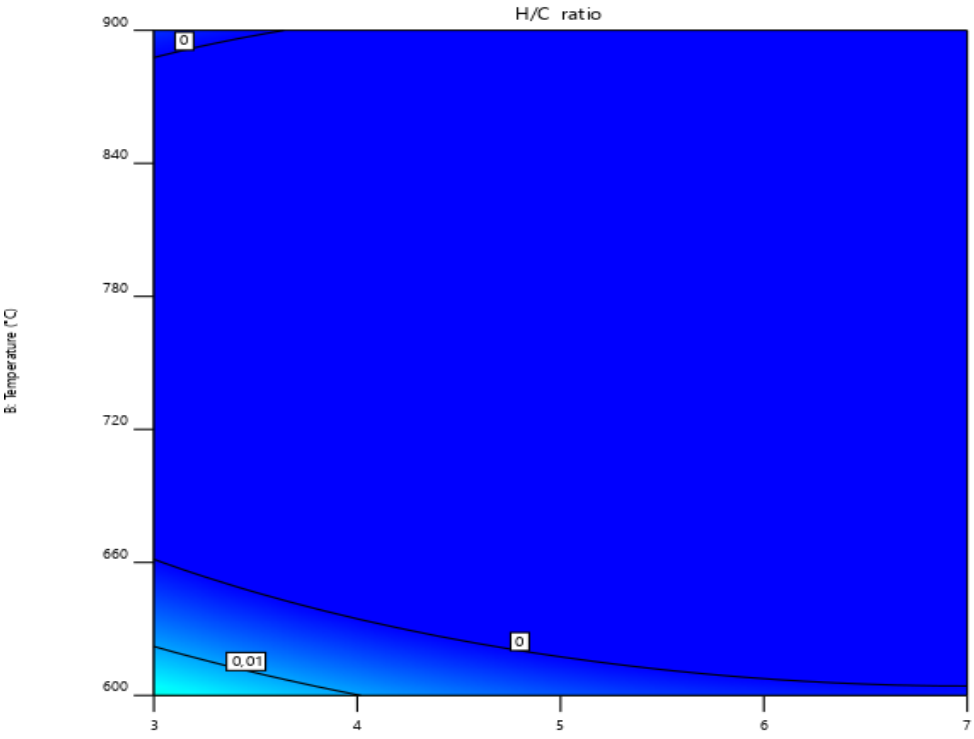


Figure 4.42 graphic of SBAC H/C ratio from sludge S without discard coal

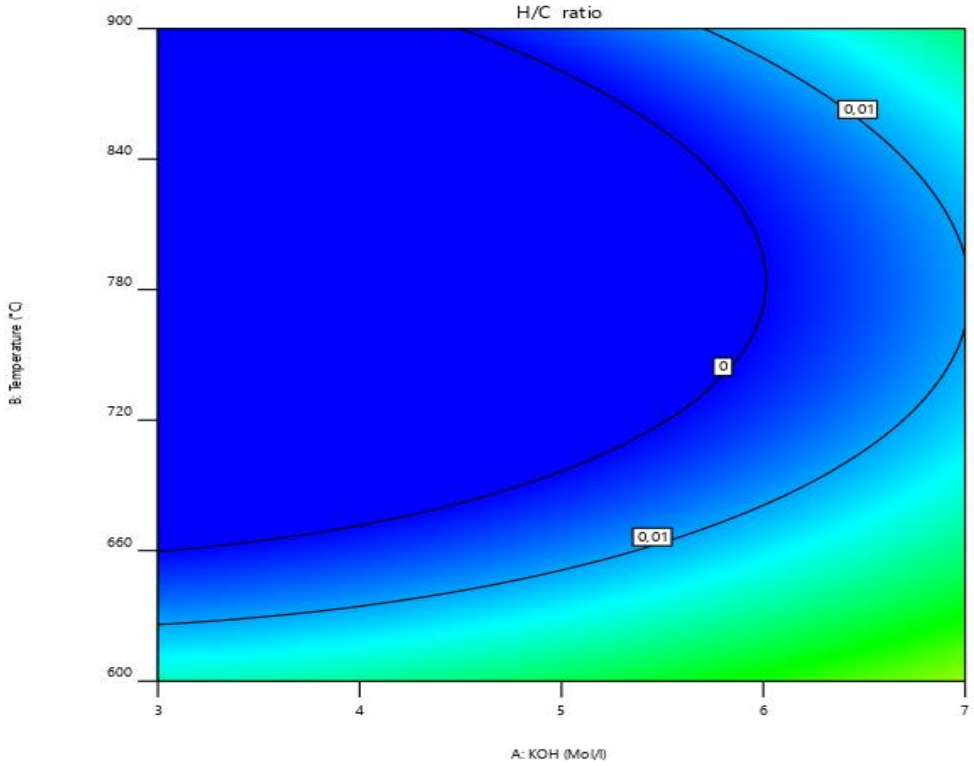


Figure 4.43 graphic of SBAC H/C ratio from sludge S with discard coal

4.4 toxicity characteristic leaching procedure

Table 4.22 shows the results of the TCLP test; in general, the concentration of leachable heavy metals in the pyrolyzed adsorbent was lower than the precursor due to the higher thermal stability of heavy metal acquired through pyrolysis (Xue et al., 2019)

However, after pyrolysis, SC-5-900 released more heavy metals (Fe, Cr, Co, and Ni) than its precursors. This may be due to the disintegration of some stable inorganic minerals (primarily silicate and carbonate) from sludge during pyrolysis with temperature augmentation, which caused the liberation of the fixed metals from the lattice (Z. Li et al., 2018).

Table 4.22 Heavy metal concentration leached with TCLP procedure from precursors and sorbents

	Elements (mg/l)							
	Cu	Zn	Pb	Ni	Co	Cr	Fe	Mn
D	3,534	0,0498	18,99	0,329	0,0061	0,000	0,670	0,000
S	3,228	0,0970	25,11	0,000	0,332	0,000	0,145	0,006
Discard Coal	3,520	0,2773	27,46	0,000	0,336	0,000	0,000	0,005
Com-AC	0,897	0,1238	0,58	0,073	0,713	0,575	0,000	0,068
SC-3-600	3,154	0,1247	24,93	4,064	0,326	0,000	0,000	0,007
SC-5-900	1,922	0,2474	20,09	4,236	0,752	1,555	17,092	2,798
DC-5-750	3,191	0,0379	24,99	0,000	0,279	0,000	0,000	0,003
DC-7-900	3,306	0,0294	24,81	0,000	0,489	0,000	0,000	0,000

CHAPTER 5: WET OXIDATION AND ADSORPTION TEST

5.1 Modification

5.1.1 FT-IR

As shown in Figure 5.1, The impact of oxidation on functionalities is visible with the appearance of peaks in the modified adsorbent in the vicinity of 1600 cm^{-1} literally 1550-1575 cm^{-1}, which can be associated with nano-aromatic C=O and symmetric COO- stretching involved in the formation of carboxylic functional groups(Teng et al., 2015) or C=C bond of the aromatic skeleton ring of adsorbent (Park et al., 2018) while declining in -OH (3640 cm^{-1}) and -CH (2901-2988 cm^{-1}) stretching compound maybe due to their solubility/affinity with H_2SO_4, Com-AC does not possess functional group.

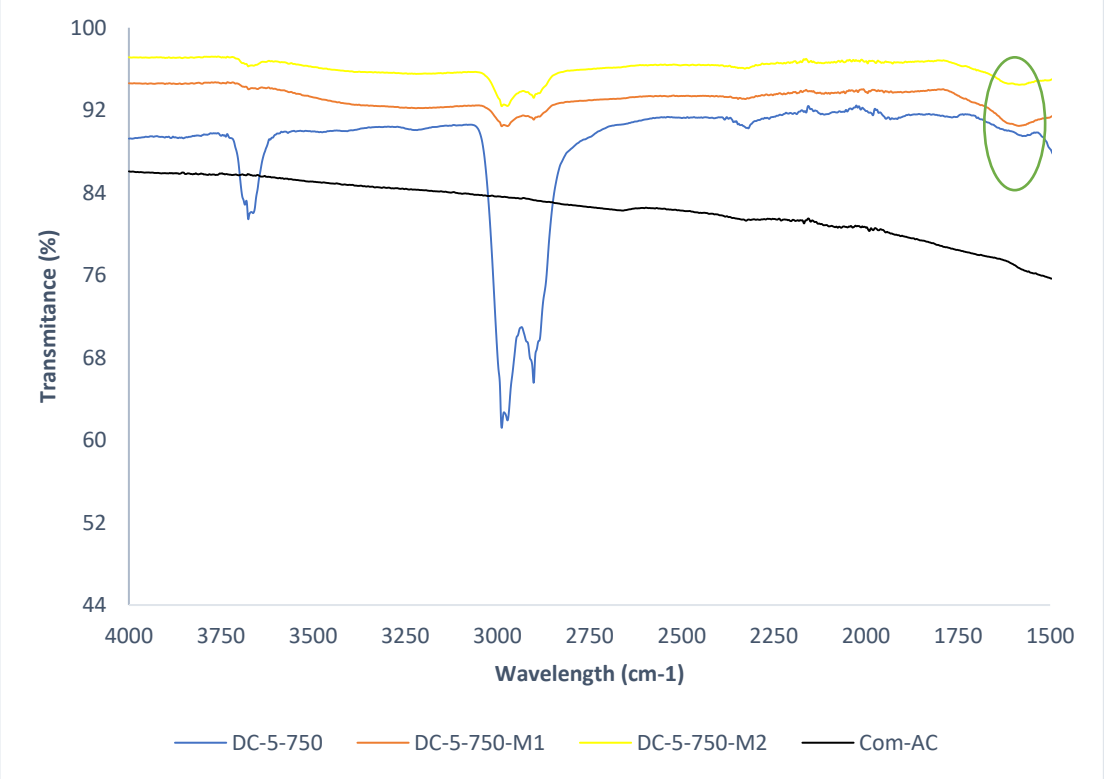


Figure 5.1 FT-IR spectra of Com-AC, DC-5-750 and its 2 modified sorbents

5.1.2 Morphology

Because of the corrosive H_2SO_4-adsorbent surface interaction (Zhang et al., 2015) and the collapse of the pore structure located at the carbon edge (Li et al., 2019), the surface

of the modified adsorbent (Figure 5.2.b) has fewer irregularities than the unmodified adsorbent (Figure 5.2.a) and Com-AC (Figure 5.2.c).

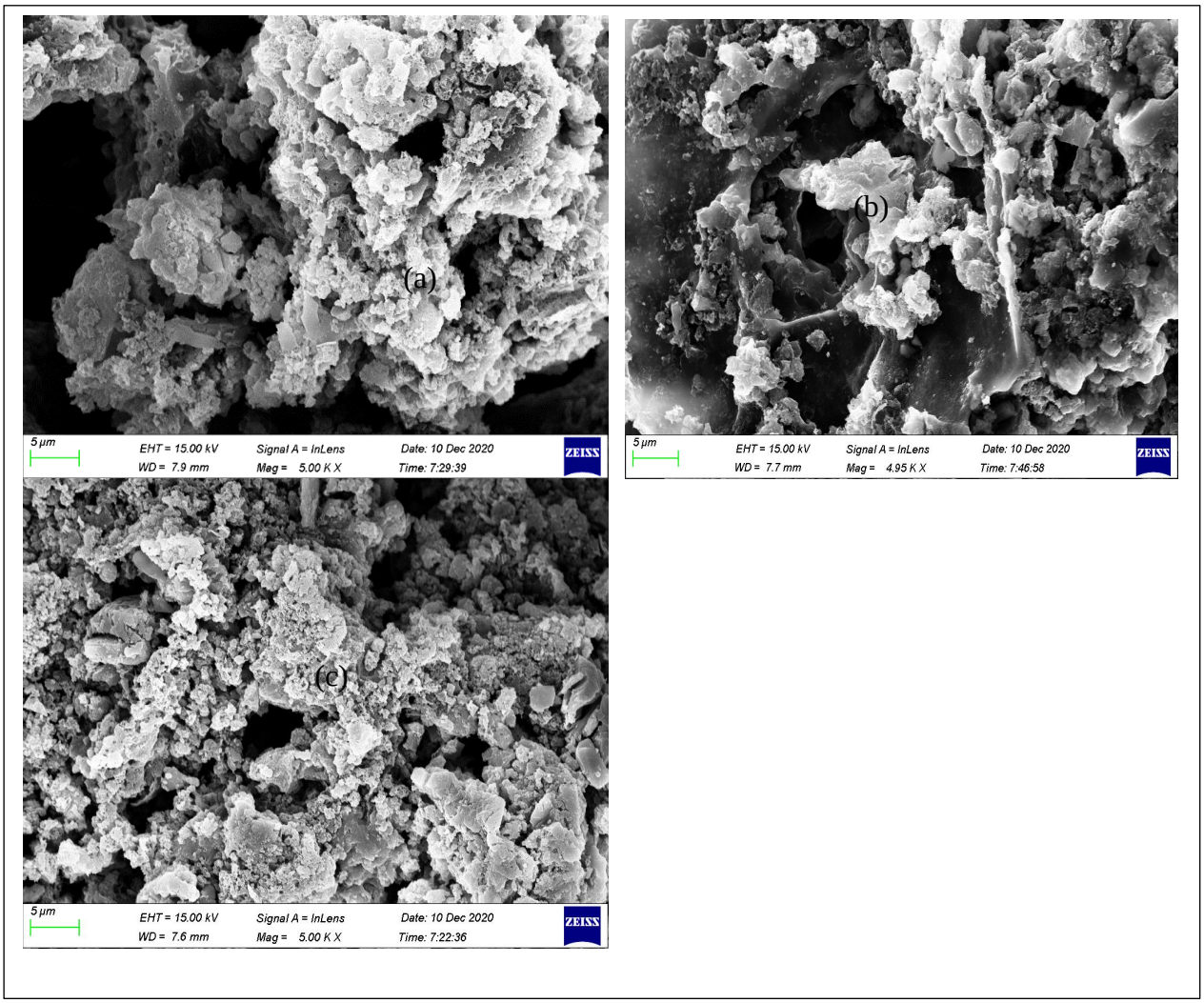


Figure 5.2 morphology of (a) DC-5-750, (b) DC-5-750 M1 and (c) Com-AC

5.1.3 **XRD**

In comparison to the unmodified sorbent, there is an increase in the large peak (2θ = 25,3°) linked to amorphous or graphite and an increase in the peak linked to quartz (2θ = 30°), possibly due to a decrease or solubilisation of other minerals (feldspar and illite), as shown in Figure 5.3.

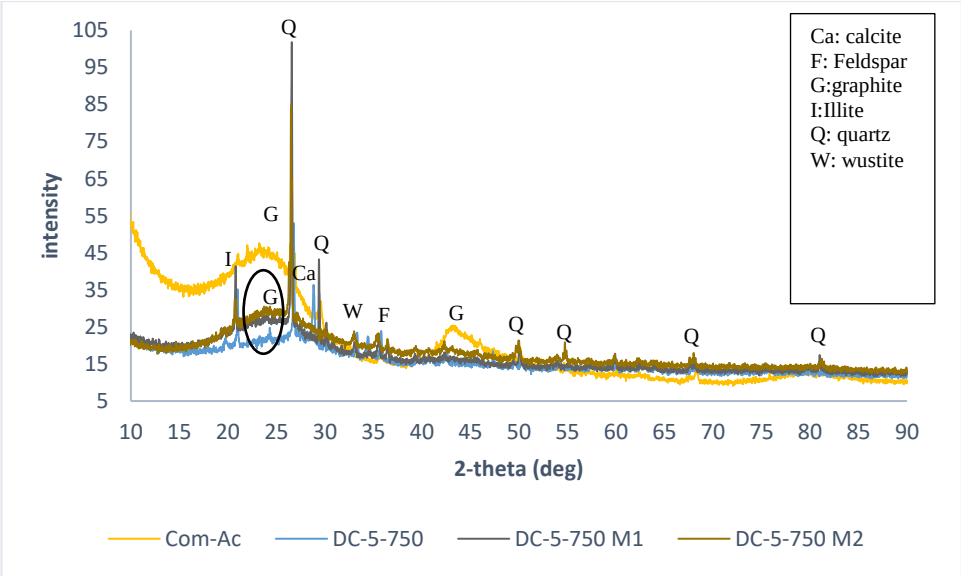


Figure 5.3 XRD pattern of Com-AC, unmodified (DC-5-750) and its modified sorbent

5.1.4 **Porosity and ultimate analysis**

Oxidation with APS did not significantly alter carbon composition from final analysis findings (Table 5.1 and additional information in appendix F), as the largest deviation was 6.771 percent (from DC-5-750: 23,612 percent to DC-5-750M2:30, 383), while the disparity with other sorbents (SC-3-600, SC-5-900, DC-7-900) did not exceed 2 percent. According to the porosity structure results (Table 5.2), the adsorbent derived from sludge S exhibited a remarkable surface area shrinkage, for example, SC-3-600 exhibited a surface area of 281,72 m^2/g that levelled off to 68,22 m^2/g and 46,673 m^2/g when treated with a solution of 1M and 2M, respectively, due to micropore occlusion(Daud & Houshamnd, 2010) and/or thinness of walls (Aburub & Wurster, 2006). In the case of DC-5-750, there was a small reduction in surface area (7,28-30,57 m^2/g) followed by a levelling up of micropore area after modification initially from 124,14 m^2/g to 157,36 m^2/g and 176,11 m^2/g after modification with 1M APS and 2M APS. The surface area of the DC-7-900 was 247,57 m^2/g until modifications such as micropore and mesopore collapse increased the surface area to 285,59 m^2/g for the DC-7-900M1 and 295,31 m^2/g for the DC-7-900M2. This effect may be caused by the reagents etching the surface of activated carbon (Ang et al., 2020).

Table 5.1 Physical structure and ultimate analysis results of SBAC after and before modifications

Adsorbent	Modification conditions	S_{BET} (m^2/g)	S_{meso} (m^2/g)[a]	S_{micro} (m^2/g)[b]	V_{tot} (cm^3/g)[c]	V_{micro} (cm^3/g)d	Pore size (nm)e	C (%)	H (%)
Com-AC	-	609,209	195,74	336,236	0,469	0,165	3,14	78,411	0,000
SC-3-600	Unmodified	281,72	90,942	123,49	0,342	0,075	4,857	45,227	0,7411
	1M APS	68,227	24,098	35,241	0,0953	0,0175	5,58	47,411	1,007
	2M APS	46,573	19,631	14,807	0,085	0,0073	9,02	46,394	1,017
SC-5-900	Unmodified	422,09	222,394	111.15	0,453	0,0495	4,296	2,014	0,000
	2M APS	313,05	61,156	223,75	0,291	0,117	3,604	1,891	0,000
DC-5-750	Unmodified	312,79	100,212	124,14	0,366	0,0898	4,681	23,612	0,454
	1M APS	305.51	115,232	157.36	0,421	0,0741	4,51	29,901	1,087
	2M APS	282,22	77,816	176,113	0,299	0,0083	4,244	30,383	1,019
DC-7-900	Unmodified	247,57	129.83	175,60	0,265	0,0320	4,28	15,460	0,000
	1M APS	285,59	117,275	133,148	0,302	0,0666	4,099	14,831	0,0075
	2M APS	295,31	103,47	121,553	0,289	0,061	3,923	15,111	0,0079

a from BJH adsorbed 170 nm and 300 nm diameter

b from t-plot method

c by Single point adsorption total pore volume of pores less than 235,930 Å diameter at P/Po = 0.99

d by t-plot method

e from BJH Adsorption average pore diameter (4V/A by BET)

5.2 Adsorption Tests Application

5.2.1 **Nitrate**

preliminary evaluation test

As shown in Figure 5.4 at this stage the unmodified adsorbent performed better than the oxidised which can be imputed to the fact that the late one is prone to have highly deprotonated surface at lower pH. The adsorption capacity declined with time except for Com-AC which vary merely from 16,32 mg/g to 13,2 mg/g for a contact time of 180 min and 360 min respectively. Moreover, a considerable amount of nitrate ions was released in the solution from SBAC (DC-5-750M1 and SC-5-900M2) at 360 min and at 720 min (appendix H). Fluoride ions at a concentration of 11,2 g/l, 71,24 g/l, and 49,72 g/l were detected in solution treated with Com-AC, DC-5-750M1 and DC-7-900M1 respectively, and finally Cl^- concentrations overtook initial concentration (141,5 mg/l: originated from HCl with pH adjustment) 770 mg/l and 695 mg/l were measured in the aliquot solution treated with Com-AC and DC-5-750M2. This observation maybe attributed to the release of elements contained in the adsorbent ash in the liquid phase (Kameyama et al., 2016) or adsorption equilibrium phenomenon in which due to saturation site of adsorption site beyond optimum equilibrium contact time the rate of desorption prevailed over the adsorption rate followed by a decline in adsorbent performance (Liadi et al., 2018).

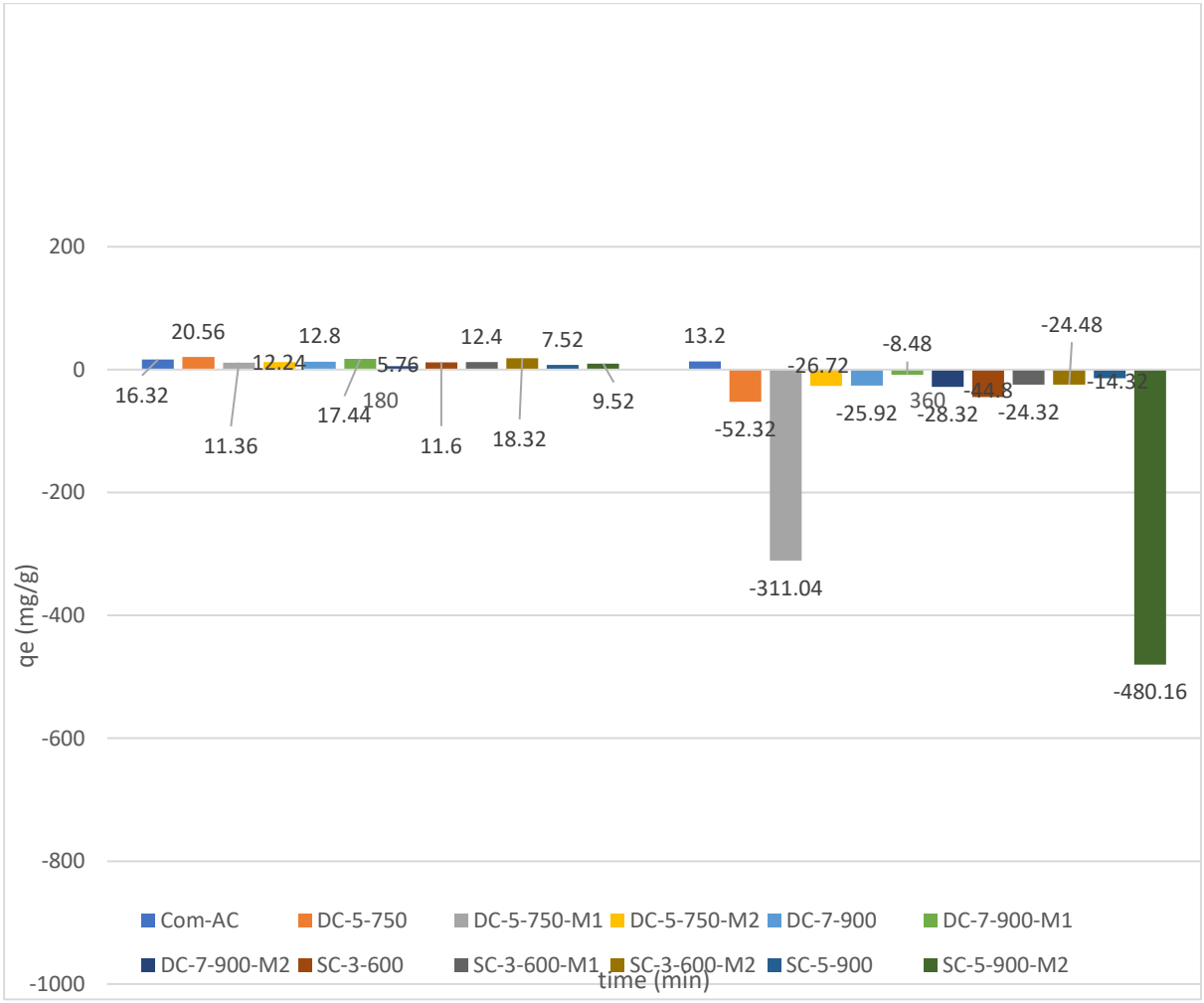


Figure 5.4 preliminary adsorption capacity evaluation of nitrate adsorption

Effect of contact time and kinetics models

Figure 5.5 depicts the trend of nitrate adsorptions as a function of time. First, the adsorption capacity of all sorbents was insignificant before 30 minutes of contact time probably due to resistance of film diffusion (external diffusion) as part of the adsorption steps process (Tan & Hameed, 2017); second, the adsorption capacity of Com-AC, DC-5-750, and DC-5-750M1 was 16,32 mg/g,20,56 mg/g and 11, 06 mg/g.

The upward trend can be attributed to the second (pore diffusion) and third (surface reaction) phases of adsorption, which are thought to counteract lower component resistance, especially the former, in which there is little adsorptive resistance (Tan & Hameed, 2017) and/or nitrate ions occupying accessible adsorption sites as the process progresses (Mazarji et al., 2017; Nassar et al., 2020; Xia et al., 2020) weakening the interaction between sorbate and adsorbent surface (Xia et al., 2020).

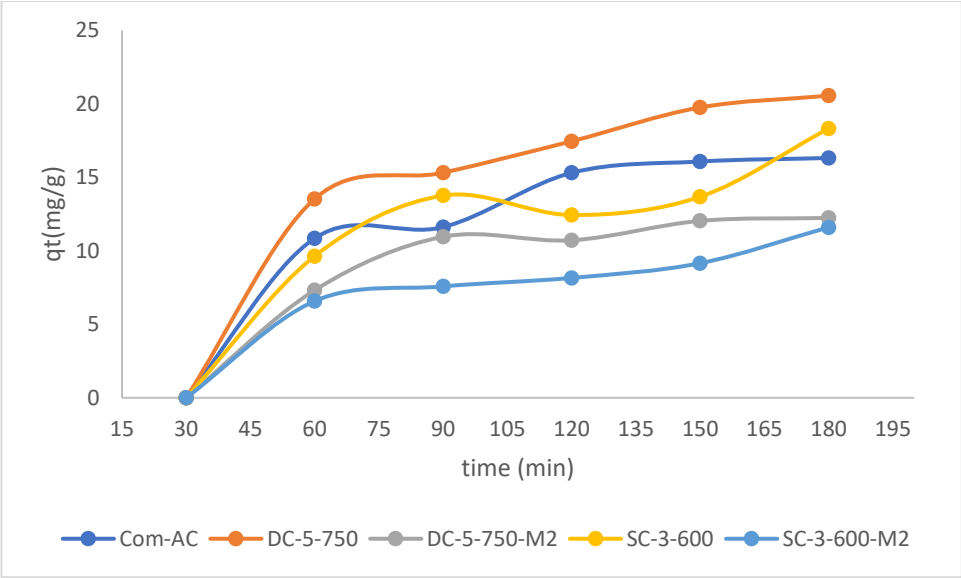


Figure 5.5 effect of time on nitrate adsorption capacity

Figures 5.6 and 5.7 depict the modelling of pseudo first order (PFO) and pseudo second order (PSO), respectively, with the parameters recorded in Table 5.2. It can be shown that only Com-AC suited the PFO model (R^2=0,9693) better than PSO (R^2=0,8569), but the other sorbents fitted the PSO model better with a lower coefficient correlation.

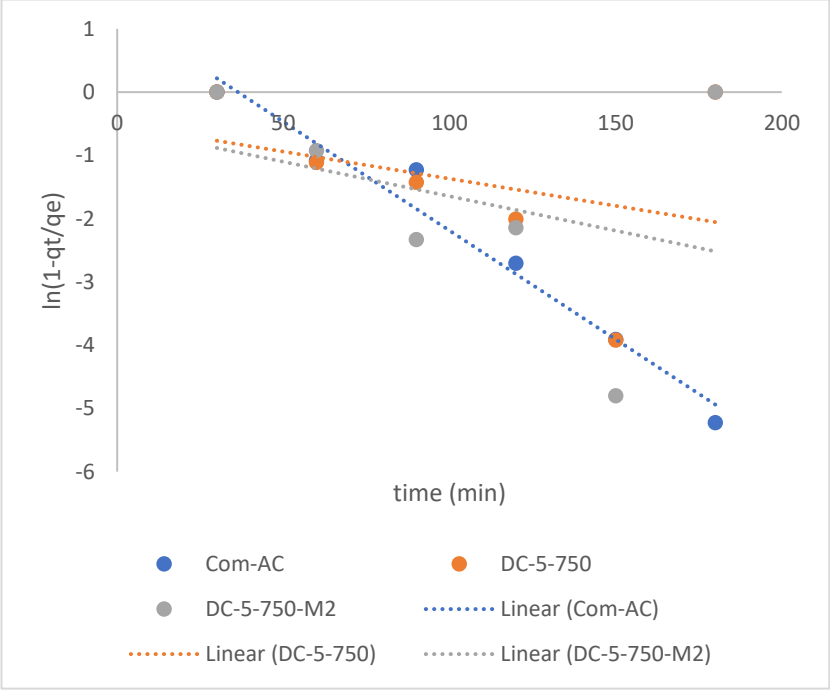


Figure 5.6 nitrate PSO kinetic model plot

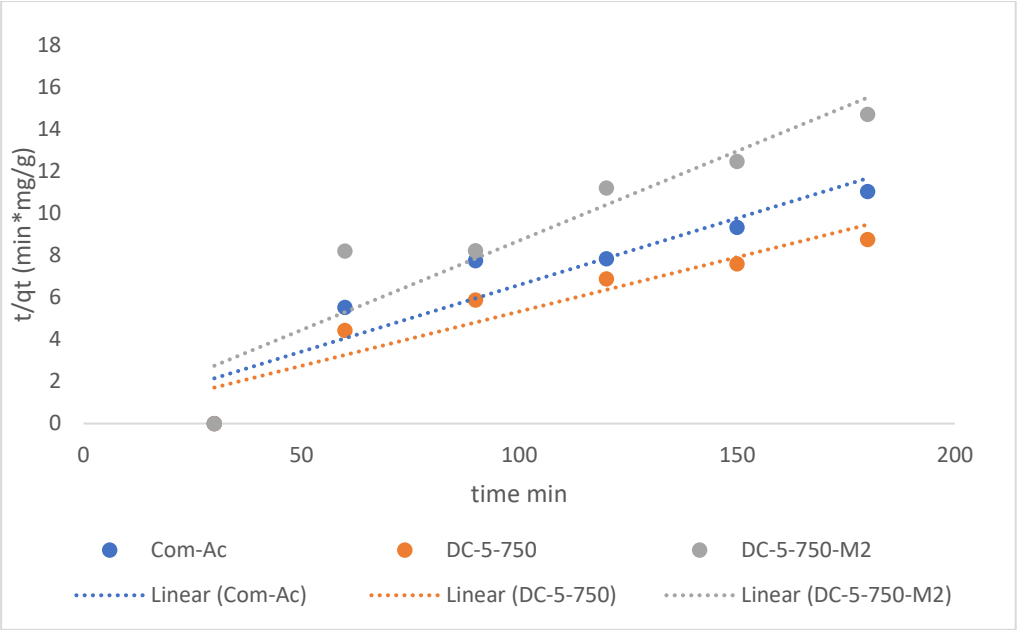


Figure 5.7 nitrate PSO kinetic plots

The diffusion line plot of each sorbent in the intraparticle model (Figure 5.8) does not pass through the axis origin point, indicating that the process mechanism was not exclusively regulated by this model as claimed by previous studies (Bhatnagar et al., 2008; Mazarji et al., 2017)

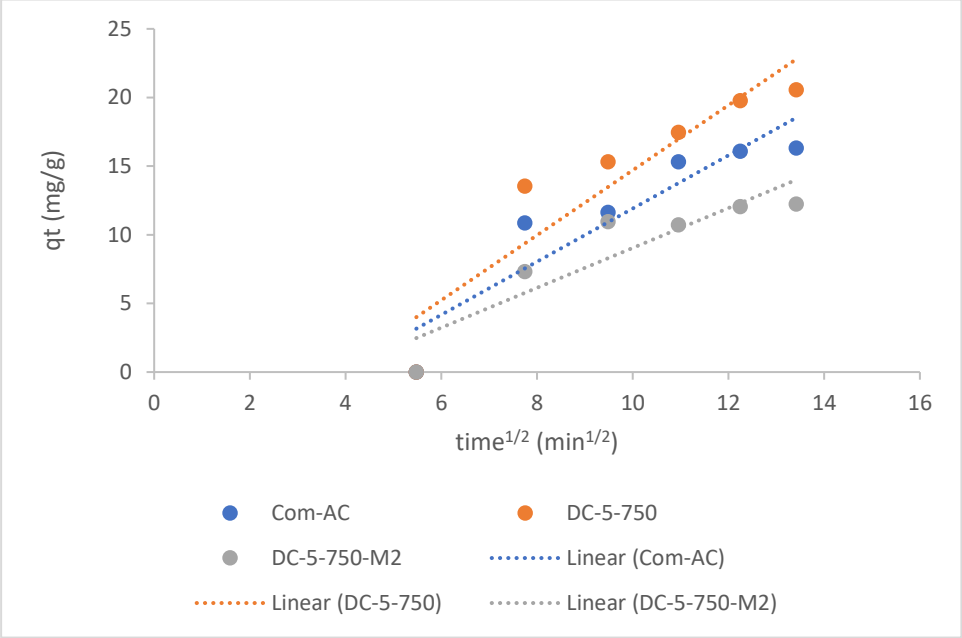


Figure 5.8 intraparticle model diffusion of nitrate adsorption

Except for Com-AC, which adopted the PFO model (R^2 =0,9683), the remaining adsorbents followed the PSO model, but with low R^2 values of 0.7859 and 0.793 for SC-3-600 and SC-3-600 M1 respectively.

Table 5.2 Parameters of PFO, PSO kinetics and intraparticle diffusion nitrate model

	Com-AC	DC-5-750	DC-5-750M1	SC-3-600	SC-3-600M1
Pseudo first order					
Qe (mg/g)	3,49	N/A	N/A	N/A	N/A
$K_1(min^{-1})$	0,0344	N/A	N/A	N/A	N/A
R^2	0,9683	0,108	0,1128	0,1543	0,1186
Pseudo second order					
Qe (mg/g)	15,748	19,342	11,764	15,797	10,277
K_2 (g. $mg^{-1}.min^{-1}$)	0,016	0,016	0,037	0,0072	0,0091
R^2	0,8569	0,8698	0,8663	0,7859	0,793
Interparticle diffusion					
K_{id} ($g.mg^{-1}. min^{-0,5}$)	2,327	2,367	1,451	1,937	1,2479
C	-14,032	-8,966	-5,475	-7,8526	-5,159
R^2	0,8953	0,8525	0,8287	0,8446	0,8827

Effect of pH

The effect of pH was investigated by varying the pH solution from 2 to 10 with increments of 2 as shown in Figure 5.9. pH was a key factor since the process was pH dependable, as the adsorption declined with pH augmentation in the case of DC-5-750 (pHpzc=6,6) from 20,56 mg/g at pH 2, to 6,24 mg/g at pH 6, and 4,2 at pH 10, as shown in Figure 5.9. A similar trend was observed with Com-AC (pHpzc=10,3) and DC-5-750M2 (pHpzc=3,1) where at pH 2 the adsorption capacity was 16,32 mg/g and 12,24 mg/g respectively, at pH6 11,12 mg/g and 9,6 mg/g respectively, at pH10 6mg/g and 1,8mg/g. This trend was more likely linked to (i) favourable conditions of nitrate uptake resulted by electrostatic attraction as adsorbent surface bears positive charge (ii) in basic media competition of nitrate ions with hydroxyl ions as reported in previous publications undertook with carbon-based activated carbon material (Nassar et al., 2020; Nunell et al., 2012; Xia et al., 2020).

On top of the aforementioned reasons, it is possible that the modified SBAC's poor performance is due to the addition of an acidic functional group, which dissociation (deprotonation) beyond pHpzc provides more binding sites for cationic sorbate than the unmodified (Daud & Houshamnd, 2010; Gokce & Aktas, 2014). However, in a peer review dedicated to nitrate adsorption (Bhatnagar et al., 2013), it was stated that carbon clothes oxidised with 4M H_2SO_4 had a higher nitrate adsorption capacity of 2,03 mmol/g than the unmodified 1,01 mmol/g. The outperformance was

linked to the highly surface protonation of the modified sorbents which strengthen electrostatic attraction.

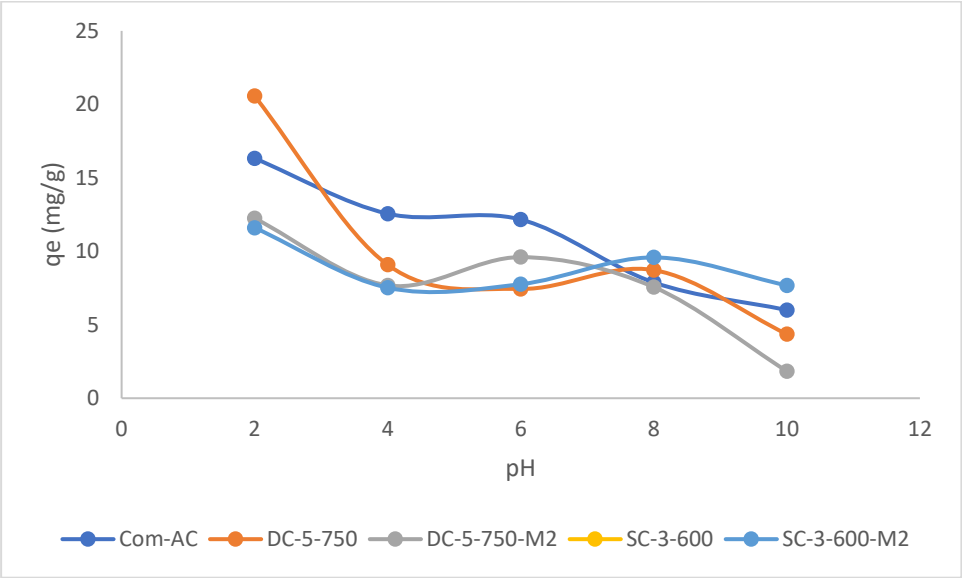


Figure 5.9 Effect of pH solution on nitrate adsorption

Effect of initial concentration and isotherm models

The adsorption capacity increased with initial nitrate concentration augmentation due to the tendency that the driving force of the concentration gradient becomes prominent to break the mass transfer resistance obstacle between the solid and liquid interface (Hadi et al., 2015), nonetheless as illustrated in Figure 5.10 and 5.11 the improvement of sorbent adsorption capacity engendered a decrease in the proportion of impurities uptake since some of them remain in the solution because of adsorbent site saturation (Devi & Saroha, 2017).

For instance in case of Com-AC, DC-5-750, DC-5-750M2 and SC-3-600 adsorption capacity at the lowest initial concentration (10 mg/l) was 5,78 mg/g, 8,50 mg/g, 6,28 mg/g and 8,51 mg/g respectively, at 50 mg/l it was 16,32 mg/g, 20,56 mg/g, 12,24 mg/g and 18,32 mg/g respectively and the highest initial concentration (90mg/l) 13 mg/g, 23,98 mg/g,14,65 mg/g and 18,778 mg/g while the proportion of nitrate removed exhibited the opposite trend at the lowest initial concentration (10 mg/l) it was 27,78 %, 40,87%, 30,19 % and 40,91 percent then decreased at initial concentration of 50 mg/l to 16,32%, 20,56%, 12,4% and 18,32 % finally at the highest initial concentration it was 8,93%, 13,14%, 8,03% and 10,29 % respectively.

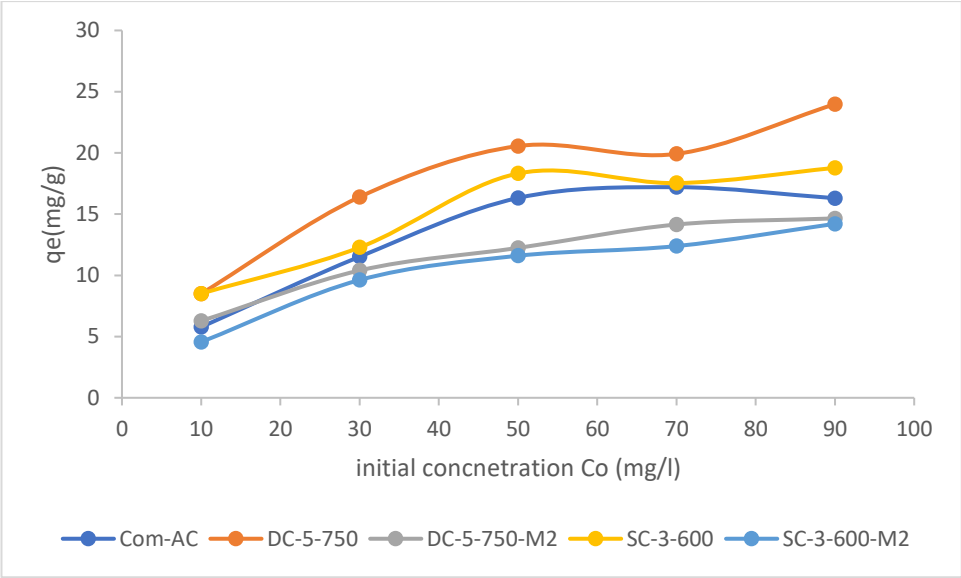


Figure 5.10 effect of initial nitrate concentration on adsorbent adsorption capacity

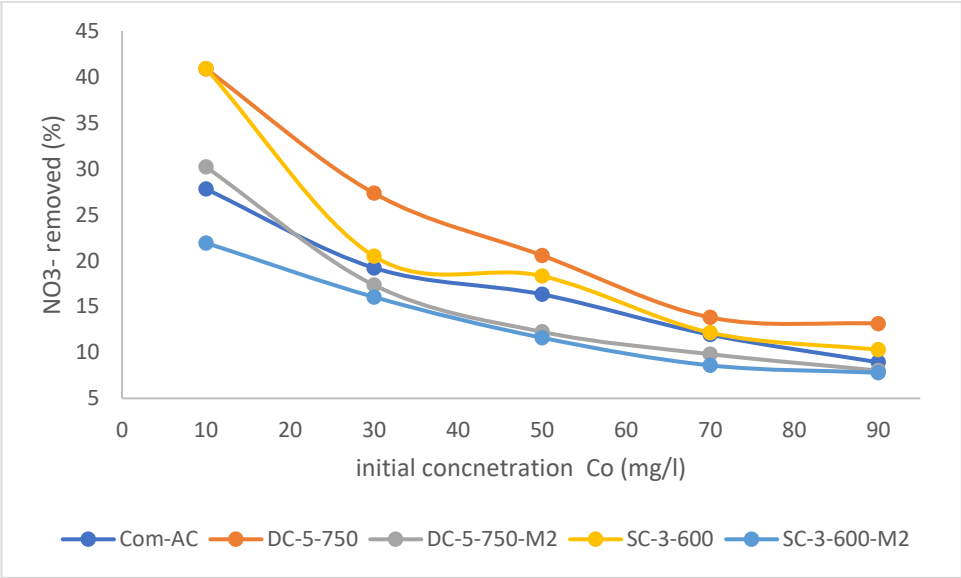


Figure 5.11 effect of nitrate adsorption initial concentration on percentage adsorbent uptake

The lines in Figures 5.12 and 5.13 show the Langmuir and Freundlich isotherms to elucidate the nitrate removal mechanism.

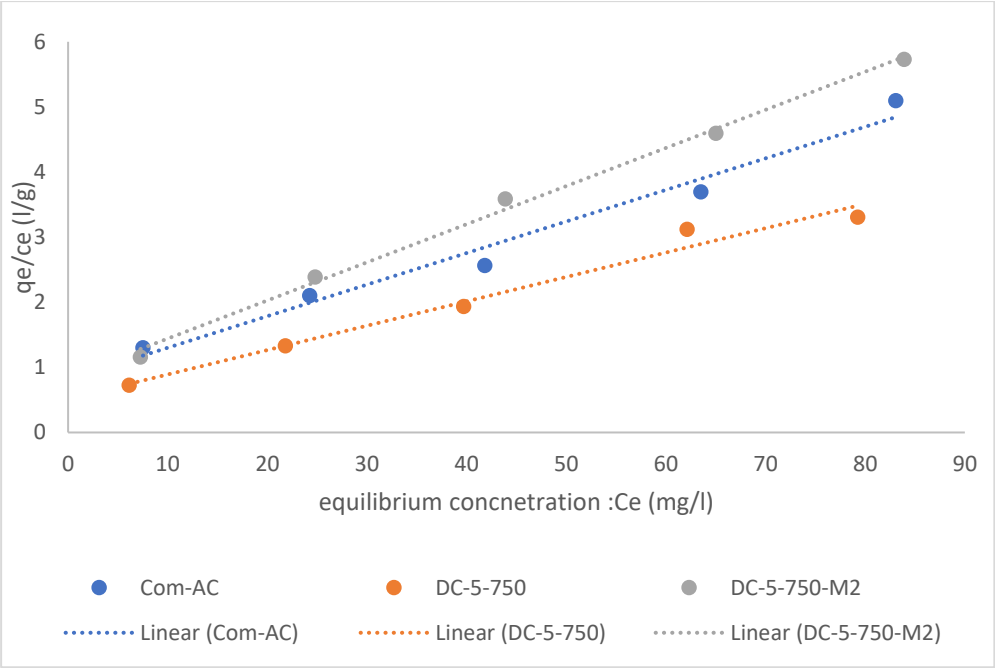


Figure 5.12 Langmuir isotherm plot of nitrate adsorption

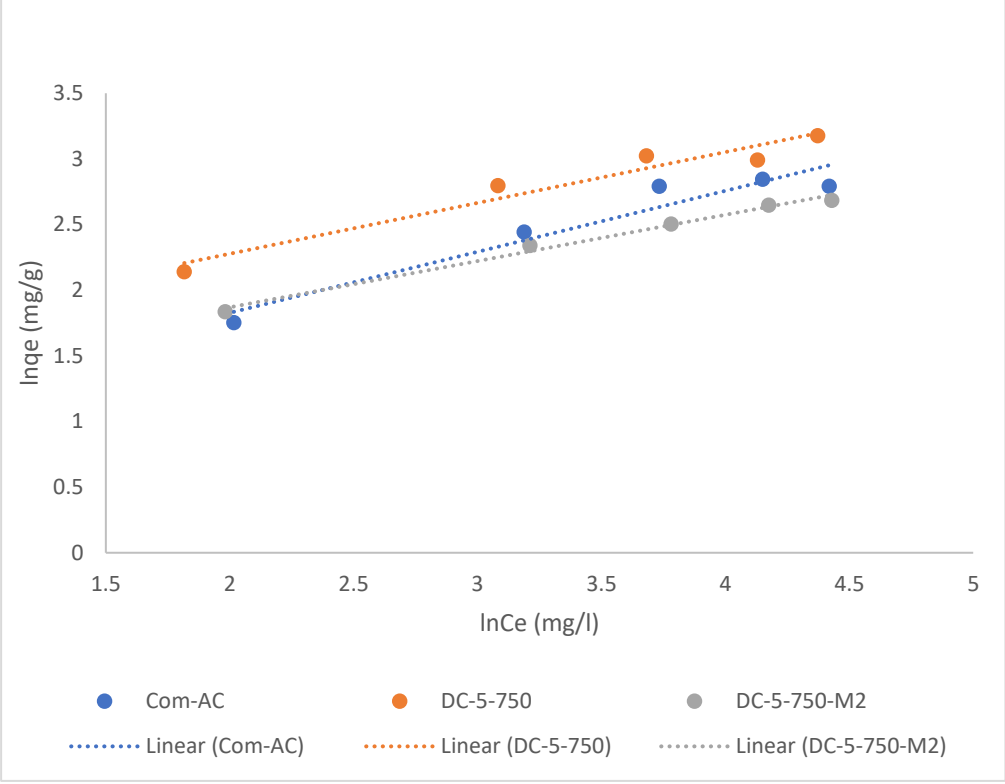


Figure 5.13 Freundlich isotherm plot of nitrate adsorption

The Langmuir isotherm defined the adsorption process better with a higher R^2 than the Freundlich model, which assumed that all adsorbents involved followed a monolayer surface (Tan & Hameed, 2017).

The value of the dimensionless parameter R_L ranging between 0 and 1 indicated that the adsorption of nitrate was favourable on all Langmuir sorbent surface. Adsorption is unfavourable if R_L>1 (Mazarji et al., 2017) and 1/n value of Freundlich parameters were in all cases <0,5 suggesting that nitrate was easily adsorbed (Fan et al., 2016).

Table 5.3 Value of isotherms parameters of nitrate removal

Langmuir	Com-AC	DC-5-750	DC-5-750M1	DC-7-900	DC-7-900M1
Qm (mg/g)	20,618	26,737	17,064	21,276	17,513
B (L/mg)	0,8165	0,5165	0,8561	0,5437	1,2918
R_L	0,109-0,0134	0,1622-0,021	0,1045-0,0128	0,1553-0,02	0,0718-0,0085
R^2	0,9759	0,9772	0,9959	0,9813	0,9967
Freundlich					
K_F (mg/g) $(l/mg)^{1/n}$	2,454	4,4942	3,2072	4,744	1,8323
1/n (l/mg)	0,4648	0,3873	0,3552	0,322	0,4724
R^2	0,9264	0,9455	0,9901	0,9317	0,9583

As shown in Table 5.4, the nitrate adsorption capacity recorded in this study is neither excessively high nor excessively low when compared to other studies and the adsorbent performances were acceptable under the stated conditions.

Table 5.4 Comparison of Langmuir maximum capacity with literature

Adsorbent type	Surface area (m^2/g)	Solution pH	Concentration range (mg/l)	Q_m (mg/g)	Reference
Sawdust AC* with KOH	768	2	8,5-510	25,49	(Nunell et al., 2012)
Commercial AC	1424	2	8,5-510	19,54	
Urea treated AC	192	2	8,5-680	38,82	(Nunell et al., 2015)
Thermally post-treat AC	772	2	8,5-680	25,49	
AC modified with CETAB*	901	7	40-200	21,51	(Mazarji et al., 2017)
Metal modified biochar	155,08	-	50-1500	32,23	(Long et al., 2019)
$ZnCl_2$ olive stone AC	1480	4	100-300	5,525	(Nassar et al., 2020)
Municipal sewage sludge biochar	2,82	2	20-100	2,1127	(Revilla et al., 2020)
Commercial AC	603,209	2	10-90	20,618	This work
DC-5-750	312,79	2	10-90	26,737	
DC-5-750M2	282,22	2	10-90	17,064	

AC*= Activated carbon and CETAB= cetyl trimethyl Ammonium bromide

Thermodynamic Analysis

The thermodynamics parameters ΔH° (kJ/mol)and ΔS° (KJ/mol/K) were deducted from the slope (-ΔH°/R) and the intercept plot (ΔS°/R) from ln (qe/ce) vs 1/T also known as Van't Hoff equation plot (Fan et al., 2016; Jung et al., 2019) whereas the free energy ΔG° (kJ/mol) was deducted from equation (2.7).

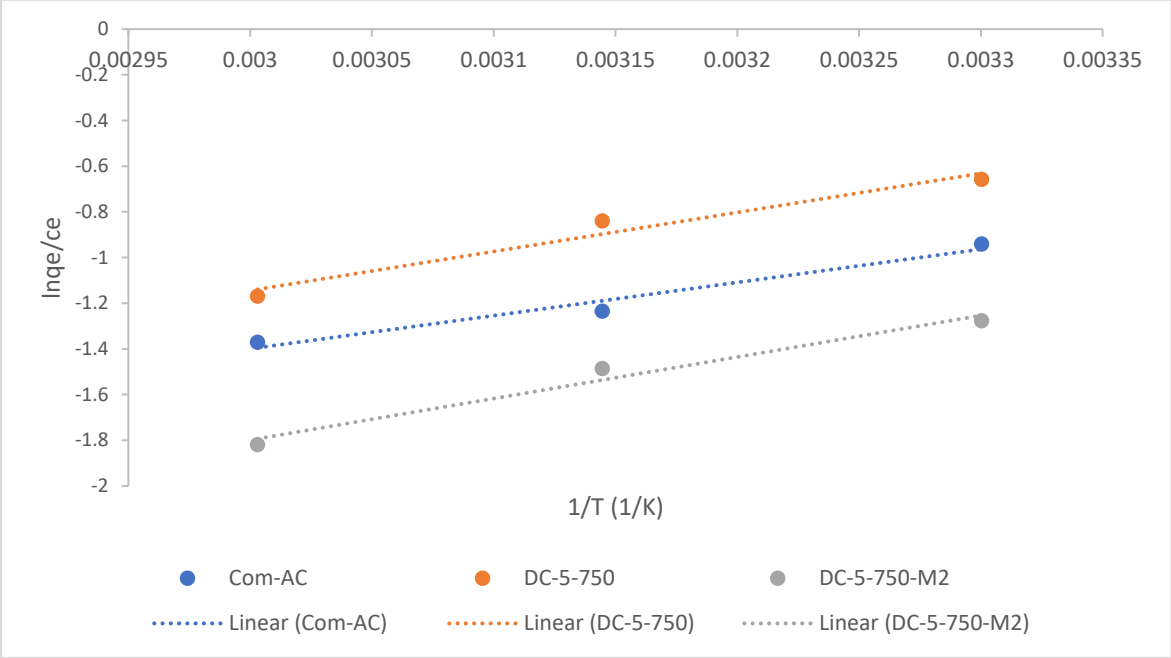


Figure 5.14 plot of nitrate ln(qe/ce) vs 1/T

Based on the thermodynamic parameters values in Table 5.5, it can be concluded that regardless of the adsorbent used in nitrate removal, the process was exothermic as the value of H° was negative with increasing randomness at the solid/liquid surface as the entropy value was negative. Previous research showed that nitrate adsorption on activated carbon-based adsorbents was exothermic (Mazarji et al., 2017; Nassar et al., 2020), and that G increased with temperature incrementation, suggesting that adsorption occurred spontaneously at lower temperatures. When temperatures ranged from 283K to 313K, nitrate adsorption with a commercial activated carbon (Aktivkohle Hydraffn CC8X30) with G>0 was confirmed, and it was suggested that the process could be spontaneous at lower temperatures(Nassar et al., 2020).

Table 5.5 Value of nitrate adsorption thermodynamic parameters

	Adsorbents				
	Com-AC	DC-5-750	DC-5-750-M2	SC-3-600	SC-3-600-M2
Slope	1452,9	1709,3	1816,4	2308,4	1733,8
Intercept	-5,785	-6,272	-7,248	-8,4367	-7,0793
R^2	0,968	0,9629	0,9754	0,9927	0,9816
H° (KJ/Mol)	-12,0794	-14,2111	-15,1015	-19,192	-14,4148
S° (KJ/mol/K)	-0,0481	-0,05215	-0,06026	-0,07014	-0,05886
ΔG at temp (K):					
303	2,49382	1,588938	3,157192	2,061208	3,418949
318	3,21527	2,37112	4,06109	3,113349	4,301808
333	3,93672	3,153301	4,964988	4,165489	5,184668

5.2.2 Methyl red Removal

The low-cost adsorbents synthesized in this study have mesopores feature, which are well suited for medium-sized absorption particles from aqueous solution (Li et al., 2016).

Preliminary evaluation test

As shown in Figure 5.15, adsorption increases with time with the exception of Com-AC, where the change was negligible (from 123 mg/g at 90 min to 121 mg/g at 180 min), owing to the fact that the equilibrium had already been reached. Despite having the highest surface area SC-5-900 (422,09 m^2/g) and SC-5-900M2 (313 m^2/g), its q_e were lower than other sorbents, most likely due to lower carbon content (Table 5.1) or a lack of acidic functional group as they deplete with temperature augmentation (Devi & Saroha, 2016), this finding highlights the importance of functional group presence.

As shown in Figure 5.15, the sorbent with the highest adsorption potential was 127,634 mg/g DC-5-750 M1 and 124,376 mg/g DC-7-900 M1, and it was chosen, along with the unmodified sorbents (DC-5-750 and DC-7-900), for further studies because of its superior performance to Com-AC (121,10 mg/g).

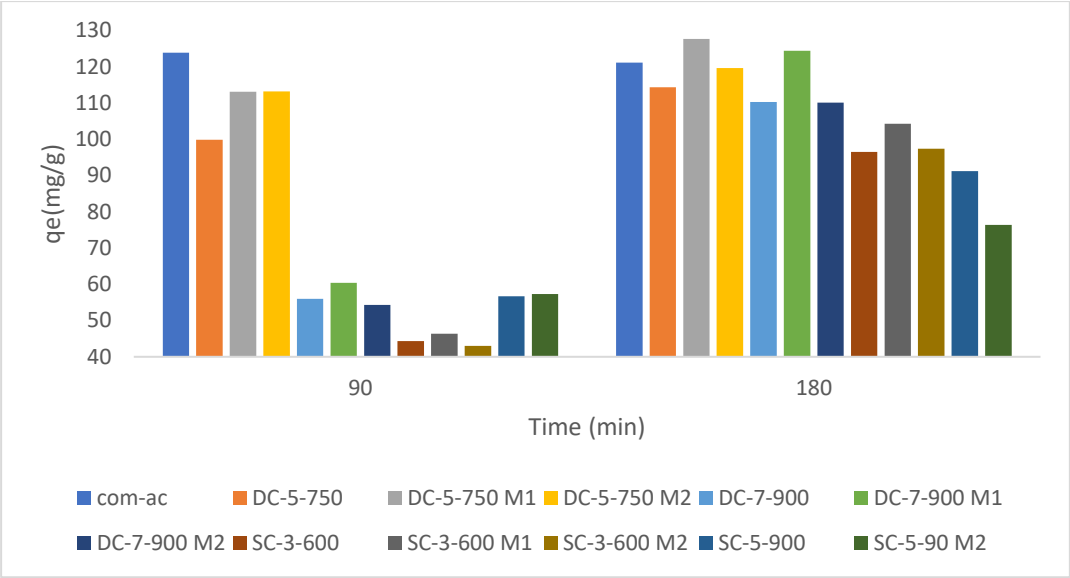


Figure 5.15 preliminary adsorption capacity results of MR adsorption

Effect of time and kinetics model

Figure 5.16 shows the adsorption capacity over a contact time period of 30 min to 180 min, in the case of Com-AC adsorption capacity rose slightly from 109,63 mg/g at 30 min to 123,868 mg/g at 90 min and 121,107 mg/g at 180 min; while DC-5-750 and DC-5-750M1 exhibited sharp augmentation from 83,08 mg/g and 113 mg/g at 30 min to 113,126 mg/g and 123,8 mg/g at 90, respectively.

The rapid increase at the start of the process may be due to the abundant existence of adsorption sites; however, as dye degradation occurs, there is less available site for impurities, resulting in a decrease in the adsorption rate (Ahmad et al., 2015). A similar assumption was invoked for MR removal using activated carbon derived apple custard (Khan et al., 2018).

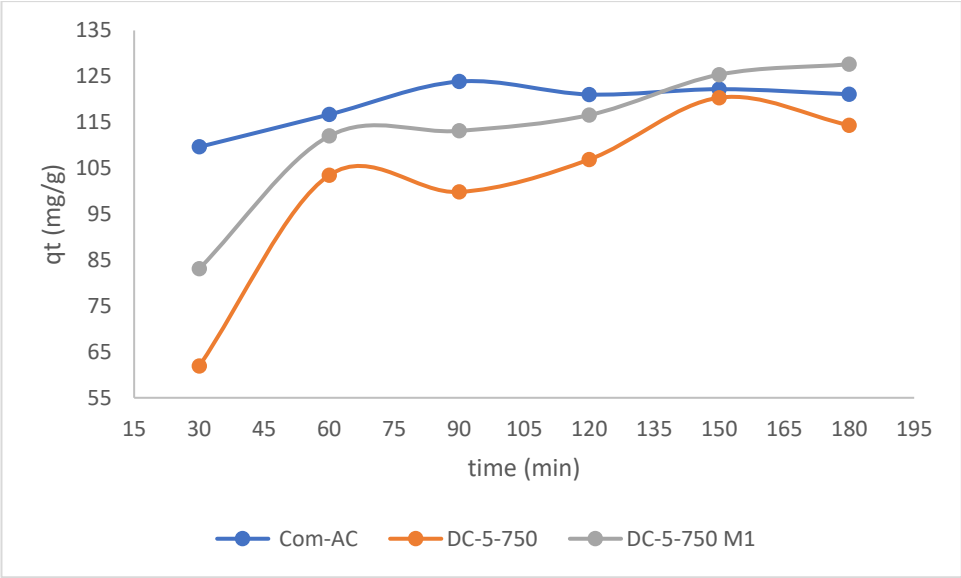


Figure 5.16 effect of contact time on adsorption capacity of MR

The plot of pseudo first-order (PFO), pseudo-second order kinetics (PSO) are depicted in Figures 5.17 and 5.18.

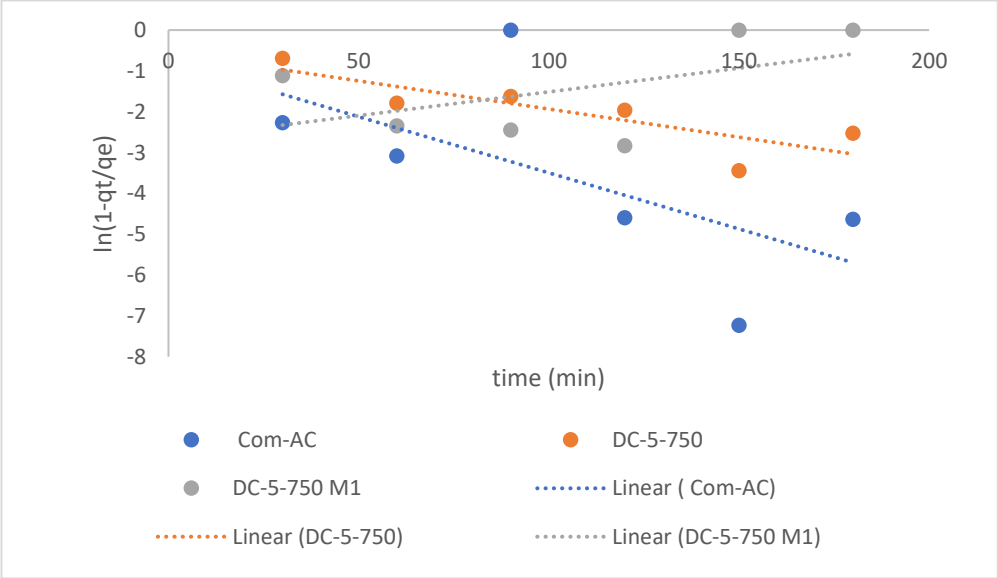


Figure 5.17 methyl red PFO kinetic model

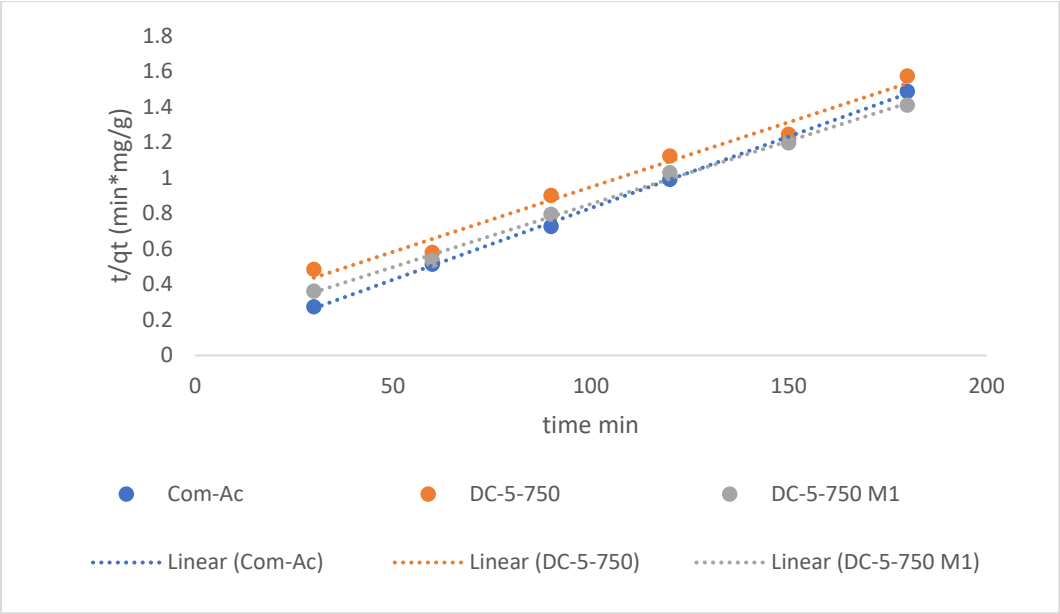


Figure 5.18 methyl red PSO kinetic model

The intraparticle diffusion model line plotted in Figure 5.19 did not pass through the origin because it was not probably the only mechanism that regulated the process, and the parameters values are reported in Table 5.6.

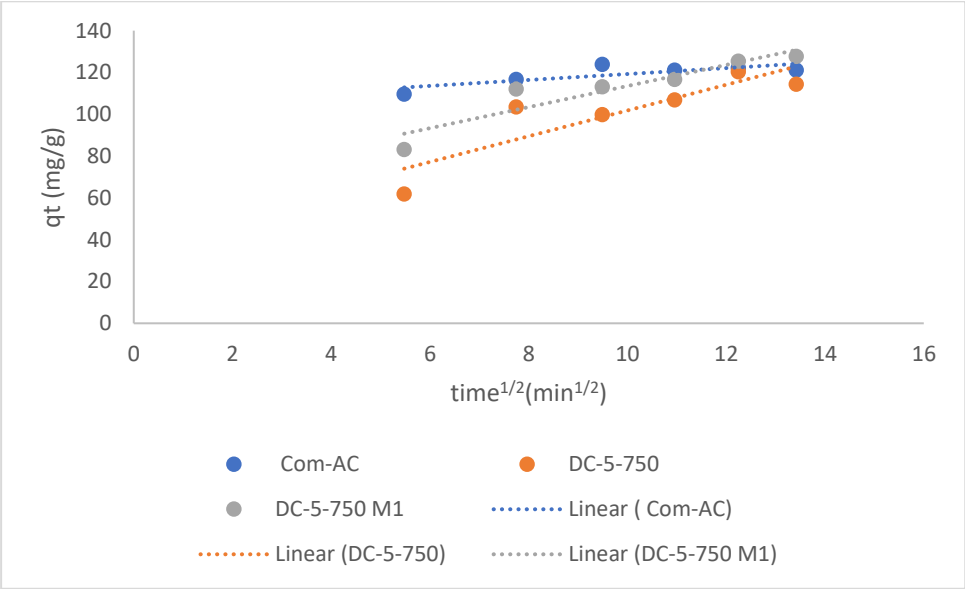


Figure 5.19 methyl red intraparticle diffusion model

Table 5.6 Parameters value of methyl red PFO and PSO kinetic and intraparticle model

	Com-AC	DC-5-750	DC-5-750M1	DC-7-900	DC-7-900M1
Pseudo first order					
Qe (mg/g)	NA	NA	NA	NA	NA
$K_1(min^{-1})$	NA	NA	NA	NA	NA
R^2	0,3935	0,7036	0,2932	0,619	0,5439
Pseudo second order					
Q_e (mg/g)	123,456	136,986	140,84	131,578	136,98
K_2 ($g*mg^{-1}*min^{-1}$)	$2,84\ 10^{-3}$	$2,44\ 10^{-4}$	$3,55\ 10^{-4}$	$1,82\ 10^{-4}$	$2,169\ 10^{-4}$
R^2	0,9815	0,9815	0,9966	0,9831	0,9779
Interparticle diffusion					
K_{id}	1,4188	6,1545	5,045	6,165	5,802
C	105,07	40,275	63,086	27,736	40,181
R^2	0,643	0,7726	0,8644	0,978	0,9509

Effect of pH

The effect of the pH solution is shown in Figure 5.20. The pHpzc of the modified adsorbents with the introduction of oxide groups induced a change from neutral 6,6 (DC-5-750) to acidic after modifications (pH=3,1) DC-5-750-M1 and basic (pH=10.2) for Com-AC. Overall the dye uptake decline with pH augmentation, this downward trend can be ascribed to the electrostatic attraction between the negatively charged surface of the modified adsorbent and the cationic dye (Ahmad et al., 2015; Khan et al., 2018), and the outperformance at pH2 may be attributed to the competition of adsorbent of H^+ and dye. Adsorption of modified adsorbent, which exhibited lower pHpzc than unmodified was more pH dependable due to electrostatic attraction between the adsorbent negatively charge and positive MR below pH4 (Khan et al., 2018), at pH4 the adsorption capacity of DC5-750M1 and DC-7-900M1 was 127.634mg/g and 117.176 mg/g respectively, from pH6, pH8 and pH10 MR and the adsorbents were both negatively charge the adsorption capacity declined from pH6 97,488mg/g for DC-5-750M1 and 109.278 for DC-7-900M1 at pH10 it was 81.854 mg/g for DC-5-750M1 and 71,028 mg/g for DC-7-900M1. The results further show that for the modified adsorbent at pH≤4 the adsorption mechanism was related to electrostatic attraction and to hydrogen bonding at pH ≥ 6 (Jung et al., 2019).

However, in the case of Com-AC, the pH had no significant impact on the adsorption capacity; at pH 2 and pH 10, it was 101.894 mg/g and 113.04 mg/g,

respectively, possibly because the electrostatic attraction mechanism was not very pronounced (Guo et al., 2017).

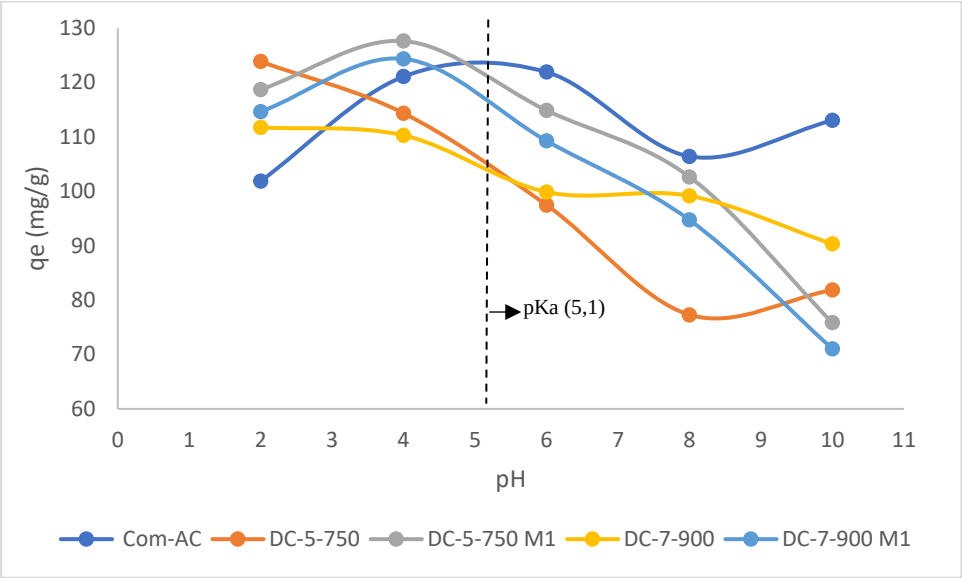


Figure 5.20 effect of solution pH on MR adsorption capacity of adsorbent

Effect of initial concentration and the isotherm models

Figures 5.21 and 5.22 display the difference in adsorbent capacity and dye absorption percentage as a function of initial concentration. As the initial pollutant concentration rises, so does the adsorbent's dye adsorption capacity, thus reducing the proportion extracted due to a stronger driving force to counter mass transfer and less available adsorption site for fraction removed (Afroze & Sen, 2018; Yagub et al., 2014)

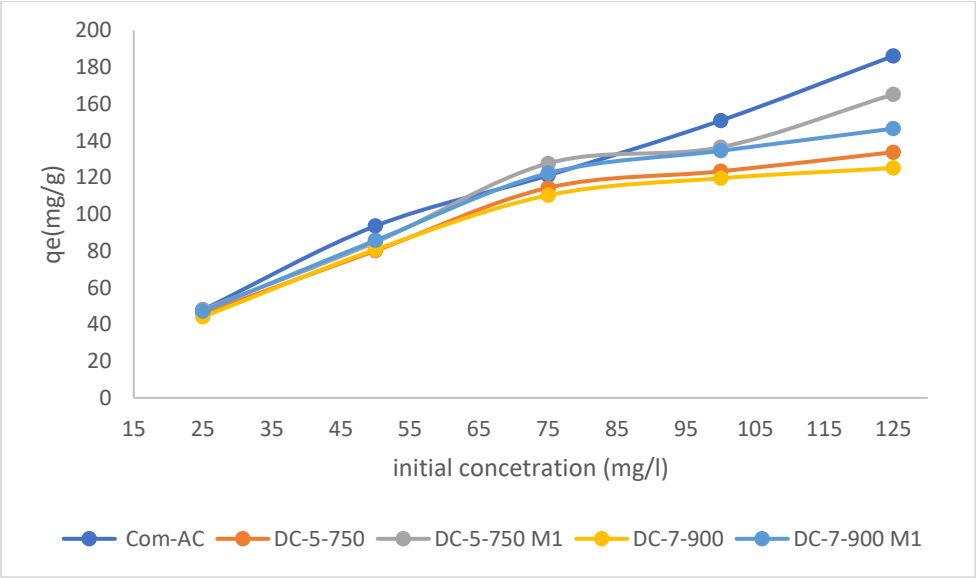


Figure 5.21 adsorption capacity of sorbent in fonction of MR initial concentration

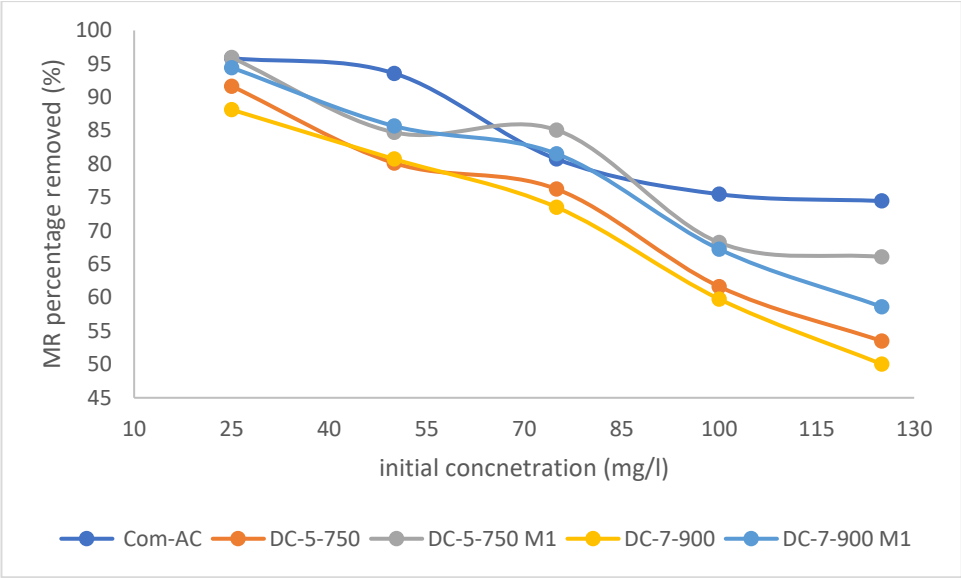


Figure 5.22 MR percentage removed in function of initial concentration

The mechanism of MR adsorption is depicted in Figures 5.23 and 5.24 by the Langmuir and Freundlich isotherms.

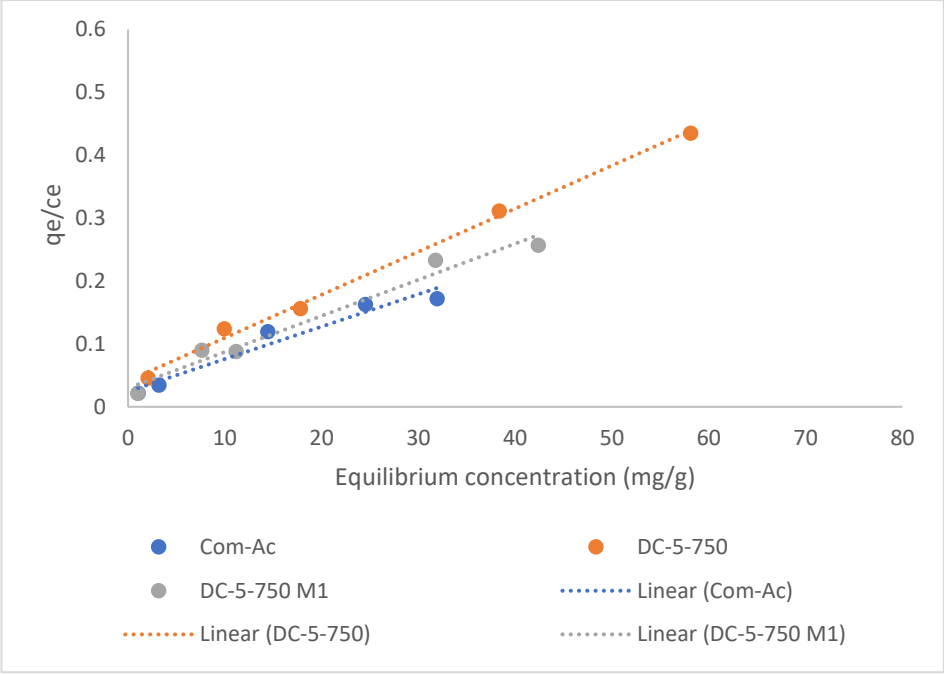


Figure 5.23 Langmuir isotherm plot of MR adsorption

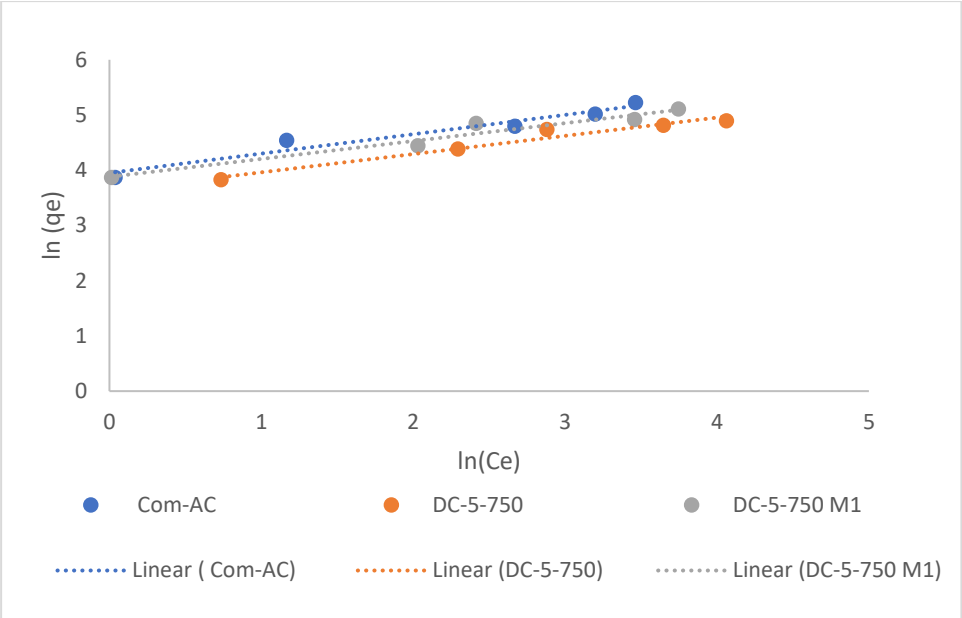


Figure 5.24 Freundlich Isotherm plot of MR adsorption

The Langmuir model defined the process better than the Freundlich model since, with a higher R^2, MR adsorption could not be more beneficial at higher concentrations because the R_L value was moving away from unity and closer to zero because adsorption is irreversible if $R_L=0$, unfavourable if >1, and favourable if $0<R_L<1$ (Gupta & Garg, 2015; Zhang et al., 2015).

Table 5.7 Parameters value of Langmuir and Freundlich isotherm

Langmuir	Com-AC	DC-5-750	DC-5-750M1	DC-7-900	DC-7-900M1
Qm (mg/g)	196,07	147,058	175,438	136,986	156,25
B (L/mg)	0,2082	0,1645	0,1919	0,1648	0,2229
R_L	0,1617-0,037	0,1946-0,0461	0,1724-0,04	0,1953-0,0463	0,1521-0,0346
R^2	0,9515	0,9955	0,9707	0,9992	0,9967
Freundlich					
K_F (mg/g) $(l/mg)^{1/n}$	51,997	37,765	48,443	33,794	45,141
1/n (l/mg)	0,035	0,3306	0,324	0,345	0.3199
R^2	0,9492	0,957	0,9463	0,9242	0,9578

In Table 5.8 shows that the adsorbent used in this study did not have the highest overall monolayer adsorption potential (q_m) when compared to other published data.

Table 5.8 Comparison of adsorption capacity with literature values

Adsorbent type	Surface area (m^2/g)	Solution pH	Concentration range	$Q_{m\ (mg/g)}$	Reference
NaOH lemongrass leaves AC*	834,04	2	25-500	76,923	(Ahmad et al., 2019)
KOH durian seed AC	980,62	-	25-500	384,62	(Ahmad et al., 2015)
Iron modified AC	153,32	-	-	526	(Saleh & Al-Absi, 2017)
K_2CO_3 custard apple AC	431,05	5	80-120	171,23	(Khan et al., 2018)
H_3PO_4 custard apple AC	1065	4	80-120	435,25	
Woody biochar	4.96	-	-	156,25	(Ding et al., 2016)
COM-AC	630,209	4	25-125	196,07	This work
DC-5-750	312,79	4	25-125	147,058	
DC-5-750M1	305,51	4	25-125	175,438	

AC=Activated carbon

Effect of ionic strength

The effect of ionic strength was evaluated by diluting MR in a solution of NaCl with concentrations of 0, 0.01 M and 0,05M and adjusting the pH at 4 as shown in Figure 5.25. The adsorption capacity of Com-AC and unmodified adsorbents increased with NaCl concentration augmentation from 121,08 mg/g to 129,42 mg/g, 114,43 mg/g to 125,31 mg/g and 110,29 mg/g to 122,85 mg/g respectively while opposite results

were observed with the oxidised sorbents (from 127,63 mg/g to 117, 08 mg/g for DC-5-750M1 and 122,296 mg/g to 119,612 mg/g for DC-7-900M1). This is probably due to the competition of Na^+ cations and the screening effect of Cl^- anions in case of the modified adsorbents where the adsorption took place at the external surface (Jung et al., 2019) while in case of Com-AC and the unmodified SBAC it may be possible that aggregation of dye under salt ions force resulted in the extent of an adsorbent surface that may have led to a rise in adsorption capacity with higher NaCl concentration (Al-Degs et al., 2008).

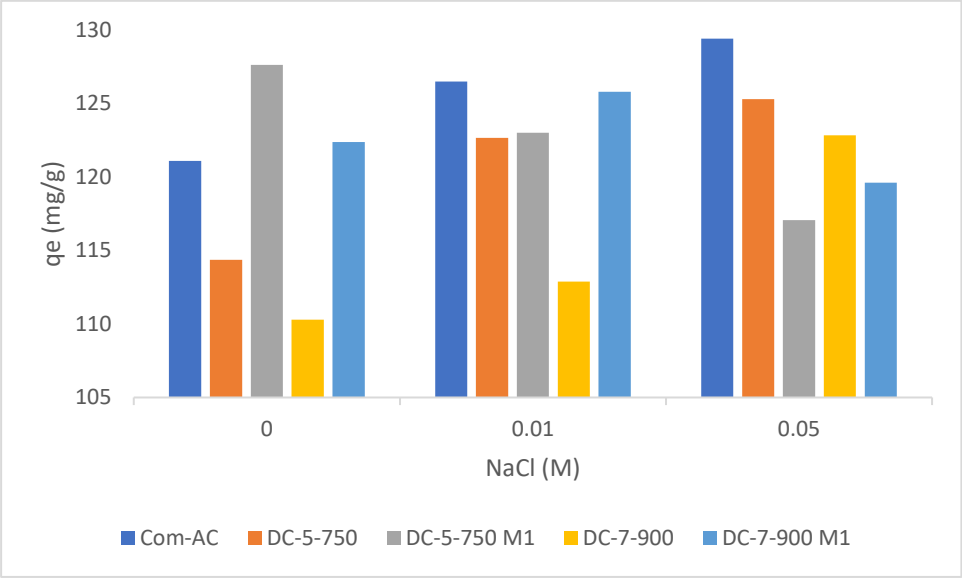


Figure 5.25 effect of ionic strength

Thermodynamic Analysis

The thermodynamics parameters and the coefficient correlations are summarized in Table 5.10.

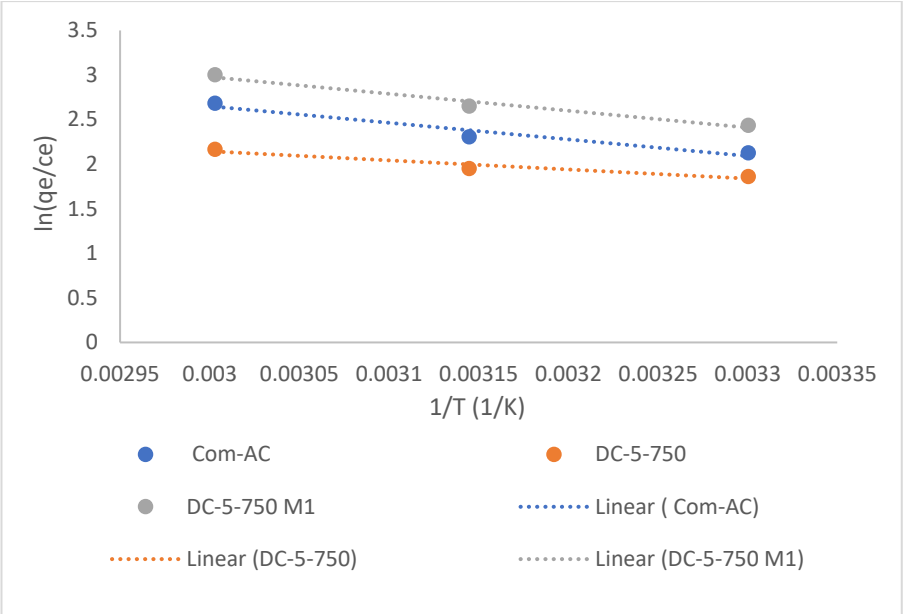


Figure 5.26 plot of ln(qe/ce) vs 1/T of MR adsorption

The free energy (ΔG°: kJ/mol) were negative with values comprise between -20 kJ/mol and 0 kJ/mol for all the adsorbents suggesting that the adsorption process was physical, spontaneous and feasible while a positive value of ΔH suggests that the process was endothermic at low temperature. Surface modification led to a slight increase in ΔH values i.e. the unmodified sorbent DC-5-750 and DC-7-900 had an enthalpy of 8,4986 kJ/mol and 10,4166 kJ/mol respectively compared to the oxidised sorbent DC-5-750 M1 and DC-7-900M1 with enthalpy of 15,8 kJ/mol and 13,7 kJ/mol respectively. Similar previous observation was recorded for Pb(II) adsorption with nitric modified activated carbon, in which the modified adsorbent had an enthalpy of 24,54 kJ/mol and the unmodified adsorbent was -11,66 kJ/mol (Yao et al., 2016).

Previous published studies have shown that MR adsorption with activated carbon adsorbent is an endothermic process (Ahmad et al., 2015, 2019; Khan et al., 2018). If ΔH < 40 kJ/mol the Van der Waal's force can be attributed to physical adsorption, if 50 kJ/mol < ΔH <200 kJ/mol the Van der Waal's force is related to chemisorption (Fan et al., 2016).

Table 5.9 Value of thermodynamic parameter of MR adsorption

	Adsorbents				
	Com-AC	DC-5-750	DC-5-750 M1	DC-7-900	DC-7-900 M1
intercept	-1863,5	-1022,2	-1895,7	-1252,9	1648,3
Slope	8,241	5,2214	8,666	5,8215	7,6424
R^2	0,9491	0,9384	0,974	0,9729	0,9679
ΔH° (KJ/Mol)	15,4931	8,4986	15,7608	10,4166	13,7040
ΔS° (KJ/mol/K)	0,0685	0,0434	0,0720	0,0484	0,0635
ΔG (kJ/mol) at temp (K):					
303	-5,2671	-4,6549	-6,0700	-4,2486	-5,5483
318	-6,2948	-5,3060	-7,1508	-4,9746	-6,5014
333	-7,3226	-5,9572	-8,2315	-5,7006	-7,4545

CHAPTER 6: CONCLUSIONS

This study was undertaken to evaluate the synthesis of bio-adsorbent from locally accessible low-cost feedstocks, and was motivated by the fact that, on the one hand, sewage sludge is an unavoidable waste produced by Wastewater Treatment Plants, and its disposal management raises concerns about soil and groundwater contamination, as well as the associated costs, and, on the other hand, the challenges represented by waste discard coal.

Two types of municipal wastewater sewage sludge were collected, the secondary sludge, which was a dissolved air flotation stage outlet was labelled as (D), while the digested and dewatered (with filter belt) sludge (primary and secondary) ready for disposal was referred to respectively as (D) and (S). The numerical factors of design surface response were KOH concentration: 3, 5 and 7M and the pyrolysis temperature 600 °C, 750°C, 900°C; whereas the sludge type D or S mixed/ unmixed to discard coal, in a proportion of 1:1were part of categorical factors. 8 responses were investigated using surface response methodology: R1 (Specific surface area: m^2/g), R2 (micropore surface area/total surface area*100: %), R3 (CEC: meq/100g), R4 (pHpzc), R5 (Acidity: mmol/g), R6 (Basicity: mmol/g), R7 (N/C ratio) and R8 (H/C ratio).

The results showed that activation with KOH was potent for cavity promotion, which was accentuated by the addition of discard coal, i.e. S-3-600 and D-5-600 had surface areas of 54,39 m^2/g and 76,03 m^2/g, respectively, but with discard coal it levelled up to approximately three-quarters (281,72 m^2/g: SC-3-600) and two-thirds (149,39 m^2/g: DC-5-600). At 60 °C, ammonium persulfate (APS) concentrations of 1M and 2M dissolved in 1M H_2SO_4 solution were used to modify the adsorbent. Adsorbents were chosen for oxidation based on the surface area of the sludge feedstock, for sludge D: DC-5-750: 312,72 m^2/g, 23,61 percent C and DC-7-900: 312,72 m^2/g, 23,61 percent C, S: SC-5-900: 422,09 m^2/g and 2,014 percent C, SC-3-600: 281,72 m^2/g and 45,22 percent C.

Surface area decreased significantly in the case of SBAC derived from Sludge S from 281,72 m^2/g to 46,573 m^2/g (SC-3-600) and 422,09 m^2/g (SC-5-900) to 313,05 m^2/g (SC-3-600) in comparison to those derived from D after modifications with 2M APS solution in similar conditions, the difference was not important. The DC-5-750

has 312,72 m^2/g to 282,22 m^2/g and the DC-7-900 has 247,57 m^2/g to 295,3 m^2/g. SEM observation revealed a polished surface after oxidation, and FT-IR analysis revealed the introduction of acidic functional groups. The pseudo kinetic model better represented the adsorption process using the synthesized AC whether for nitrate or methyl red and diffusion was not found to be the sole controlling mechanism. The Langmuir maximum adsorption potential q_m (mg/g) for nitrate is as follows: DC-5-750 (26,735mg/g) > Com-AC (20,618 mg/g) > DC-7-750M1 (17,064 mg/g) and for methyl red, Com-AC (196,07 mg/g) > DC-5-750M2 (175, 438 mg/g) > DC-7-750 (147,058 mg/g). Thermodynamic analysis further showed that nitrate uptake was exothermic and spontaneous at lower temperatures, with S< 0, while MR uptake was endothermic, feasible, and spontaneous, with S >0. Overall, the performances of the synthesized bio-adsorbents were found adequate for the removal of MR and nitrate and that surface modifications were more profitable for dye adsorption.

For prospects studies in connexion with similar topic as recommendation to fill the knowledge gap we can suggest to explore XPS analysis, zeta potential determination and column adsorption.

BIBLIOGRAPHY

Aburub, A., & Wurster, D. E. (2006). Phenobarbital interactions with derivatized activated carbon surfaces. *Journal of Colloid and Interface Science*, *296*(1), 79–85.

Acheampong, M. A. (2020). *Sustainable Gold Mining Wastewater Treatment by Sorption Using Low-Cost Materials: UNESCO-IHE PhD Thesis*. CRC Press.

Afroze, S., & Sen, T. K. (2018). A Review on Heavy Metal Ions and Dye Adsorption from Water by Agricultural Solid Waste Adsorbents. *Water, Air, & Soil Pollution*, *229*(7), 225. https://doi.org/10.1007/s11270-018-3869-z

Ahmad, M. A., Ahmad, N., & Bello, O. S. (2015). Modified durian seed as adsorbent for the removal of methyl red dye from aqueous solutions. *Applied Water Science*, *5*(4), 407–423. https://doi.org/10.1007/s13201-014-0208-4

Ahmad, M. A., Ahmed, N. B., Adegoke, K. A., & Bello, O. S. (2019). Sorption studies of methyl red dye removal using lemon grass (Cymbopogon citratus). *Chemical Data Collections*, *22*, 100249.

Al-Degs, Y. S., El-Barghouthi, M. I., El-Sheikh, A. H., & Walker, G. M. (2008). Effect of solution pH, ionic strength, and temperature on adsorption behavior of reactive dyes on activated carbon. *Dyes and Pigments*, *77*(1), 16–23.

Aliakbari, Z., Younesi, H., Ghoreyshi, A. A., Bahramifar, N., & Heidari, A. (2018). Production and characterization of sewage-sludge based activated carbons under different post-activation conditions. *Waste and Biomass Valorization*, *9*(3), 451–463.

Almahbashi, N., Kutty, S., Ayoub, M., Noor, A., Salihi, I., Al-Nini, A., Jagaba, A., Aldhawi, B., & Ghaleb, A. (2020). Optimization of Preparation Conditions of Sewage sludge based Activated Carbon. *Ain Shams Engineering Journal*.

Al-Malack, M. H., & Dauda, M. (2017). Competitive adsorption of cadmium and phenol on activated carbon produced from municipal sludge. *Journal of Environmental Chemical Engineering*, *5*(3), 2718–2729.

Álvarez-Merino, M. A., López-Ramón, V., & Moreno-Castilla, C. (2005). A study of the static and dynamic adsorption of Zn (II) ions on carbon materials from aqueous solutions. *Journal of Colloid and Interface Science*, *288*(2), 335–341.

Ang, T. N., Young, B. R., Taylor, M., Burrell, R., Aroua, M. K., Chen, W.-H., & Baroutian, S. (2020). Enrichment of surface oxygen functionalities on activated carbon for adsorptive removal of sevoflurane. *Chemosphere*, *260*, 127496.

Asuquo, E., Martin, A., Nzerem, P., Siperstein, F., & Fan, X. (2017). Adsorption of Cd (II) and Pb (II) ions from aqueous solutions using mesoporous activated carbon adsorbent: Equilibrium, kinetics and characterisation studies. *Journal of Environmental Chemical Engineering*, *5*(1), 679–698.

Bandosz, T. J. (2006). *Activated carbon surfaces in environmental remediation*. Elsevier.

Bansal, R. C., & Goyal, M. (2005). *Activated Carbon Adsorption*. CRC Press.

Bhadra, B. N., Seo, P. W., & Jhung, S. H. (2016). Adsorption of diclofenac sodium from water using oxidized activated carbon. *Chemical Engineering Journal*, *301*, 27–34.

Bhatnagar, A., Hogland, W., Marques, M., & Sillanpää, M. (2013). An overview of the modification methods of activated carbon for its water treatment applications. *Chemical Engineering Journal*, *219*, 499–511.

Bhatnagar, A., Ji, M., Choi, Y., Jung, W., Lee, S., Kim, S., Lee, G., Suk, H., Kim, H., & Min, B. (2008). Removal of nitrate from water by adsorption onto zinc chloride treated activated carbon. *Separation Science and Technology*, *43*(4), 886–907.

Björklund, K., & Li, L. Y. (2017). Adsorption of organic stormwater pollutants onto activated carbon from sewage sludge. *Journal of Environmental Management*, *197*, 490–497.

Boehm, H. P. (2002). Surface oxides on carbon and their analysis: A critical assessment. *Carbon*, *40*(2), 145–149.

Boualem, T., Debab, A., de Yuso, A. M., & Izquierdo, M. (2014). Activated carbons obtained from sewage sludge by chemical activation: Gas-phase environmental applications. *Journal of Environmental Management*, *140*, 145–151.

Cechinel, M. A. P., & de Souza, A. A. U. (2014). Study of lead (II) adsorption onto activated carbon originating from cow bone. *Journal of Cleaner Production*, *65*, 342–349.

Dai, Y., Zhang, K., Li, J., Jiang, Y., Chen, Y., & Tanaka, S. (2017). Adsorption of copper and zinc onto carbon material in an aqueous solution oxidized by ammonium peroxydisulphate. *Separation and Purification Technology*, *186*, 255–263.

Daud, W. M. A. W., & Houshamnd, A. H. (2010). Textural characteristics, surface chemistry and oxidation of activated carbon. *Journal of Natural Gas Chemistry*, *19*(3), 267–279.

de Andrés, J. M., Orjales, L., Narros, A., de la Fuente, M. del M., & Rodríguez, M. E. (2013). Carbon dioxide adsorption in chemically activated carbon from sewage sludge. *Journal of the Air & Waste Management Association*, *63*(5), 557–564.

De Filippis, P., Palma, L., Petrucci, E., Scarsella, M., & Verdone, N. (2013). Production and characterization of adsorbent materials from sewage sludge by pyrolysis. *Chem. Eng. Trans*, *32*.

De Gisi, S., Lofrano, G., Grassi, M., & Notarnicola, M. (2016). Characteristics and adsorption capacities of low-cost sorbents for wastewater treatment: A review. *Sustainable Materials and Technologies*, *9*, 10–40.

Devi, P., & Saroha, A. K. (2016). Improvement in performance of sludge-based adsorbents by controlling key parameters by activation/modification: A critical review. *Critical Reviews in Environmental Science and Technology*, *46*(21–22), 1704–1743.

Devi, P., & Saroha, A. K. (2017). Utilization of sludge based adsorbents for the removal of various pollutants: A review. *Science of the Total Environment*, *578*, 16–33.

Diffo, B. K., Elimbi, A., Cyr, M., Manga, J. D., & Kouamo, H. T. (2015). Effect of the rate of calcination of kaolin on the properties of metakaolin-based geopolymers. *Journal of Asian Ceramic Societies*, *3*(1), 130–138.

Ding, G., Wang, B., Chen, L., & Zhao, S. (2016). Simultaneous adsorption of methyl red and methylene blue onto biochar and an equilibrium modeling at high concentration. *Chemosphere*, *163*, 283–289.

Domingo-Garcia, M., Lopez-Garzon, F., & Perez-Mendoza, M. (2000). Effect of some oxidation treatments on the textural characteristics and surface chemical nature of an activated carbon. *Journal of Colloid and Interface Science*, *222*(2), 233–240.

Donahue, C. J., & Rais, E. A. (2009). Proximate analysis of coal. *Journal of Chemical Education*, *86*(2), 222.

dos Reis, G. S., Adebayo, M. A., Lima, E. C., Sampaio, C. H., & Prola, L. D. (2016). Activated carbon from sewage sludge for preconcentration of copper. *Analytical Letters*, *49*(4), 541–555.

dos Reis, G. S., Mahbub, M. K. B., Wilhelm, M., Lima, E. C., Sampaio, C. H., Saucier, C., & Dias, S. L. P. (2016). Activated carbon from sewage sludge for removal of sodium diclofenac and nimesulide from aqueous solutions. *Korean Journal of Chemical Engineering*, *33*(11), 3149–3161.

dos Reis, G. S., Wilhelm, M., de Almeida Silva, T. C., Rezwan, K., Sampaio, C. H., Lima, E. C., & de Souza, S. M. G. U. (2016). The use of design of experiments for the evaluation of the production of surface rich activated carbon from sewage sludge via microwave and conventional pyrolysis. *Applied Thermal Engineering*, *93*, 590–597.

DWA. (2013a). *National Water Resource Strategy water equitable and sustainable future*. Department of Water Affairs.

DWA. (2013b, July 4). *National Water Resource Strategy*. Centre for Environmental Rights. https://cer.org.za/news/national-water-resource-strategy

Fan, S., Tang, J., Wang, Y., Li, H., Zhang, H., Tang, J., Wang, Z., & Li, X. (2016). Biochar prepared from co-pyrolysis of municipal sewage sludge and tea waste for the adsorption of methylene blue from aqueous solutions: Kinetics, isotherm, thermodynamic and mechanism. *Journal of Molecular Liquids*, *220*, 432–441.

Feng, N., Wei, F., Zhu, M., & Guo, X. (2018). Adsorption of Cd2+ in aqueous solutions using KMnO4-modified activated carbon derived from Astragalus residue. *Transactions of Nonferrous Metals Society of China*, *28*(4), 794–801.

Figueiredo, C., Lopes, H., Coser, T., Vale, A., Busato, J., Aguiar, N., Novotny, E., & Canellas, L. (2018). Influence of pyrolysis temperature on chemical and physical properties of biochar from sewage sludge. *Archives of Agronomy and Soil Science*, *64*(6), 881–889.

Gokce, Y., & Aktas, Z. (2014). Nitric acid modification of activated carbon produced from waste tea and adsorption of methylene blue and phenol. *Applied Surface Science*, *313*, 352–359.

Gómez-Pacheco, C., Rivera-Utrilla, J., Sánchez-Polo, M., & López-Peñalver, J. (2012). Optimization of the preparation process of biological sludge adsorbents for application in water treatment. *Journal of Hazardous Materials*, *217*, 76–84.

Gong, X. (2013). *Modification and utilization of sewage sludge-based activated carbon as metal adsorbents*. University of The British Columbia.

Guo, T., Yao, S., Chen, H., Yu, X., Wang, M., & Chen, Y. (2017). Characteristics and adsorption study of the activated carbon derived from municipal sewage sludge. *Water Science and Technology*, *76*(7), 1697–1705.

Gupta, A., & Garg, A. (2015). Primary sewage sludge-derived activated carbon: Characterisation and application in wastewater treatment. *Clean Technologies and Environmental Policy*, *17*(6), 1619–1631.

Hadi, P., Xu, M., Ning, C., Lin, C. S. K., & McKay, G. (2015). A critical review on preparation, characterization and utilization of sludge-derived activated carbons for wastewater treatment. *Chemical Engineering Journal*, *260*, 895–906.

Han, X., Lin, H., & Zheng, Y. (2015). Adsorptive denitrogenation and desulfurization of diesel using activated carbons oxidized by (NH4) 2S2O8 under mild conditions. *The Canadian Journal of Chemical Engineering*, *93*(3), 538–548.

Herselman, J., & Moodley, P. (2009). *Guidelines for the Utilisation and Disposal of Wastewater Sludge Volume 5: Requirements for thermal sludge management practices and for commercial products containing sludge*. Departement of Water and Forestery.

Herselman, J., Steyn, C. E., & Snyman, H. (2006). Dedicated land disposal of wastewater sludge in South Africa: Leaching of trace elements and nutrients. *Water Science and Technology*, *54*(5), 139–146.

Hobbs, P. J., & Cobbing, J. E. (2007). *Hydrogeological assessment of acid mine drainage impacts in the West Rand Basin, Gauteng Province*.

Huang, H., Yang, T., Lai, F., & Wu, G. (2017). Co-pyrolysis of sewage sludge and sawdust/rice straw for the production of biochar. *Journal of Analytical and Applied Pyrolysis*, *125*, 61–68.

Hui, T. S., & Zaini, M. A. A. (2015). Potassium hydroxide activation of activated carbon: A commentary. *Carbon Letters (Carbon Lett.)*, *16*(4), 275–280.

Jung, K., Lee, S. Y., & Lee, Y. J. (2019). Optimized preparation of activated carbon from municipal sewage sludge and application to the adsorption of azo dye from aqueous solutions. *Environmental Progress & Sustainable Energy*, *38*(s1), S267–S276.

Kacprzak, M., Neczaj, E., Fijałkowski, K., Grobelak, A., Grosser, A., Worwag, M., Rorat, A., Brattebo, H., Almås, Å., & Singh, B. R. (2017). Sewage sludge disposal strategies for sustainable development. *Environmental Research*, *156*, 39–46.

Kameyama, K., Miyamoto, T., Iwata, Y., & Shiono, T. (2016). Influences of feedstock and pyrolysis temperature on the nitrate adsorption of biochar. *Soil Science and Plant Nutrition*, *62*(2), 180–184.

Khan, E. A., Shahjahan, & Khan, T. A. (2018). Adsorption of methyl red on activated carbon derived from custard apple (Annona squamosa) fruit shell: Equilibrium isotherm and kinetic studies. *Journal of Molecular Liquids*, *249*, 1195–1211. https://doi.org/10.1016/j.molliq.2017.11.125

Lee, Y.-E., Kim, I.-T., & Yoo, Y.-S. (2018). Stabilization of high-organic-content water treatment sludge by pyrolysis. *Energies*, *11*(12), 3292.

Leng, L., Yuan, X., Huang, H., Shao, J., Wang, H., Chen, X., & Zeng, G. (2015). Bio-char derived from sewage sludge by liquefaction: Characterization and application for dye adsorption. *Applied Surface Science*, *346*, 223–231.

Li, J., Xing, X., Li, J., Shi, M., Lin, A., Xu, C., Zheng, J., & Li, R. (2018). Preparation of thiol-functionalized activated carbon from sewage sludge with coal blending for heavy metal removal from contaminated water. *Environmental Pollution*, *234*, 677–683.

Li, L. Y., Gong, X., & Abida, O. (2019). Waste-to-resources: Exploratory surface modification of sludge-based activated carbon by nitric acid for heavy metal adsorption. *Waste Management*, *87*, 375–386.

Li, N., Ma, X., Zha, Q., Kim, K., Chen, Y., & Song, C. (2011). Maximizing the number of oxygen-containing functional groups on activated carbon by using ammonium persulfate and improving the temperature-programmed desorption characterization of carbon surface chemistry. *Carbon*, *49*(15), 5002–5013.

Li, Y., Li, Y., Li, L., Shi, X., & Wang, Z. (2016). Preparation and analysis of activated carbon from sewage sludge and corn stalk. *Advanced Powder Technology*, *27*(2), 684–691.

Li, Z., Deng, H., Yang, L., Zhang, G., Li, Y., & Ren, Y. (2018). Influence of potassium hydroxide activation on characteristics and environmental risk of heavy metals in chars derived from municipal sewage sludge. *Bioresource Technology*, *256*, 216–223.

Liadi, M. A., Mu'azu, N. D., Jarrah, N., Zubair, M., Alagha, O., Al-Harthi, M. A., & Essa, M. H. (2020). Comparative performance study of ZnCl2 and NaOH sludge based activated carbon for simultaneous aqueous uptake of phenolic compounds. *International Journal of Environmental Analytical Chemistry*, 1–25.

Liadi, M. A., Tawabini, B., Shawabkeh, R., Jarrah, N., Oyehan, T. A., Shaibani, A., & Makkawi, M. (2018). Treating MTBE-contaminated water using sewage sludge-derived activated carbon. *Environmental Science and Pollution Research*, *25*(29), 29397–29407.

Liang, Q., Liu, Y., Chen, M., Ma, L., Yang, B., Li, L., & Liu, Q. (2020). Optimized preparation of activated carbon from coconut shell and municipal sludge. *Materials Chemistry and Physics*, *241*, 122327.

Libhaber, M., & Orozco-Jaramillo, Á. (2012). *Sustainable Treatment and Reuse of Municipal Wastewater: For decision makers and practising engineers*. Iwa publishing.

Lin, Q., Cheng, H., & Chen, G. (2012). Preparation and characterization of carbonaceous adsorbents from sewage sludge using a pilot-scale microwave heating equipment. *Journal of Analytical and Applied Pyrolysis*, *93*, 113–119.

Long, L., Xue, Y., Hu, X., & Zhu, Y. (2019). Study on the influence of surface potential on the nitrate adsorption capacity of metal modified biochar. *Environmental Science and Pollution Research*, *26*(3), 3065–3074.

Lu, H., Zhang, W., Wang, S., Zhuang, L., Yang, Y., & Qiu, R. (2013). Characterization of sewage sludge-derived biochars from different feedstocks and pyrolysis temperatures. *Journal of Analytical and Applied Pyrolysis*, *102*, 137–143.

Machida, M., Chensun, S., Amano, Y., & Imazeki, F. (2015). Adsorptive removal of Pb (II) ions from aqueous solution by (NH4) 2S2O8 oxidized activated carbons. *Bulletin of the Chemical Society of Japan*, *88*(1), 127–132.

Marsh, H., & Reinoso, F. R. (2006). *Activated carbon*. Elsevier.

Masindi, V., Chatzisymeon, E., Kortidis, I., & Foteinis, S. (2018). Assessing the sustainability of acid mine drainage (AMD) treatment in South Africa. *Science of the Total Environment*, *635*, 793–802.

Mazarji, M., Aminzadeh, B., Baghdadi, M., & Bhatnagar, A. (2017). Removal of nitrate from aqueous solution using modified granular activated carbon. *Journal of Molecular Liquids*, *233*, 139–148.

Mmonatau, M. M. M. (2018). *Production of activated carbon fibers and carbon nanotubes from Ion exchange resins*. University of the Witwatersrand,Johanneburg.

Mohamed, E. F., Andriantsiferana, C., Wilhelm, A.-M., & Delmas, H. (2011). Competitive adsorption of phenolic compounds from aqueous solution using sludge-based activated carbon. *Environmental Technology*, *32*(12), 1325–1336.

Monsalvo, V. M., Mohedano, A. F., & Rodriguez, J. J. (2011). Activated carbons from sewage sludge: Application to aqueous-phase adsorption of 4-chlorophenol. *Desalination*, *277*(1–3), 377–382.

Moreno-Castilla, C., Carrasco-Marín, F., & Mueden, A. (1997). The creation of acid carbon surfaces by treatment with (NH4) 2S2O8. *Carbon*, *35*(10–11), 1619–1626.

Moreno-Castilla, C., Ferro-Garcia, M., Joly, J., Bautista-Toledo, I., Carrasco-Marin, F., & Rivera-Utrilla, J. (1995). Activated carbon surface modifications by nitric acid, hydrogen peroxide, and ammonium peroxydisulfate treatments. *Langmuir*, *11*(11), 4386–4392.

Moreno-Castilla, C., López-Ramón, M., & Carrasco-Marın, F. (2000). Changes in surface chemistry of activated carbons by wet oxidation. *Carbon*, *38*(14), 1995–2001.

Mulopo, J. (2017). Electrochemical recovery of hydrogen from coal acid mine drainage for the enhancement of sulphate reduction using grass cellulose as carbon source. *Water and Environment Journal*, *31*(3), 302–309.

Nassar, H., Zyoud, A., El-Hamouz, A., Tanbour, R., Halayqa, N., & Hilal, H. S. (2020). Aqueous nitrate ion adsorption/desorption by olive solid waste-based carbon activated using ZnCl2. *Sustainable Chemistry and Pharmacy*, *18*, 100335.

Nunell, G., Fernández, M., Bonelli, P., & Cukierman, A. (2012). Conversion of biomass from an invasive species into activated carbons for removal of nitrate from wastewater. *Biomass and Bioenergy*, *44*, 87–95.

Nunell, G. V., Fernandez, M. E., Bonelli, P. R., & Cukierman, A. L. (2015). Nitrate uptake improvement by modified activated carbons developed from two species of pine cones. *Journal of Colloid and Interface Science*, *440*, 102–108.

Nunthaprechachan, T., Pengpanich, S., & Hunsom, M. (2013). Adsorptive desulfurization of dibenzothiophene by sewage sludge-derived activated carbon. *Chemical Engineering Journal*, *228*, 263–271.

Pam, A. A., Abdullah, A. H., Tan, Y. P., & Zainal, Z. (2018). Batch and fixed bed adsorption of Pb (II) from aqueous solution using EDTA modified activated carbon derived from palm kernel shell. *BioResources*, *13*(1), 1235–1250.

Park, J., Jung, M., Jang, H., Lee, K., Attia, N. F., & Oh, H. (2018). A facile synthesis tool of nanoporous carbon for promising H 2, CO 2, and CH 4 sorption capacity and selective gas separation. *Journal of Materials Chemistry A*, *6*(45), 23087–23100.

Perrich, J. R. (2018). *Activated carbon adsorption for wastewater treatment*. CRC press.

Reig, F. B., Adelantado, J. G., & Moreno, M. M. (2002). FTIR quantitative analysis of calcium carbonate (calcite) and silica (quartz) mixtures using the constant ratio method. Application to geological samples. *Talanta*, *58*(4), 811–821.

Revilla, P. N. D., Maguyon-Detras, M. C., Migo, V. P., & Alfafara, C. G. (2020). *Nitrate removal from aqueous solution by adsorption using municipal solid waste-derived activated biochar*. *778*(1), 012135.

Rio, S., Faur-Brasquet, C., Le Coq, L., Courcoux, P., & Le Cloirec, P. (2005). Experimental design methodology for the preparation of carbonaceous sorbents from sewage sludge by chemical activation—application to air and water treatments. *Chemosphere*, *58*(4), 423–437.

Rivera-Utrilla, J., Sánchez-Polo, M., Gómez-Serrano, V., Alvarez, P., Alvim-Ferraz, M., & Dias, J. (2011). Activated carbon modifications to enhance its water treatment applications. An overview. *Journal of Hazardous Materials*, *187*(1–3), 1–23.

Rösner, T., & Van Schalkwyk, A. (2000). The environmental impact of gold mine tailings footprints in the Johannesburg region, South Africa. *Bulletin of Engineering Geology and the Environment*, *59*(2), 137–148.

Saleh, T. A., & Al-Absi, A. A. (2017). Kinetics, isotherms and thermodynamic evaluation of amine functionalized magnetic carbon for methyl red removal from aqueous solutions. *Journal of Molecular Liquids*, *248*, 577–585.

Shaarani, F., & Hameed, B. (2011). Ammonia-modified activated carbon for the adsorption of 2, 4-dichlorophenol. *Chemical Engineering Journal*, *169*(1–3), 180–185.

Shafeeyan, M. S., Daud, W. M. A. W., Houshmand, A., & Shamiri, A. (2010). A review on surface modification of activated carbon for carbon dioxide adsorption. *Journal of Analytical and Applied Pyrolysis*, *89*(2), 143–151.

Sheha, D., Khalaf, H., & Daghestani, N. (2013). Experimental design methodology for the preparation of activated carbon from sewage sludge by chemical activation process. *Arabian Journal for Science and Engineering*, *38*(11), 2941–2951.

Sheldrick, B. (1984). *Analytical methods manual 1984*. Land Resource Research Institute Ottawa, Ontario, Canada.

Shi, L., Zhang, G., Wei, D., Yan, T., Xue, X., Shi, S., & Wei, Q. (2014). Preparation and utilization of anaerobic granular sludge-based biochar for the adsorption of methylene blue from aqueous solutions. *Journal of Molecular Liquids*, *198*, 334–340.

Simate, G. S., & Ndlovu, S. (2014). Acid mine drainage: Challenges and opportunities. *Journal of Environmental Chemical Engineering*, *2*(3), 1785–1803.

Singh, N. B., Nagpal, G., Agrawal, S., & Rachna. (2018). Water purification by using Adsorbents: A Review. *Environmental Technology & Innovation*, *11*, 187–240. https://doi.org/10.1016/j.eti.2018.05.006

Smith, B. C. (1998). *Infrared spectral interpretation: A systematic approach*. CRC press.

Smith, K., Fowler, G., Pullket, S., & Graham, N. D. (2009). Sewage sludge-based adsorbents: A review of their production, properties and use in water treatment applications. *Water Research*, *43*(10), 2569–2594.

Snyman, H., & Herselman, J. (2006). *Requirements for the agricultural use of sludge*. Water Research Commission.

Song, X., Liu, H., Cheng, L., & Qu, Y. (2010). Surface modification of coconut-based activated carbon by liquid-phase oxidation and its effects on lead ion adsorption. *Desalination*, *255*(1–3), 78–83.

Stats SA. (2018). *Mid-year population estimates 2018* (No. P0302).

Stats SA. (2019). *Gross domestic product 4th quarter 2018*. Statistic South Africa.

Taenzana, B. (2011). *Adsorption of cadmium, nickel and lead on modified natural zeolite*. University of the Witwatersrand,Johanneburg.

Tamai, H., Nagoya, H., & Shiono, T. (2006). Adsorption of methyl mercaptan on surface modified activated carbon. *Journal of Colloid and Interface Science*, *300*(2), 814–817.

Tan, K. L., & Hameed, B. H. (2017). Insight into the adsorption kinetics models for the removal of contaminants from aqueous solutions. *Journal of the Taiwan Institute of Chemical Engineers*, *74*, 25–48. https://doi.org/10.1016/j.jtice.2017.01.024

Tao, H.-C., Zhang, H.-R., Li, J.-B., & Ding, W.-Y. (2015). Biomass based activated carbon obtained from sludge and sugarcane bagasse for removing lead ion from wastewater. *Bioresource Technology*, *192*, 611–617.

Tascón, J. M. (2012). *Novel carbon adsorbents*. Elsevier.

Teng, W., Wu, Z., Fan, J., Zhang, W., & Zhao, D. (2015). Amino-functionalized ordered mesoporous carbon for the separation of toxic microcystin-LR. *Journal of Materials Chemistry A*, *3*(37), 19168–19176.

Tesfamariam, E. H. (2010). *Sustainable use of sewage sludge as a source of nitrogen and phosphorus in cropping systems*. University of pretoria.

Tsechansky, L., & Graber, E. (2014). Methodological limitations to determining acidic groups at biochar surfaces via the Boehm titration. *Carbon*, *66*, 730–733.

Velghe, I., Carleer, R., Yperman, J., Schreurs, S., & D'Haen, J. (2012). Characterisation of adsorbents prepared by pyrolysis of sludge and sludge/disposal filter cake mix. *Water Research*, *46*(8), 2783–2794.

Wang, X., Xu, X., Liang, X., Wang, Y., Liu, M., Wang, X., Xia, S., Zhao, J., Yin, D., & Zhang, Y. (2011). Adsorption of copper (II) onto sewage sludge-derived materials via microwave irradiation. *Journal of Hazardous Materials*, *192*(3), 1226–1233.

Wang, Z., Xie, L., Liu, K., Wang, J., Zhu, H., Song, Q., & Shu, X. (2019). Co-pyrolysis of sewage sludge and cotton stalks. *Waste Management*, *89*, 430–438.

Worch, E. (2012). *Adsorption technology in water treatment: Fundamentals, processes, and modeling*. Walter de Gruyter.

Xia, F., Yang, H., Li, L., Ren, Y., Shi, D., Chai, H., Ai, H., He, Q., & Gu, L. (2020). Enhanced nitrate adsorption by using cetyltrimethylammonium chloride pre-loaded activated carbon. *Environmental Technology*, *41*(27), 3562–3572.

Xu, C., Cheng, H.-W., Li, G.-S., Lu, C.-Y., Lu, X.-G., Zou, X.-L., & Xu, Q. (2017). Extraction of metals from complex sulfide nickel concentrates by low-temperature chlorination roasting and water leaching. *International Journal of Minerals, Metallurgy and Materials*, *24*(4), 377–385. Scopus. https://doi.org/10.1007/s12613-017-1417-2

Xu, G., Yang, X., & Spinosa, L. (2015). Development of sludge-based adsorbents: Preparation, characterization, utilization and its feasibility assessment. *Journal of Environmental Management*, *151*, 221–232.

Xue, Y., Wang, C., Hu, Z., Zhou, Y., Xiao, Y., & Wang, T. (2019). Pyrolysis of sewage sludge by electromagnetic induction: Biochar properties and application in adsorption removal of Pb (II), Cd (II) from aqueous solution. *Waste Management*, *89*, 48–56.

Yagub, M. T., Sen, T. K., Afroze, S., & Ang, H. M. (2014). Dye and its removal from aqueous solution by adsorption: A review. *Advances in Colloid and Interface Science*, *209*, 172–184.

Yang, B., Liu, Y., Liang, Q., Chen, M., Ma, L., Li, L., Liu, Q., Tu, W., Lan, D., & Chen, Y. (2019). Evaluation of activated carbon synthesized by one-stage and two-stage co-pyrolysis from sludge and coconut shell. *Ecotoxicology and Environmental Safety*, *170*, 722–731.

Yao, S., Zhang, J., Shen, D., Xiao, R., Gu, S., Zhao, M., & Liang, J. (2016). Removal of Pb (II) from water by the activated carbon modified by nitric acid under microwave heating. *Journal of Colloid and Interface Science*, *463*, 118–127.

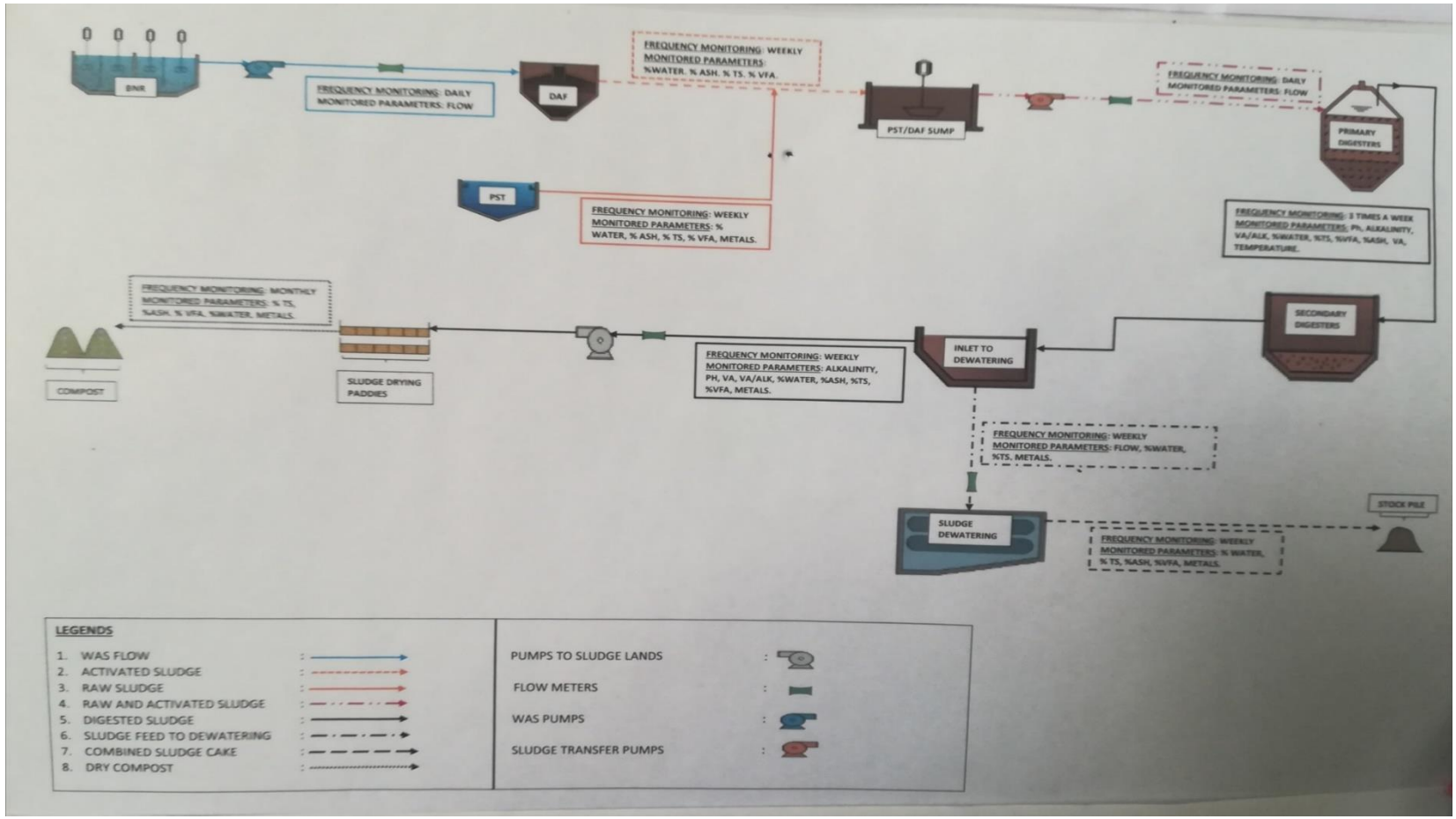
Zeng, F., Liao, X., Hu, H., & Liao, L. (2018). Effect of potassium hydroxide activation in the desulfurization process of activated carbon prepared by sewage sludge and corn straw. *Journal of the Air & Waste Management Association*, *68*(3), 255–264.

Zhang, G., Shi, L., Zhang, Y., Wei, D., Yan, T., Wei, Q., & Du, B. (2015). Aerobic granular sludge-derived activated carbon: Mineral acid modification and superior dye adsorption capacity. *RSC Advances*, *5*(32), 25279–25286.

Zhang, J., Shao, J., Jin, Q., Li, Z., Zhang, X., Chen, Y., Zhang, S., & Chen, H. (2019). Sludge-based biochar activation to enhance Pb (II) adsorption. *Fuel*, *252*, 101–108.

APPENDICES

APPENDIX A: Flowsheet of ERWAT Midvaal WWTP



APPENDIX B: Titrant volume in ml used for neutralization of 10 ml titrant aliquot

			$NaHCO_3$		**Na2CO3**		**NaOH**		**HCl**	
			HCl volume		**HCl volume**		**HCl volume**		**NaOH Volume**	
Sample	Run	sample	TEST1	TEST 2	TEST 1	TEST 2	TEST 1	TEST 2	TEST 1	TEST 2
1	18	D-3-600	8,5	8,9	14,7	14,2	15	14,5	6,4	6
2	22	D-3-750	7,2	7,5	14,7	14,2	8,6	8,4	8,6	8
3	3	D-5-600	8,2	7,9	13,5	13,6	9,3	9,5	9,4	8,8
4	6	D-5-900	10	10	16	16,3	10,4	9,9	7,4	7,1
5	11&15	D-7-600	9,7	9,2	9,6	9,9	11,2	10,8	7,4	7,9
6	20&23	DC-3-900	8	8,4	17	16,4	8,8	9,1	7,3	7,8
7	17	DC-5-600	9	9,2	15,5	16,1	10,3	10,4	7,1	6,8
8	8	DC-5-750	9,4	9,6	13,8	13,3	16,3	16,9	7,1	6,6
9	10&19	DC-7-900	10,1	9,8	15,7	16	9,5	9	7	7,4
10	7	S-3-600	9,8	9,6	17,3	17,6	8,8	8,7	7,2	7,6
11	5	S-3-900	8,3	8,6	14,1	13,8	10,4	10,9	7,8	7,4
12	16	S-5-600	8,8	9,2	17,4	17,9	9,7	9,1	7	7,6
13	14&2	S-7-900	9,9	10,1	17,8	17,6	9,8	9,7	6,7	7
14	13&4	SC-3-600	9,1	9,6	14,8	14,6	8,9	8,5	6,9	6,4
15	1	SC-3-900	9,3	8,8	18,1	10,4	10,1	9,9	6,5	6,8
16	21	SC-5-900	9,9	10,2	15,9	16,5	9,6	9,8	6,8	7
17	12	SC-7-600	8,4	8,8	18,3	18,4	10,2	10	7,5	7
18	9	SC-7-750	10,3	9,7	15,6	15,2	9,4	9,8	6,5	7,2
Com-AC			9,8	9,7	18,3	18,5	8,6	9,1	5,9	6,4

APPENDIX C: Concentration of exchangeable ions

				Elements (mg/l)				Exchangeable cation				CEC (meq/100g)
Sample	Run	labelled	Sludge type	Ca2+	Mg2+	K+	Na+	Ca2+ (1)	Mg2+ (2)	K+ (3)	Na+ (4)	(1)+(2)+(3)+(4)
1	18	D-3-600	D	1,601	0,011	17,036	0,000	7,989	0,046	43,589	0,000	51,624
2	22	D-3-750	D	3,013	0,494	47,337	0,321	15,036	2,033	121,120	1,398	139,586
3	3	D-5-600	D	0,000	0,467	48,643	0,458	0,000	1,922	124,461	1,991	128,373
4	6	D-5-900	D	12,430	1,705	27,746	2,797	186,087	21,046	212,974	36,505	456,613
5	11&15	D-7-600	D	7,853	1,772	17,481	1,556	58,783	10,934	67,092	10,151	146,959
6	20&23	DC-3-900	D	17,322	0,832	26,282	0,339	86,441	3,425	67,247	1,473	158,586
7	17	DC-5-600	D	10,896	1,072	21,505	3,285	54,374	4,409	55,023	14,291	128,097
8	8	DC-5-750	D	7,261	1,125	32,496	0,000	36,234	4,627	83,145	0,000	124,007
9	10&19	DC-7-900	D	6,442	0,197	19,836	0,449	32,147	0,811	50,754	1,954	85,667
10	7	S-3-600	S	13,460	0,448	32,339	1,150	67,169	1,841	82,745	5,002	156,758
11	5	S-3-900	S	8,054	0,242	22,108	1,607	40,192	0,996	56,567	6,990	104,745
12	16	S-5-600	S	18,797	0,634	36,612	0,177	93,802	2,610	93,677	0,769	190,858
13	14&2	S-7-900	S	12,510	0,911	36,603	2,639	62,428	3,749	93,654	11,479	171,311
14	13&4	SC-3-600	S	9,592	2,989	19,820	1,465	47,867	12,297	50,713	6,371	117,247
15	1	SC-3-900	S	9,705	0,610	24,448	0,430	48,431	2,508	62,553	1,871	115,363
16	21	SC-5-900	S	18,260	2,514	42,780	3,030	91,122	10,344	109,458	13,178	224,103
17	12	SC-7-600	S	19,981	0,903	38,915	0,165	99,711	3,715	99,571	0,717	203,714
18	9	SC-7-750	S	15,550	0,394	22,504	0,124	77,599	1,621	57,581	0,540	137,340
Com-AC				31,413	1,601	11,219	0,421	156,759	6,589	28,706	1,831	193,885
D				1,601	17,638	3,460	0,000	7,989	72,571	8,853	0,000	89,414
S				1,601	11,733	17,840	2,237	7,989	48,275	45,646	9,731	111,642
Discard coal				1,601	4,716	26,974	2,474	7,989	19,401	69,017	10,763	107,170

APPENDIX D: Final pH for point of zero charge determination

Samples	labelled												
	D-3-600	**2**	**3**	**4**	**5**	**6**	**7**	**8**	**9**	**10**	**11**	**12**	Init pH
1		2,27	5,15	7,02	7,38	7,29	7,33	7,39	7,72	7,54	9,61	10,95	Final Ph
	D-3-750	**2**	**3**	**4**	**5**	**6**	**7**	**8**	**9**	**10**	**11**	**12**	Init pH
2		2,33	4,07	5,97	6,82	6,59	6,78	7,08	7,52	8,21	9,43	10,1	Fin Ph
	D-5-600	**2**	**3**	**4**	**5**	**6**	**7**	**8**	**9**	**10**	**11**	**12**	Init pH
3		2,26	3,89	5,16	5,34	5,8	5,57	5,68	6,44	7,08	7,93	10,2	Fin Ph
	D-5-900	**2**	**3**	**4**	**5**	**6**	**7**	**8**	**9**	**10**	**11**	**12**	Init pH
4		2,92	7,31	9,31	9,47	9,58	9,61	9,02	9,62	9,58	9,84	11,27	Fin Ph
	D-7-600	**2**	**3**	**4**	**5**	**6**	**7**	**8**	**9**	**10**	**11**	**12**	Init pH
5		2,13	3,33	4,26	4,86	4,66	5,57	5,19	6,68	4,98	9,74	11,18	Fin Ph
	DC-3-900	**2**	**3**	**4**	**5**	**6**	**7**	**8**	**9**	**10**	**11**	**12**	Init pH
6		3,45	4,14	4,53	7,86	7,89	7,87	7,84	8,07	8,72	9,68	10,85	Fin Ph
	DC-5-600	**2**	**3**	**4**	**5**	**6**	**7**	**8**	**9**	**10**	**11**	**12**	Init pH
7		2,1	3,04	4,01	4,55	4,55	4,56	5,06	5,69	6,16	7,57	11,35	Fin Ph
	DC-5-750	**2**	**3**	**4**	**5**	**6**	**7**	**8**	**9**	**10**	**11**	**12**	Init pH
8		3,74	6,5	7,44	7,63	7,45	7,58	7,64	8,1	8,22	9,85	10,86	Fin Ph
	DC-7-900	**2**	**3**	**4**	**5**	**6**	**7**	**8**	**9**	**10**	**11**	**12**	Init pH
9		4,37	9,59	9,99	10,1	10,16	10,14	10,15	10,07	10,39	10,36	10,89	Fin Ph
	S-3-600	**2**	**3**	**4**	**5**	**6**	**7**	**8**	**9**	**10**	**11**	**12**	Init pH
10		2,44	3,79	5,24	5,63	5,85	5,83	6,58	7,12	7,28	7,66	10,5	Fin Ph
	S-3-900	**2**	**3**	**4**	**5**	**6**	**7**	**8**	**9**	**10**	**11**	**12**	Init pH
11		2,12	3,39	6,59	7,34	9,61	8,22	8,63	8,61	9,12	9,81	11,23	Fin Ph
	S-5-600	**2**	**3**	**4**	**5**	**6**	**7**	**8**	**9**	**10**	**11**	**12**	Init pH
12		3,23	5,98	6,62	6,79	6,6	6,76	7,06	7,23	7,17	7,36	8,58	Fin Ph
	S-7-900	**2**	**3**	**4**	**5**	**6**	**7**	**8**	**9**	**10**	**11**	**12**	Init pH
13		2,49	4,23	5,9	6,64	7	6,83	6,62	6,69	7,03	9,04	10,59	Fin Ph
	SC-3-600	**2**	**3**	**4**	**5**	**6**	**7**	**8**	**9**	**10**	**11**	**12**	Init pH
14		2,13	3,14	4,2	5,92	4,7	5,24	5,11	5,67	7,48	9,23	10,81	Fin Ph
15	SC-3-900	**2**	**3**	**4**	**5**	**6**	**7**	**8**	**9**	**10**	**11**	**12**	Init pH

		2,93	4,82	6,96	6,83	6,88	7,064	7,16	7,08	7,1	8,34	11,12	Fin Ph
16	SC-5-900	**2**	**3**	**4**	**5**	**6**	**7**	**8**	**9**	**10**	**11**	**12**	Init pH
		4,12	7,57	8,22	8,5	8,68	8,36	8,52	8,5	8,85	9,13	11,27	Fin Ph
17	SC-7-600	**2**	**3**	**4**	**5**	**6**	**7**	**8**	**9**	**10**	**11**	**12**	Init pH
		2,47	3,87	5,12	5,72	5,78	5,7	5,87	5,83	5,83	6,9	11,19	Fin Ph
18	SC-7-750	**2**	**3**	**4**	**5**	**6**	**7**	**8**	**9**	**10**	**11**	**12**	Init pH
		4,04	6,65	7,18	7,54	7,67	7,62	7,52	7,61	7,58	8,31	10,92	Fin Ph
19	CAC	**2**	**3**	**4**	**5**	**6**	**7**	**8**	**9**	**10**	**11**	**12**	Init pH
		2,48	7,32	10,4	10,35	10,39	10,68	10,64	10,42	10,67	10,93	10,86	Fin Ph

APPENDIX E: Ultimate analysis of unmodified SBAC and modified.

		Elements (%)								Average (%)			
SBAC	modifications conditions	C		N		H		S		C	N	H	S
SC-3-600	unmodified	44,848	45,606	-0,218	-0,221	0,735	0,747	0,413	0,413	45,227	-0,219	0,741	0,413
	M1	48,539	46,283	1,575	1,566	1,008	1,002	0,301	0,299	47,411	1,571	1,005	0,300
	M2	46,267	46,521	1,569	1,577	1,025	1,010	0,287	0,289	46,394	1,573	1,017	0,288
SC-5-900	unmodified	2,025	2,003	0,414	0,419	-0,552	-0,558	0,663	0,670	2,014	0,416	-0,555	0,666
	M2	1,889	1,893	1,779	1,769	0,000	0,000	0,000	0,000	1,891	1,774	0,000	0,000
DC-5-750	unmodified	23,809	23,416	-0,763	-0,751	0,458	0,450	0,127	0,124	23,612	-0,757	0,454	0,126
	M1	29,250	30,552	1,755	2,010	1,051	1,123	0,026	0,031	29,901	1,883	1,087	0,029
	M2	30,634	30,132	1,901	1,870	1,027	1,012	0,000	0,000	30,383	1,885	1,019	0,000
DC-7-900	unmodified	15,376	15,545	-0,796	-0,805	-0,293	-0,296	0,000	0,000	15,460	-0,800	-0,295	0,000
	M1	14,955	14,707	1,936	1,904	0,079	0,078	0,000	0,000	14,831	1,920	0,079	0,000
	M2	15,099	15,122	1,895	1,913	0,076	0,073	0,000	0,000	15,111	1,904	0,075	0,000

APPENDIX F: Ultimate analysis of precursors, SBAC and Com-AC

		Elements (%)				Average (%)				Ratio	
SABC	Sample	C	N	H	S	C	N	H	S	N/C	H/C
D-3-600		17,9893	-0,5719	1,1173	0,4035						
	1	18,2858	-0,8679	1,1357	0,4101	18,1376	-0,7199	1,1265	0,4068	0,0000	0,0621
D-3-750		3,0491	0,4261	-0,4725	0,8210						
	2	3,0323	0,4237	-0,4699	0,8165	3,0407	0,4249	-0,4712	0,8188	0,1397	0,0000
D-5-600		8,9485	-0,1621	0,1294	0,0211						
	3	8,7902	-0,1586	0,1266	0,0207	8,8694	-0,1604	0,1280	0,0209	0,0000	0,0144
D-5-900		2,1690	0,3611	-0,5392	0,8745						
	4	2,2174	0,3692	0,5392	0,8941	2,1932	0,3651	0,0000	0,8843	0,1665	0,0000
D-7-600		2,7124	0,4375	-0,4630	0,7466						
	5	2,6824	0,4327	-0,4578	0,7383	2,6974	0,4351	-0,4604	0,7424	0,1613	0,0000
DC-3-900		12,9052	-1,0586	-0,3546	-0,1600						
	6	12,6901	-1,0410	-0,3487	-0,1573	12,7977	-1,0498	-0,3517	-0,1587	0,0000	0,0000
DC-5-600		57,2879	0,2080	1,5097	-0,0626						
	7	57,6010	0,2092	1,5179	-0,0630	57,4444	0,2086	1,5138	-0,0628	0,0036	0,0264
DC-5-750		23,8085	-0,7634	0,4578	0,1265						
	8	23,4161	-0,7508	0,4503	0,1245	23,6123	-0,7571	0,4540	0,1255	0,0000	0,0192
DC-7-900		15,3755	-0,7960	-0,2930	0,0000						
	9	15,5454	-0,8048	-0,2963	0,0000	15,4605	-0,8004	-0,2947	0,0000	0,0000	0,0000
S-3-600		47,8371	-0,1767	1,0292	1,1280						
	10	47,0440	-0,1737	1,0122	1,1470	47,4406	-0,1752	1,0207	1,1375	0,0000	0,0215
S-3-900		1,7500	-0,4044	-0,5821	3,9840						
	11	1,7301	-0,4000	-0,5757	3,9404	1,7401	-0,4022	-0,5789	3,9622	0,0000	0,0000
S-5-600		8,8245	-0,3725	-0,1966	0,1699						
	12	8,8736	-0,3746	-0,1977	0,1708	8,8491	-0,3735	-0,1972	0,1703	0,0000	0,0000
S-7-900		1,7876	0,5347	-0,5376	1,1081						
	13	1,7876	0,5377	-0,5065	1,1143	1,7876	0,5362	-0,5221	1,1112	0,3000	0,0000
SC-3-600		44,8485	-0,2178	0,7349	0,4129						
	14	45,6059	-0,2211	0,7473	0,4129	45,2272	-0,2195	0,7411	0,4129	0,0000	0,0164
SC-3-900		6,9966	0,6933	-0,3405	0,7010						
	15	6,9574	0,6890	-0,3386	0,6970	6,9770	0,6912	-0,4103	0,6990	0,0991	0,0000
SC-5-900		2,0250	0,4141	-0,5518	0,6628						
	16	2,0032	0,4186	-0,5579	0,6701	2,0141	0,4163	-0,5549	0,6664	0,2067	0,0000
SC-7-600		21,6051	-0,3651	1,1189	1,0457						
	17	21,7231	-0,3671	1,1250	1,0514	21,6641	-0,3661	1,1219	1,0485	0,0000	0,0518
SC-7-750		14,0060	0,5384	-0,1035	1,0825						
	18	14,1614	0,5389	-0,1047	1,0945	14,0837	0,5387	-0,1041	1,0885	0,0382	0,0000
		78,6275	-0,0997	-0,8631	0,0000						
CAC	19	78,1935	-0,0992	-0,8631	0,0000	78,4105	-0,0994	-0,8631	0,0000	0,0000	0,0000
		36,412	5,511	5,006	1,997						
D		36,610	5,541	5,033	2,008	36,511	5,526	5,020	2,002	0,151	0,137
		36,842	5,244	2,696	2,239						
S		36,438	5,186	2,667	2,264	36,640	5,215	2,681	2,251	0,142	0,073

	43,015	2,435	-1,690	2,422						
Discard Coal	43,251	2,412	-1,700	2,435	43,133	2,424	-1,695	2,429	0,056	0,000

Appendix G: Preliminary results of methyl red adsorption

volume	10	ml
sorbent mass	5	Mg
pH	4	
initial Co	75	mg/ml

C e at t(min):	Com-AC	DC-5-750	DC-5-750 M1	DC-5-750 M2	DC-7-900	DC-7-900 M1	DC-7-900 M2	SC-3-600	SC-3-600 M1	SC-3-600
90	13,066	25,086	18,437	18,426	47,014	44,821	47,854	52,829	51,814	53
180	14,4464	17,818	11,183	15,193	19,854	12,812	19,932	26,738	22,8833	26
qe (mg/g)										
90	123,868	99,828	113,126	113,148	55,972	60,358	54,292	44,342	46,372	43
180	121,1072	114,364	127,634	119,614	110,292	124,376	110,136	96,524	104,2334	9
% removal										
90	82,578667	66,552	75,417333	75,432	37,3147	40,238667	36,194667	29,5613	30,914667	28
180	80,738133	76,2427	85,089333	79,742667	73,528	82,917333	73,424	64,3493	69,488933	